Strengthening of Al-based composites by microstructural modifications

D I S S E R T A T I O N

zur Erlangung des akademischen Grades

Doktor - Ingenieur

(Dr.-Ing.)

Vorgelegt

der Fakultät Maschinenwesen

der Technische Universität Dresden

von

Hafiz Rub Nawaz Shahid

geboren am 15. March 1981 in Sargodha (Pakistan)

Dedicated to;

Dr. Ruth Katherina Martha Pfau

Born: 1929, Leipzig, Germany

Dedicated her life to fight against the leprosy outbreaks in Pakistan

Died: 2017, Karachi, Pakistan

&

Mr. Abdul Sattar Edhi

Born: 1928, Bantva, India

Pakistani philanthropist, ascetic, and humanitarian

Died: 2016, Karachi, Pakistan

Abstract

The strengthening of aluminum matrix composites can be achieved by incorporating hard phase particles in the matrix. The strengthening of the composites depends on the ability of the reinforcement to bear the load and on the microstructural changes induced by the reinforcement addition. The microstructural strengthening is mainly associated with dislocation multiplication, matrix partitioning and Orowan strengthening effects. The strength increases by increasing the reinforcement volume fraction as well as by reducing the size of the reinforcing particles. Additionally, strengthening of composites can be achieved by microstructural modifications through the proper reaction between matrix and reinforcement. Strengthening can also be efficiently attained by the creation of harmonic structures: bimodal microstructures generated by controlled milling of the particulate precursors, which consist of coarse-grained cores embedded in a continuous fine-grained matrix.

In this thesis, aluminum based composites are synthesized using ball milling followed by consolidation through hot pressing. Starting from the in-situ creation of intermetallic reinforcements in Al-Mg composites, the research proceeds towards the in-situ microstructural modification in Al-Fe$_3$Al composites. Finally, Al-Fe$_3$Al composites with harmonic structure are successfully produced. The consolidated composites are characterized to analyze the effect of the microstructural changes on the mechanical properties.

Lightweight Al-Mg metal matrix composites are synthesized from elemental powder mixtures of aluminum and magnesium using pressure-assisted reactive sintering. The aim is to analyze the effect of the initial volume percent of magnesium on the microstructural modifications and development of the in-situ intermetallic reinforcements. The effect of the reaction between aluminum and magnesium on the mechanical properties of the composites due to the formation of β-Al$_3$Mg$_2$ and γ-Al$_{12}$Mg$_{17}$ intermetallics is also investigated. The formation of the intermetallic compounds progressively consumes aluminum and magnesium and induces strengthening of the composites: the yield and compressive strengths increase with increasing the content of intermetallic reinforcement at the expense of the plastic deformation.

In the next stage, the effectiveness of the reaction between matrix and reinforcement as a strengthening method for further improving the mechanical performance composites is investigated for the Al-Fe$_3$Al system. To achieve this aim, *transformed* and *non-transformed* composites are produced by hot pressing at different temperatures. Phase analysis and microstructural characterization of the transformed composites reveal the formation of a

double-shell-reinforcement with Al_5Fe_2 and $Al_{13}Fe_4$ intermetallics surrounding the Fe_3Al phase, while the Al matrix is progressively consumed with increasing the reinforcement content. In order to analyze the phase sequence induced by the $Al-Fe_3Al$ reaction, composites consisting of Al matrix and a single mm-sized Fe_3Al particle were synthesized through hot pressing at 823, 873 and 903 K. The microstructural investigations and phase identifications suggest that in-situ phase transformation occurs through atomic diffusion of aluminum in Fe_3Al and the formation of in-situ intermetallics (Al_5Fe_2 and $Al_{13}Fe_4$) takes place exclusively within the original Fe_3Al particles. The phase transformation during hot pressing induces significant strengthening: the ranges of yield and compressive strengths increase from 70-360 MPa and 200-500 MPa for the non-transformed composites to 400-1800 MPa and 550-1800 MPa for the transformed materials. This occurs at the expense of the plastic deformation, which is generally reduced in the transformed composites. The yield strength of both transformed and non-transformed composites follows the iso-stress model when the characteristic structural features (i.e. strengthening phases and matrix) are taken into account.

At the end, the concept of harmonic structures is extended to metal matrix composites by analyzing the effectiveness of such bimodal microstructures as a strengthening method for composites consisting of a pure Al matrix reinforced with Fe_3Al particles. The purpose of the study is to examine the microstructural variations induced by ball milling of the $Al-Fe_3Al$ composite powder mixtures and how such variations influence the resulting microstructure and mechanical response of the bulk composite specimens synthesized by hot-pressing.

Preferential microstructural refinement limited to the surface of the particles, where the Fe_3Al phase is progressively fragmented, occurs during ball milling of the $Al-Fe_3Al$ composite powder mixtures. The refined surface becomes the continuous fine-grained matrix that encloses macro-regions with coarser reinforcing particles in the harmonic composites synthesized during subsequent powder consolidation. The generation of the bimodal microstructure has a significant influence on the strength of the harmonic composites, which exceeds that of the conventional material by a factor of 2 while retaining considerable plastic deformation. Finally, modeling of the mechanical properties indicates that the strength of the harmonic composites can be accurately described by taking into account both the volume fraction of reinforcement and the characteristic microstructural features describing the harmonic structure.

The results of the current research work demonstrate that powder metallurgy (i.e. ball milling followed by hot consolidation) can be successfully used to produce high strength

aluminum based composites reinforced by intermetallics. The findings indicate that phase transformation and reinforcement arrangement based microstructural modifications can significantly enhance the strength of the composites. The strength and deformability of the composites depends on the volume fraction and arrangement of the reinforcement along with the interfacial reaction between the initial components.

Kurzfassung

Die Verstärkung von Aluminium-Matrix-Verbundwerkstoffen kann durch die Integration von Hartphasenpartikeln in die Matrix erreicht werden. Die Festigkeitssteigerung der Komposite ist abhängig davon, wie die Verstärkungsphase die einwirkenden Kräfte aufnehmen kann und zudem von den Auswirkungen der Verstärkungsphase auf das Werkstoffgefüge. Die Verfestigung wird zurückgeführt auf Versetzungsmultiplikation, Matrixpartitionierung und Orowan-Verstärkungseffekte. Die Festigkeit steigt durch Erhöhung des Volumenanteils der Verstärkungsphase sowie durch die Reduktion der Größe der Verstärkungsphase. Darüber hinaus kann die Festigkeitssteigerung von Verbundwerkstoffen durch eine Gefügemodifikation verbunden mit einer Reaktion zwischen Matrix und Verstärkungsphase erreicht werden. Die Festigkeitssteigerung kann auch durch die Schaffung harmonischer Strukturen, d.h. durch ein bimodales Gefüge, erfolgen. Dieses wird erzeugt durch kontrolliertes Mahlen der partikelförmigen Precursor-Phase, die dann aus grobkörnigen Kerngebieten bestehen, eingebettet in eine kontinuierliche feinkörnige Matrix.

In dieser Arbeit werden Verbundwerkstoffe auf Aluminiumbasis durch Hochenergiemahlen und anschließender Konsolidierung durch Heißpressen hergestellt. Ausgehend von der in-situ Herstellung intermetallischer Verstärkungsphasen in Al-Mg-Verbundwerkstoffen werden außerdem in-situ Gefügemodifikationen in Al-Fe_3Al-Verbundwerkstoffen betrachtet. Al-Fe_3Al-Verbundwerkstoffe mit harmonischer Struktur konnten dabei erfolgreich hergestellt werden. Anschließend wurde der Einfluss der mikrostrukturellen Veränderungen auf die mechanischen Eigenschaften analysiert.

Al-Mg-Metallmatrix-Verbundwerkstoffe werden aus den Pulvergemischen von elementarem Aluminium und Magnesium durch druckunterstütztes reaktives Sintern hergestellt. Das Ziel ist es, den Einfluss des anfänglichen Volumenanteils von Magnesium auf die mikrostrukturellen Veränderungen und die Entstehung der in-situ intermetallischen Verstärkungsphase zu analysieren. Zudem wird der Einfluss der Reaktion zwischen Aluminium und Magnesium und die damit verbundene Bildung der intermetallischen Phasen β-Al_3Mg_2 und γ-$Al_{12}Mg_{17}$ auf die mechanischen Eigenschaften der Verbundwerkstoffe untersucht. Die Bildung der intermetallischen Phasen verbraucht zunehmend Aluminium und Magnesium und bewirkt eine Verfestigung der Verbundwerkstoffe: Die Streckgrenze und die Druckfestigkeit steigen mit zunehmendem Gehalt an intermetallischer Verstärkungsphase auf Kosten der plastischen Verformung.

In der nächsten Phase wird im Al-Fe$_3$Al-System die Wirksamkeit der Reaktion zwischen Matrix und Verstärkungsphase als festigkeitssteigernde Maßnahme zur weiteren Verbesserung der mechanischen Eigenschaften untersucht. Dafür werden *transformierte* und *nicht-transformierte* Verbundwerkstoffe durch Heißpressen bei unterschiedlichen Temperaturen hergestellt. Phasenanalyse und mikrostrukturelle Charakterisierung der transformierten Verbundwerkstoffe zeigten die Bildung der intermetallischen Phasen Al$_5$Fe$_2$ und Al$_{13}$Fe$_4$, die als Verstärkungsphase mantelförmig um die die Fe$_3$Al-Phase angeordnet sind. Die Al-Matrix wird dabei mit steigendem Anteil an Verstärkungsphase zunehmend verbraucht. Um die durch die Al-Fe$_3$Al-Reaktion induzierte Phasenfolge zu analysieren, wurden Verbundwerkstoffe, bestehend aus Al-Matrix und einem einzigen mm-großen Fe$_3$Al-Partikel durch Heißpressen bei 823, 873 und 903 K synthetisiert. Die Gefüge- und Phasenanalyse deuten darauf hin, dass die In-situ-Phasenumwandlung durch atomare Diffusion von Aluminium in Fe$_3$Al erfolgt und die Bildung von in-situ intermetallischen Phasen (Al$_5$Fe$_2$ und Al$_{13}$Fe$_4$) ausschließlich innerhalb der ursprünglichen Fe$_3$Al-Partikel stattfindet. Die Phasenumwandlung beim Heißpressen führt zu einer signifikanten Festigkeitssteigerung: Die Streckgrenze und die Druckfestigkeit erhöhen sich von 70-360 MPa und 200-500 MPa für die nicht umgewandelten Verbundwerkstoffe auf 400-1800 MPa und 550-1800 MPa für die umgewandelten Materialien. Damit verbunden ist jedoch auch eine verringerte plastische Verformbarkeit in den umgewandelten Kompositen. Die Streckgrenze von transformierten und nicht transformierten Verbundwerkstoffen folgt dem Iso-Stress-Modell, wenn die charakteristischen strukturellen Merkmale (d.h. Verstärkungsphasen und Matrix) berücksichtigt werden.

Schließlich wird das Konzept der harmonischen Strukturen für Metallmatrix-Verbundwerkstoffe erweitert, indem die Wirksamkeit solcher bimodaler Gefüge als Verstärkungsmethode für Verbundwerkstoffe aus einer reinen Al-Matrix verstärkt mit Fe$_3$Al-Partikeln betrachtet wird. Ziel der Studie ist es, die Gefügeveränderungen zu untersuchen, die durch das Hochenergiemahlen der Al-Fe$_3$Al-Verbundpulvermischungen induziert werden. Weiterhin soll der Einfluss des so veränderten Gefüges auf das mechanische Verhalten der durch Heißpressen synthetisierten Verbundproben charakterisiert werden.

Die beabsichtigte Kornfeinung beschränkt sich auf die Oberfläche der Partikel, wo die Fe$_3$Al-Phase während der Kugelmahlung der Al-Fe$_3$Al-Verbundpulvermischungen nach und nach fragmentiert wird. In den bei der anschließenden Pulverkonsolidierung erzeugten harmonisierten Kompositen wird die feinkörnige Oberfläche zur kontinuierlichen feinkörnigen Matrix, die Makroregionen mit grobkörnigen Verstärkungspartikeln umschließt. Die

Erzeugung der bimodalen Gefüge hat einen signifikanten Einfluss auf die Festigkeit der harmonischen Verbundwerkstoffe, die die des konventionellen Materials um den Faktor 2 übertrifft, ohne die plastische Verformbarkeit zu beeinträchtigen. Zudem zeigt die Modellierung der mechanischen Eigenschaften, dass die Festigkeit der harmonischen Verbundwerkstoffe genau beschrieben werden kann, indem sowohl der Volumenanteil der Verstärkungsphase als auch die charakteristischen Gefügemerkmale der harmonischen Struktur berücksichtigt werden.

Die Ergebnisse der vorliegenden Arbeit zeigen, dass die Pulvermetallurgie (d.h. Hochenergiemahlen mit anschließendem Heißpressen) erfolgreich eingesetzt werden kann, um hochfeste Verbundwerkstoffe auf Aluminiumbasis mit intermetallischer Verstärkungsphase herzustellen. Die Ergebnisse zeigen, dass durch Phasenumwandlung und durch die Anordnung von Verstärkungsphasen hervorgerufene Gefügeveränderungen die Festigkeit der Verbundwerkstoffe signifikant erhöht werden kann. Die Festigkeit und Verformbarkeit der so erzeugten Komposite hängt vom Volumenanteil und der Anordnung der Verstärkungsphase sowie der Grenzflächenreaktion zwischen den Ausgangskomponenten ab.

Contents

Chapter 1. Introduction

Aluminum matrix composites (AMCs) are attractive materials for applications in automotive, aircraft and transportation industries because of their low density, high specific strength, stiffness, workability, good thermal stability and enhanced resistance to wear, corrosion and fatigue [Yas17, Sur03]. Particulate-reinforced AMCs synthesized by solid-state powder metallurgy (e.g. through pressure-assisted sintering) are of particular interest thanks to the excellent control over fundamental microstructural features, including size, morphology and distribution of the reinforcing phase [Ger05, Tor03], which allows the development of advanced materials with customized properties.

The strengthening of composites is based on the incorporation of a hard phase in a metallic matrix to improve the properties compared to the unreinforced material [Scu09a, Moy07, Kai06]. According to the shear lag model, strengthening of a composite depends on the load bearing ability of the reinforcement: the soft matrix transfers the applied stress to the reinforcing particles, which share the stress and strengthen the composite [Dav93, Nar86]. Simultaneously, the addition of the reinforcement generates microstructural variations in the matrix, which enhance the strength of the composites by Orowan strengthening, matrix partitioning and dislocation multiplication [Kra93, Ars88, Vog86]. As a composite is cooled down during synthesis, the difference between the coefficient of thermal expansion of matrix and reinforcement leads to the formation of dislocations at the matrix-reinforcement interface. These thermally-induced dislocations as well improve the strength of the composites [Scu09b, Ars91, Mil91, Ars86].

Both load bearing and microstructural strengthening effects coexist and are related to the distribution, volume fraction and size of the reinforcement [Scu09b, Ram96]. The strength increases with increasing the reinforcement volume fraction as well as by reducing the size of the reinforcing phase [Sur13b, Gan05, Cha01], provided that the reinforcing particles are homogeneously dispersed in the matrix and no significant reinforcement clustering occurs. Particular important for large volume fractions of reinforcement and/or small particle size is the reduction of the matrix ligament size (λ), which can be regarded as the average distance between adjacent reinforcing particles, and results in a similar strengthening as the Hall-Petch effect observed for grain refinement [Scu09b].

More unconventional strengthening methods include (*i*) controlled interfacial reactions between matrix and reinforcement during processing or, subsequently, by post processing heat treatments to obtain microstructural changes and phase transformations capable to further enhance the strength of the composites [Ali14, Lap10a, Scu09a, El08, Ken08, Tan05] and (*ii*) microstructural modifications induced by ball milling of the composite powder mixtures [Bal15, Kim12, Sur01a]. Ball milling, which consists of high-energy collisions of the grinding balls with the particles, is a flexible and commonly used method of de-agglomeration, size reduction and homogeneous dispersion of the reinforcing particles within the matrix [Cha12, Cor11, Koc97]. Protracted ball milling leads to microstructural refinement by deforming, fracturing and cold welding of the composite powder [Kim12, Sur01b]. Such microstructural modifications can induce substantial strengthening in composites without the need to increase the volume fraction of the reinforcing phase [Bal15, Sur13b, Kim12].

Recently, metallic particulate reinforcements, including metallic glasses [Alj12, Scu09a] and complex intermetallic phases, such as quasicrystals and complex metallic alloys [Ali12a, Lap10b, Scu09b], have been successfully used as reinforcements in AMCs synthesized by powder metallurgy (P/M). The use of metallic reinforcements instead of conventional ceramics provides economical production and recyclability of AMCs [Dav93]. In addition, metallic reinforcements display improved wettability and reduced difference of thermal expansion with the metallic matrix, [Tan04, Tjo00] which may thus lead to the creation of a stronger interface between matrix and reinforcement [Yu06].

Phase transformations and microstructural changes during processing or afterward during heat treatment can occur in composite materials due to the interfacial reaction between matrix and reinforcement. The effect of the transformation on the properties of the composites depends upon the nature of the reaction products, their bonding with the surrounding phases, and the volumetric changes involved in the transformation [Kai06, Has02a]. Interfacial reactions can, therefore, be used to enhance the mechanical properties of composites. An explicative example of this behavior is given by the Al-based composites reinforced with Al-Cu-Fe quasicrystals, where the reaction between the Al matrix and the quasicrystalline particles forms a new reinforcing phase, the ω-Al_7Cu_2Fe [Ali14, El08, Ken08]. The new microstructure leads to enhanced strength of the composites at both room and high temperatures.

Ex-situ as well as in-situ addition of Al-Mg-intermetallics have been used to strengthen either aluminum or magnesium matrix composites [Par18, Mal16, Cha14, Scu09b, Chu06]

because of their high hardness, low density, high temperature strength and low processing cost [Ste07, Bak92]. Taking into account the excellent properties of magnesium aluminides as reinforcing particles and the involvement of only two intermetallics (β-Al_3Mg_2 and γ-$Al_{12}Mg_{17}$) in the entire Al-Mg composition range the aluminum-magnesium system was selected to analyze the effectiveness of phase transformation on the strength of aluminum-magnesium composites. Another reason behind the selection of this system is that rarely research activities on the powder metallurgical processing of aluminum-magnesium composites reinforced by magnesium aluminides starting from pure aluminum and magnesium powders are reported.

Similarly, iron-aluminides are also potential substitutes for ceramics and more expensive metallic reinforcements in AMCs [Nem16b, Cha13] due to their remarkable properties, including good mechanical behavior, low cost and considerable stability under corrosive environments [Sto98, Dee96]. Many attempts have been made to incorporate the Fe_3Al phase in composite materials using different processing routes [Pan15, Sto03, Lee02]. Therefore, the effectiveness of the reaction between matrix and reinforcement as a strengthening method for further improving the mechanical performance of the Al-Fe_3Al composites has been investigated in the next step of this research work.

Materials strengthening while retaining appreciable plastic deformation can be achieved by generating harmonic structures: bimodal heterogeneous microstructures consisting of coarse-grained cores embedded in a continuous fine-grained matrix [Vaj16, Hua15]. Such microstructures are synthesized by solid-state powder processing, for example by controlled milling of the particles followed by powder consolidation [Vaj16, Ame12]. The harmonic structure and its gradual variation of size from coarse to fine leads to enhanced strength and toughness for a variety of materials, including pure Ti, Ti-6Al-4V, steel and Co-Cr-Mo [Zha17b, Saw14, Ame12]. The advantage of the harmonic structures over other bimodal arrangements resulting from simply mixing coarse- and fine-grained particles is the creation of controlled heterogeneous microstructures, which avoids the irregular distribution of the coarse- and fine-grained areas and leads to a good reproducibility of the mechanical properties [Vaj16, Hua15].

In this work, P/M processing consisting of solid-state pressure-assisted sintering is used. P/M is a flexible route for the fabrication of composites because it gives excellent control over the microstructural features, such as volume fraction and size, shape and distribution of the

components [Tor03, Har98]. Furthermore, the possibility to control the (relatively low) processing temperature enables to govern the extent of the interfacial reaction during consolidation.

The focus of the current study is thus to investigate the effectiveness of the unconventional strengthening methods for aluminum-magnesium and aluminum-Fe$_3$Al composite systems. The interfacial reaction based strengthening was investigated for Al-Mg and Al-Fe$_3$Al composites systems by establishing chemical reaction between the initial components of the composites. The concept of harmonic structures was extended to metal matrix composites by analyzing the effectiveness of such bimodal microstructures as a strengthening method for composites consisting of a pure Al matrix reinforced with Fe$_3$Al particles.

An overview of aluminum matrix composites, matrix-reinforcement interface, and intermetallic reinforcements: i.e., iron aluminides and magnesium aluminides, is given in Chapter 2 along with the strengthening mechanisms for particulate reinforced aluminum matrix composites. The final part of Chapter 2 summarizes the powder metallurgical processing techniques used for the synthesis of particle reinforced aluminum matrix composites. Experimental procedures used in this research work to process and characterize the composites are explained in Chapter 3. The effect of the chemical reaction between aluminum and magnesium on the microstructure and mechanical properties of the Al-Mg composites due to the creation of in-situ Mg-aluminides is discussed in Chapter 4. A comparison of the microstructural and mechanical properties between non-transformed (Al+Fe$_3$Al) and transformed (Al+Fe$_3$Al+Al$_5$Fe$_2$+Al$_{13}$Fe$_4$) composites is discussed in chapter 5 along with the phase evolution sequence in the Al-Fe$_3$Al composite system and the (micro)structural modifications induced by the transformation have been correlated with the observed variations of the mechanical properties. Chapter 6 presents the microstructural variations induced in the Al-Fe$_3$Al composite powder mixtures by extended low energy ball milling. It further explains how such variations influence the thermal stability of the cold compacts and the resulting microstructure and mechanical response of the bulk composite specimens synthesized by hot-pressing. Finally, Chapter 7 gives the summary and concluding remarks.

Chapter 2. Motivation and state-of-the-art

2.1 Metal matrix composites

Metal matrix composites (MMCs) consist of at least two chemically and physically different phases, a metallic matrix and a metallic or non-metallic reinforcement. The distribution of continuous or dis-continuous reinforcements in a metallic matrix provides superior properties compared to the unreinforced material [Cha06]. Lightweight metallic matrix composites are generally produced to combine the ductility and deformability of the metallic matrix with the strength and stiffness of the reinforcement. MMCs have superior fatigue, creep, thermal and corrosion properties compared to the unreinforced matrix [Jay15]. Matrices in MMCs can be pure metals or alloy and reinforcement morphologies include fibers, whiskers and particles. Ceramics, e.g., carbides, oxides and nitrides, and metallic materials, e.g. complex metallic alloys, bulk metallic glasses and intermetallics, can be used as reinforcements [Cha06, Kai06].

Particles   Short fibers / whiskers   Continuous fibers
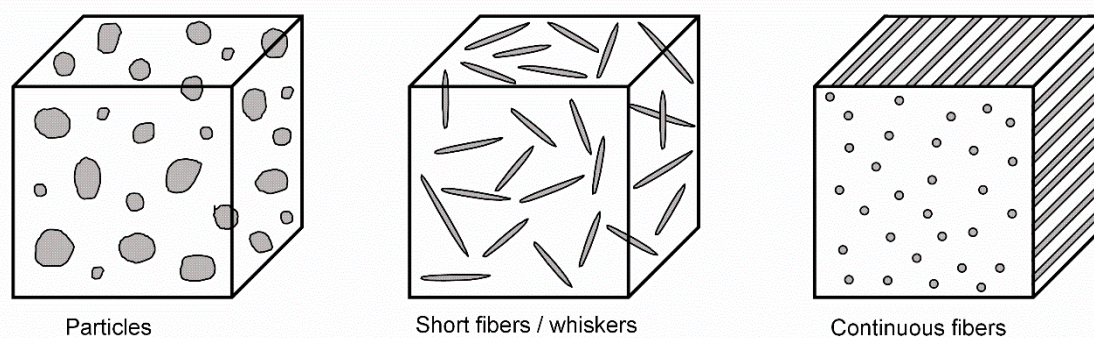
Figure 2.1 *Schematic presentation of different types of MMCs (after [Cha06, Kai06]).*

MMCs can be divided into continuous and discontinuous reinforced composites (Figure 2.1). The continuous (fiber) reinforced composites have anisotropic properties while discontinuous reinforced, i.e., particle reinforced, short fiber or whiskers reinforced composites, give isotropic properties. The particulate reinforcements exist in different shapes (e.g., spherical, round, irregular, etc.) and sizes and the aspect ratio of whiskers can vary significantly. The properties of the MMCs can be customized according to the applications by changing the volume fraction, shape, size range or aspect ratio, as well as by varying the distribution and arrangement of the reinforcement. The matrix-reinforcement interface and grain size of the matrix also play an important role in determining the properties of MMCs.

The reinforcement selection depends on a number of factors like chemical, physical and mechanical compatibility with the matrix, thermal stability, cost and geometrical properties such as size distribution and shape. Reinforcements normally have lower density and higher strength and Young's modulus in comparison to the matrix material [Cha06, Kai06].

2.1.1 Why MMCs?

Metal matrix composites find widespread engineering applications in aircraft, automotive and electronic industries. For example, lightweight structural materials play a vital role in transport industry [All93]. The development of energy efficient and environment friendly vehicles needs stronger and stiffer lightweight materials with good toughness and deformability [Jay15, Pal12]. Only 10 % weight reduction can enhance vehicle fuel economy up to 5.5 %. For example, the reduction of 110 kg in vehicle weight increases its fuel efficiency approximately by 0.5 km/l [All93] and reduces CO_2 emission by 10 g/km [Hel03]. Alloys of aluminum, magnesium and titanium are of primary importance because of their low density and good machinability. Although aluminum, magnesium and titanium alloys are lighter than conventional automotive materials, the reduced strength of aluminum, the lower workability and poor corrosion resistance of magnesium and the higher cost of titanium limits their applications [Jay15, All93]. Another strong limiting factor is noticeable weakening of the mechanical properties of aluminum and magnesium at temperatures below 473 K [Sur03, Mor01]. Hence, to take full advantage of lightweight metallic materials, their properties need to be improved. An effective option to achieve this objective is to produce metal matrix composites [Jay15].

Polymeric matrix composites are also a prominent candidate for lightweight structural applications but MMCs defeat this group of composites where higher strength and stiffness at elevated service temperatures is desired. Thermal and electrical conductivities, radiation stability and joining characteristics of MMCs are better than polymeric matrix composites [Cha06]. Recyclability of polymeric matrix composites is also a problem [Ral97]. Similarly, MMCs are a better choice than ceramic matrix composites where higher thermal and electrical conductivities, toughness, deformability and plasticity are required. The higher processing temperatures, cost and lower shear strength of ceramic matrix composites are other factors for their limited applications [Hag16, Ral97].

Although MMCs are expensive replacements for the conventional materials, the overall improved performance of the component due to the use of MMCs results in a total cost

reduction [Kai06, Cha06, All93]. However, researchers are focusing to develop the cost effective processing techniques for MMCs to improve their properties and application areas [Yas17, Har98].

2.1.2 *Aluminum matrix composites*

Aluminum matrix composites (AMCs) contain aluminum or its alloys as matrix reinforced with continuous or discontinuous metallic or non-metallic reinforcement [Sur03]. Aluminum based MMCs are extensively investigated and the most widely produced because of their lower density than conventional structural materials, e.g. steels and cast iron, better oxidation resistance and reduced reactivity with common commercial reinforcements than other lightweight structural materials, such as titanium and magnesium [Hag16, Tor03, Mir01]. AMCs provide greater specific strength, improved high temperature properties and stiffness, enhanced abrasion and wear resistance, and controlled coefficient of thermal expansion (CTE) in comparison to the unreinforced corresponding materials. AMCs deliver superior combination of properties in comparison to the pure matrix material just by combining a suitable reinforcement in the appropriate amount that ranges from a few percent to 70 volume %. For example, the addition of 60 vol.% Al_2O_3 continuous fiber increases the modulus of elasticity of aluminum from 70 GPa to 240 GPa and reduces CTE from 24 ppm/K to 7 ppm/K [Sur03]. Similarly AMC with 9 vol.% Si and 20 vol.% SiC offers wear resistance better than grey cast iron [Hag16].

Discontinuously reinforced (whiskers or particles) AMCs are the 69 % of the annual production of MMCs, which is the largest production volume of commercial market by weight [Mir05]. The most common commercial reinforcements are SiC and Al_2O_3 [Mir05]. AMCs reinforced with silicon particles have been used in automotive industry for over 50 years in the form of a natural composite; e.g., hypereutectic aluminum-silicon alloys for their superior strength and wear properties over conventional cast alloys with low silicon content [Col95]. Modern cylinder liners for engine blocks are being manufactured by Honda using Al_2O_3 plus short carbon fiber reinforced AMCs that reduce the weight by 3.5 kg in comparison to the previous gray cast iron cylinder liners. AMCs cylinder liners provide reduced engine friction due to their increased rigidity, high temperature strength and reduced knocking due to enhanced thermal conductivity [Hag16, All93]. Similarly, Toyota has introduced pistons for diesel engines made of aluminum alloy matrix composites reinforced with Al_2O_3 short fibers that can perform at higher temperatures due to its high strength, improved fatigue behavior, reduced

wear, low thermal conductivity and low coefficient of thermal expansion [All93, Col95]. Advanced composite materials corporation (ACMC) is testing an extruded aluminum 2000 series matrix composite reinforced with 15 vol.% SiC whiskers to develop components of main landing gear for aircrafts with improved fatigue life and corrosion resistance [Imm95]. Along with the transport sector, AMCs have been used for decades in non-structural application (e.g., heat sink and hermetic seal materials for electronic circuits, load supporting cores for power transmission wires, sports goods) because of their improved performance, environmental and economic benefits [Hag16].

2.1.3 Magnesium matrix composites

Magnesium is the lightest structural elemental material (1.74 g/cm^3) and magnesium alloys are being used in transport and electronic sector because of their high specific strength, superior castability, good damping capacity and excellent machinability [Cha06, Ye04]. However, the low strength at high temperatures limits its applications to 393 K [Sar17, Cha06, Ye04]. The high temperature mechanical properties of magnesium or its alloys can be improved by producing Mg-based composites. For example, carbon fiber reinforced unidirectional magnesium matrix composites (1.8 g/cm^3) retain good mechanical properties up to 673 K; e.g., bending strength is 1000 MPa. Similarly, extruded Mg-matrix composites reinforced with in-situ Mg$_2$Si show around 200 MPa tensile strength at 573 K and composites prepared by mechanical alloying of magnesium based alloys reinforced with Fe$_3$O$_2$, and MnO$_2$ followed by hot extrusion show 600 MPa proof stress (0.2% offset value) and 300 MPa specific strength [Ye04, Yam02, Mab96]. Mg-Li alloys are attractive lightweight materials due to the very low density (0.534 g/cm^3) of lithium. Near eutectic Mg-Li compositions give some solid solution strengthening but heat treatment based precipitation strengthening is not viable for these alloys [Jay15, Wan06, Eis98]. The incorporation of reinforcements in these alloys can enhance their mechanical properties, thermal stability and thus applications; e.g., the tensile strength and modulus of elasticity of the Mg-14Li-1Al alloy have been increased from 130 to 189 MPa and 34 to 50 GPa respectively by adding 5 wt.% Al$_2$Y, at the cost of 42% reduction in ductility. In addition to pure magnesium matrix composites, the Mg-Al matrix composites have also been under the focus of the researchers for automotive applications but higher production cast, lower thermal conductivity, poor wettability of reinforcement with magnesium based matrix and detrimental matrix-reinforcement interfacial reaction restrict the use of magnesium based matrix composites in comparison to aluminum matrix composites. The potential applications of magnesium based MMCs in transport industry are connecting rods,

disk rotors, gears, gearbox bearings, piston ring grooves, and shift forks [Hag16, Jay15, Wan06, Ye04].

2.2 Particle reinforced MMCs

Particle reinforced MMCs are a class of discontinuously reinforced MMCs in which generally equiaxed particles typically varying from submicron level to 25 micron in diameter, with an aspect ratio of less than 5 are used as reinforcement [Cha06]. Typical ceramic particulate reinforcements are carbides, oxides, nitrides and borides: e.g., SiC, TiC, B_4C, WC, Al_2O_3, AlN, BN, Ti_2B [Cha06, Sur03]. Particle reinforced MMCs are more economical than fiber reinforced MMCs, possess good thermal stability and provides isotropic properties. Conventional metallurgical processing techniques including melting-casting, powder metallurgy, machining and hot forming processes, i.e., rolling, forging and extrusion, can be used to synthesis and shape these composites [Cha06, Kai06, Har98].

Particle reinforced AMCs have a number of applications in transportation and electronic housing sector like bearings, break components (discs, calipers and rotors), cylinder liners, engine blocks, pistons and transmission components: e.g., driveshaft, propshaft [Yas17, Mir05]. Driveshaft made of $6061Al + 20$ vol.% Al_2O_3 with higher specific stiffness relative to steel or aluminum drivehafts enables to make longer shafts with the equivalent diameter, which eliminates the need of two shafted joined by a connector in long vehicles. Particulate AMC (Al-alloy + 25% SiC) was introduced by Toyota and Ford in 1995 for low density brake disks, high thermal conductivity and good clogging resistance in comparison to old cast iron stuff. Similarly Al-Mg reinforced with Al_2O_3 is another promising brake material. Light frames for bicycles with high rigidity and good fatigue resistance are made of Al-alloy + 10% Al_2O_3 or 20% SiC composites [Mir05, All93].

Lockheed aerospace company uses AMC (Al-alloy + 25% SiC particles) housing for on-board electronics in aircrafts which has high specific strength, low density, good electrical conductivity and 65% more stiffness than previous one made by unreinforced 7075 aluminum. SiC particles (20-65%) reinforced aluminum alloy based composite is used to make housing for microelectronic components which is solder-able and Lightweight. The current housing is used for shielding of microwave radar and stray field communication systems due to its electrical conductivity, high thermal conductivity and low coefficient of thermal expansion that provides high dimensional stability [Mir05]. Alcoa (Aluminum Company of America) has produced a series of SiC (12.5 to 20 vol.%) reinforced AMCs with excellent high temperature

properties using 2000, 6000, 7000 and 8000 aluminum alloys as matrix [Imm95]. Particulate AMCs are being used in gas turbine engines in military aircrafts and in helicopters as rotating blade sleeves. Sports equipment like head and shaft of golf club, baseball shaft, skating and horse shoes also contains particulate AMCs [Sur03].

To enhance the commercial importance of particulate MMCs progressive research efforts are required to improve the properties of interest with the minimum processing cost. Beside the cost effective optimization of post- and preprocessing steps, the selection of proper reinforcement type and incorporation of its optimal volume fraction in the matrix is extremely important. Reinforcement and matrix can react to produce detrimental products at the interface that can deteriorate the properties. Many aspects of the particulate MMCs have not been yet thoroughly investigated beyond the basic level like addition of metallic reinforcements in MMCs, controlled inhomogeneous distribution of reinforcement and use of bimodal reinforcement are openings to a new horizon of research [Mir05].

2.3 Matrix-reinforcement interface

Interface in composites is a common boundary between matrix and reinforcement. It creates bond between matrix and reinforcement for load transfer. The properties of an interface are neither similar to the matrix nor to the reinforcement [Jay15]. Across the interface a discontinuity in the properties of the material, like chemical potential, chemical composition, elastic modulus, and CTE can be found [Met16, Jay15]. A difference in chemical potential introduced by the interface in the composite can create inter-diffusion-zones that could be preferential sites for precipitation or segregation [Cha06]. The overall composite system will try to minimize its free energy by introducing the changes in and around the interfacial zone which may involve the migration of grain boundaries, creation of dislocations, nucleation and/or propagation of crack. Ideally, an interface should promote the matrix-reinforcement wetting (intimate contact) and efficient bonding. A good interface protects the reinforcement from further chemical reactions and efficiently helps to transfer the applied load from matrix to reinforcement [Jay15, Cha06]. The following factors influence the quality of interface between matrix and reinforcement;

2.3.1 Wettability

The ability of a liquid to spread on a solid surface is called wettability [Cha06]. In case of MMCs, the wettability is the amount of work required by a melt to immerse the reinforcement. Figure 2.2 shows two different interactions of a liquid droplet with a solid

surface. The term γ stands for interface energy per unit area (also known as specific energy or surface tension [Isr11]) and The subscripts 'sl', 'lv', and 'sv' indicate the solid-liquid, liquid-vapor and solid-liquid interfaces. The angle θ between γ_{sl} and γ_{lv} is called the contact angle of the liquid with the solid and it is the measure of wettability. Perfect wetting is achieved at θ = 0°, while no wetting will occur if θ = 180°. The values of θ within the range of 0° to 180° indicate partial wettability. The contact angle depends on the number of factors, e.g., temperature, quality of the substrate surface, solid-liquid contact duration and occurrence of interfacial reactions [Jay15, Cha06].
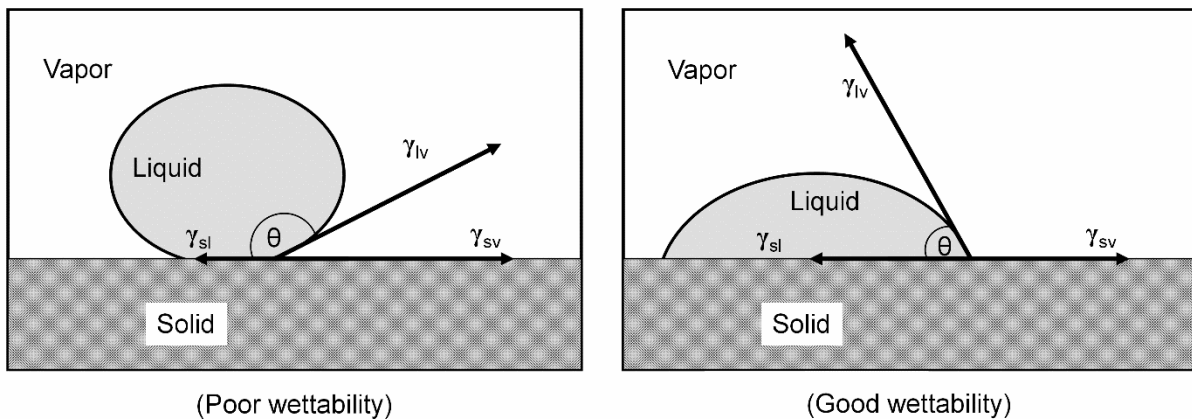

Figure 2.2 *Schematic presentation of the contact angle (θ) between liquid and solid surfaces (after [Jay15, Cha06]).*

Good wettability is an essential prerequisite for good bonding between matrix and reinforcement in the liquid state processing of MMCs but it does not mean that good wettability will always result in a good bonding because bonding depends on several other factors in addition to wettability [Jay15, Sur13a, Mor88]. Most of the ceramic-metal composite systems exhibit poor wettability. Therefore various efforts has been made to enhance the wettability like coating of the reinforcement, modification of matrix alloys and pre-treatment of reinforcements [Del87, Roh86, Kim84, Kri81].

2.3.2 Bonding

The matrix-reinforcement adhesion takes place because of the chemical bonding and/or mechanical interlocking between the surfaces [Cha06]. The chemical potential gradient due to the different compositions of matrix and reinforcement could initiate atomic transport (diffusion) across the interface. The atomic diffusion between matrix and reinforcement may result either in the diffusion bonding by forming solid solutions or in the creation of a compound as a result of a chemical reaction [Met16, Jay15]. The effectiveness of the diffusion

bonding or chemical adhesion depends upon the thickness and nature of the product emerging at the interface. An uncontrolled prolonged chemical reaction at the interface can fully or partially consume the reinforcement which may decrease its ability to bear the load. Therefore, an optimum extent of interfacial reaction is required to achieve the good adhesion with minimum loss in the reinforcement strength [Jay15, Kai06, Tre74].
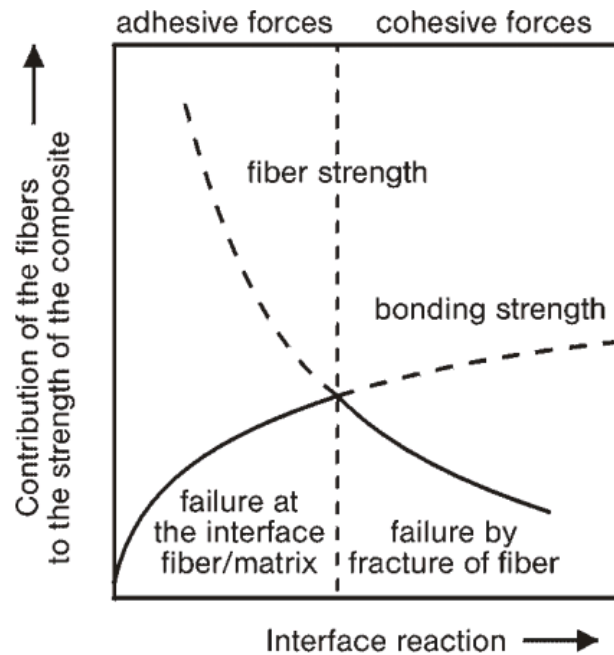

Figure 2.3 *Dependence of the shear strength on the thickness of the interfacial reaction layer in alumina reinforced nickel matrix composites [Tre74].*

Figure 2.3 shows for the alumina-nickel system that by increasing the thickness of the reaction product layer at the interface, the bonding strength increases but the fiber strength decreases [Tre74]. An optimum is achieved when the lines intersect. At this point, the composite shows maximum strength and failure occurs due to mix fracture under shear loading. In case of thinner interfaces, the failure will take place due to the matrix-reinforcement detachment and on the other hand thicker interfaces cause reduction in the reinforcement strength and composites fail due the rupture of the reinforcement. The reaction can also end up with pores or formation of brittle products at the interface, like carbides, intermetallics or oxides, which can change the composite behavior from ductile to brittle by acting as stress concentrators [Cha06].

The mechanical interlocking between two surfaces takes place due the asperities present on them. The increase of surface roughness can enhance the mechanical bonding but surface roughness beyond a critical value may decrease the adherence due to reduced wettability

[Ghu16, Cha96]. To rise the surface roughness, methods like etching, pitting, emery paper grinding and micro-hardness indentation have been employed. [Met16, Cha96, Cha78].
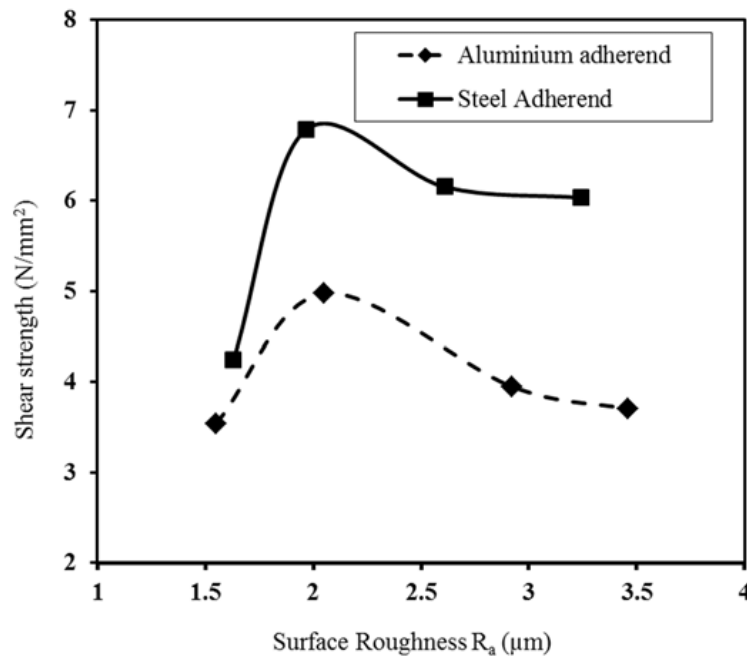

Figure 2.4 *Dependence of shear strength on the surface roughness of aluminum and mild steel adherend joints [Ghu16].*

For example, in case of adhesive bonding of aluminum or mild steel plates using epoxy resin (layered composites), it has been observed that by increasing the surface roughness the shear strength of the joint (composite) increases up to an extent and then it decreases (Figure 2.4). The drop in the shear strength at higher surface roughness values was associated with the poor wettability of the highly rough surfaces due to the formation of higher contact angle with the epoxy resin [Ghu16].

2.3.3 Thermal mismatch stresses

Thermal stresses are another significant element besides the wetting, chemical and mechanical bonding which affects the interfacial bonding. Difference in CTE between metallic matrix and ceramic reinforcement generates these thermal residual stresses at the interface. During cooling of such composites the matrix shrinks faster and more than the reinforcement because of its higher value of CTE and grips the reinforcement firmly. Such gripping has been confirmed alumina reinforced AMCs and W-filament reinforced AMCs [Cha96, Cha78]. Beside gripping of the reinforcement, the differenec in CTE creates a large zone of thermal residual stresses around the interface. If the order of magnitude of thermal mismatch stresses is equal to the yield stress of the matrix then local plastic deformation of the matrix can occur

that leads toward the generation and accumulation of vacancies and dislocations at the interface [Cha06, Kai06]. The presence of the high energy defects in relatively higher amount at the interface in comparison to the matrix speeds up the chemical reaction kinetics and/or nucleation and growth of cracks at the interface by facilitating the atomic and vacancy diffusion at elevated temperatures [Jay15, Cha06]. Thermal mismatch stresses also affect the strengthening process in non-heat treatable alloys and accelerate the precipitation hardening kinetics in heat treatable alloys [Met16, Jay15, Cha06]. Zones of higher dislocation and defect density and their effect on the properties of MMCs have been observed in SiC whiskers and alumina short fibers reinforced AMCs and W-filament reinforced Cu matrix MMC [Dlo93, Ars83, Cha72].

2.4 *Metallic reinforcements*

MMCs are normally reinforced using ceramic reinforcements because of their high values of strength, elastic modulus, hardness, along with thermal stability and low density but during the processing of MMCs two problems may arise beside the wettability [Ye04]. One problem is the reactivity of reinforcement with the matrix because many of reinforcements are not thermodynamically stable with many metallic matrices. The second complication arises from the difference in coefficient of thermal expansion (CTE) between matrix and reinforcement. Top of the list reinforcements are carbides, oxides and carbon e.g., SiC and Al_2O_3. The lightest elemental structural material magnesium reacts with all of them. Although aluminum does not show any significant chemical reaction with SiC and Al_2O_3, it reacts with carbon to form carbides. To avoid the detrimental effects of the interfacial reactions on the mechanical properties of MMCs, ceramic reinforcement with coating can be used [Kai06]. Likewise, in case of SiC reinforced AMCs the difference in CTE is 20.2×10^{-6} K^{-1}. During cooling of the MMCs which have a large difference in the CTE values of matrix and reinforcement, a thermal mismatch strain can arise which generates the local plastic deformation in the metallic matrix around the reinforcement and repeated thermal cycles can induce microstructural damages in the MMCs that lead to the poor mechanical properties [Kai06, Mor01, Ral97].

The effectiveness of the reinforcement in MMCs depends upon the load transfer ability from matrix to reinforcement, which requires a strong interface between these phases. In some systems, the matrix-reinforcement adhesion is too poor to develop MMCs, while in other cases unnecessary extended interfacial reaction due to fast kinetics and thermodynamic instabilities can generate a brittle layer around the reinforcement that can damage the properties of MMCs

[Har98]. Therefore, all combinations of matrix-reinforcements are not possible to process. Problems associated with the ceramic reinforcements like low compatibility with the lightweight metallic matrices, low ductility, low wettability and high cost have restricted their application potential. Reduction in the ductility of ceramic reinforced MMCs is due to the brittle nature of the reinforcement, interfacial reaction product and quality of the interface [Jay15, Ye04, Eus99]. Additional disadvantages of the ceramic reinforced MMCs include their low toughness, poor recyclability of metallic matrix by conventional methods and high wear of tooling during machining of the composites [Tan04, Tan03, All93]. Thus, a great demand to explore the alternative cost-effective reinforcements has shifted the focus of MMCs research towards metallic reinforcements [Jay15, Tan04]. Beside the use of elemental metallic powders of micron and submicron size [Fat15, Xue15, Gu12, Gu09, Has02b, Has02c, Has02d] the bulk metallic glasses [Alj12, Scu09a, Scu08, Yu06, Lee04], quasi-crystals [Tsa16, Ali14, Ali12a, Lap10a, Lap10b, Tan03], complex metallic alloys and various intermetallics [Scu09b, Urb04, Var02] have been used as reinforcements to develop novel MMCs.

Although the metallic reinforcements are usually heavier than ceramic reinforcements, they can lead to the formation of a stronger matrix-reinforcement interface because of their higher ductility, improved compatibility and wettability with the metallic matrix, lesser difference of CTE between the matrix and reinforcement [Yu06, Tan04, Tjo00]. Other advantages of the metallic particulate MMCs (PMMCs) are the economical production, recyclability and machinability in comparison to the ceramic reinforced PMMCs [Dav93]. Increased strengthening effect of metallic reinforcements due to better quality of the interface of the PMMCs containing metallic reinforcements in comparison to the ceramic reinforced PMMCs provide compensation for the composite weight increment [Tan04, Ye04, Tjo00].

2.4.1 Intermetallics

An intermetallic compound is a solid phase composed of two or more metallic elements present in a fixed or a narrow range of composition. Intermetallics may possess an ordered crystal structure which can differ from the parent metals [Cin13, Cot99]. Intermetallics are generally hard and show high strength and creep resistance because of their highly complex and stable crystal structure. Some of them can retain the ordered crystal structure until their melting point, for example Ni-based super alloys [Ohr02, Sto00, Mur93, Liu90]. The potential application areas for intermetallics include magnetic materials, parts for heat treatment

furnaces and aqueous/molten salt baths, hydrogen storage materials, gas turbine parts, and corrosion resistant materials [Sto00].

Figure 2.5 *Schematic representation of 2-D simple cubic lattice containing a super-lattice dislocation (paired dislocations) and two antiphase boundaries [Sto66].*

Ordered intermetallics represent different mechanical behavior than other metallic materials due to their unusual dislocation structure in the ordered lattice [Liu93]. Ordered intermetallics deform through the glide of super-lattice or partial dislocations (see Figure 2.5). The first dislocation introduces a layer of wrong bonding (antiphase domain layer) in a lattice of AB composition, while the following dislocation reinstates the atomic order. The yield strength of many ordered intermetallics (e.g., Ni- and Fe-aluminides) increases by increasing the temperature rather than decreasing and it is called anomalous yielding of intermetallics [Liu98, Liu93]. This anomaly arises due to the low mobility of the super-lattice dislocations in

the lattice. At higher temperatures the slip planes, on which the dislocation movement takes place, change from {111} to {010} by thermal activation and the dislocations mobility decreases accordingly, which means strain hardening at higher temperatures. The brittle behavior of intermetallics can be ascribed to the inadequate amount of deformation modes, low surface energy, week grain boundaries, environmental embrittlement, low dislocation movement and generation and planar slip [McK11, Liu90, Sto66]. Intermetallics have both structural and non-structural applications because of the attractive combination of physical and mechanical properties, e.g. shape memory alloys, dental amalgams, high temperature structural parts and coatings, magnetic and hydrogen storage materials, superconductors [Ohr02, Sto00, Mur93, Liu90].

Ordered aluminide intermetallics are particularly attractive for the development of high temperature service materials (573 to 1773 K) because the critical ordering temperature of these intermetallics is close to the melting temperature and their inherent density is low due to the high percentage of aluminum. Iron, nickel, niobium, cobalt and titanium based aluminides offer good specific strength (strength/mass) and resistance to oxidation, sulfidation, carburizing and corrosion at higher temperatures (around 1273 K) and in aggressive chemical environment [Cin13, Dee96, Liu90]. The alloying elements such as B, Cr, Si and Zr have been added to produce aluminides with increased deformability [Gsc03]. Grain size refinement by fast cooling or mechanical milling have also been used to improve the deformability and fracture toughness [Gsc03]. Excellent high temperature properties of intermetallics together with the lower density and elastic modulus comparable to conventional ceramics reinforcements make them suitable reinforcement materials for MMCs [Cha13, Ye04, Var02]. Generally, aluminide reinforcements increase the wear and corrosion resistance of the lightweight MMCs along with the improvement in the mechanical properties [Bai13, Cha12, Lie97].

Quasi crystals are another group of intermetallics. The interesting mechanical and physical properties of quasicrystals (QCs), such as high hardness, yield strength and elastic modulus, along with the higher compatibility with the matrix (i.e., reduced difference of CTE) and good interfacial bonding in comparison to conventional ceramic reinforcements, make them attractive reinforcements for composites [Hut04, Gia99, Urb97]. Recent reports indicate enhancement in the mechanical properties of aluminum matrix composites due to the use of QC as reinforcement [Tsa16, Ali14, Ali12a, Lap10b, El08, Tan03].

2.4.1.1 Synthesis of intermetallics

Usually, casting techniques are used to prepare the intermetallic compounds. Pure metals in pre-calculated weighted ratios are melted using arc or induction melting in an argon atmosphere or under vacuum to cast a button or an ingot [Sto98, Bak95]. Several cycles of re-melting followed by annealing are applied on the cast material to homogenize the composition. In some cases air induction melting with subsequent electroslag remelting also has been practiced successfully [Cha98a, Sto98, Bak95]. Mechanical alloying is an alternative approach to generate the intermetallic compounds from the pre-weighted mixture of elemental powders [Bas15, Dee96]. In this method powders are mechanically alloyed for long intervals of time using high energy ball mills. Initial milling leads to the formation of alloys, which may be followed by the amorphization of the alloys. Annealing or prolonged milling of amorphous phase creates the intermetallic phase [Bas15, Far15, Can14, Mha11, Boe88]. Another way of producing intermetallic powders is exothermic reaction between elemental powders e.g., exothermic reaction between aluminum and iron powders can synthesis iron-aluminides. Additionally, aluminides can be obtained by atomization and the aluminide powders can then be consolidated into the desired bulk products [Sto98, Liu97, Sik96]. Otherwise, reactive sintering during hot consolidation i.e., hot pressing or hot extrusion, of the pre-weighted and pre-mixed/alloyed elemental powders in a ball mill can be used to synthesis the intermetallics [Mas16, Kon15, Sin15, Mha13, Kra10].

2.4.1.2 Iron aluminides

Iron aluminides are low cost intermetallics because of the ease of processing and abundance of iron and aluminum. Fe-Al intermetallics have been investigated for high temperature applications for the possibility to substitute superalloys and stainless steel in some areas [Sto98, Liu97, Liu93]. Iron-aluminides are 30 % lighter than conventional structural materials that are commercially used for high temperature applications, i.e., stainless steel or nickel based super-alloys, because of the high concentration of aluminum [Egg00]. High percentage of aluminum creates a continuous and protective layer of alumina on the surface when exposed to air. Iron aluminides possess high resistance to creep, wear, oxidation and corrosion up to 873 K along with high temperature strength. They offer high electrical resistivity which rises with temperature [Sto00, Dee96].

Among all other iron aluminides, FeAl and Fe₃Al intermetallics have been examined exclusively for the crystal structure, deformation, fracture and potential application due to good strength, low cost, low density, ease of fabrication and corrosion and wear resistance [Egg00,

Sto98]. The Al-Fe phase diagram in in Figure 2.6 displays the existence several aluminides. FeAl exists in B2 (cP2) crystal lattice type (Figure 2.7) and contains ~12.8 to ~37 wt.% aluminum while Fe_3Al has ~13 to ~20 wt.% aluminum and exhibits the $D0_3$ (cF16) lattice structure at low temperatures which transforms during heating into B2 (cP2) at 723 K. Other prominent phases are: $FeAl_2$ (~48 to ~49.4 wt.% Al), orthorhombic Fe_2Al_5 (oC24 crystal structure [Bur94]) which contains ~53 to ~57 wt.% Al and monoclinic $FeAl_3$ (mostly referred as $Al_{13}Fe_4$ [Lee03b]), which is a complex metallic alloy with 102 atoms in a giant unit cell (mC102 [Gri94]) existing from ~58.5 to ~61.3 wt.% aluminum. By increasing the aluminum concentration a rise in the transition temperature from $D0_3$ to B2 lattice for the Fe_3Al phase is observed, while the FeAl phase is stable up to 1373 K [Cin13, Dee96, Liu93, Bak92]. Potential applications for iron-aluminides are in heat treatment baths (liquid/molten) and furnaces (trays, fixtures, rails and immersion heaters), automotive industry (porous filters, piston valves and exhaust system), porous filters in power generation plants and catalytic refineries, radiant pipes in heat exchangers and as substrate in catalytic conversion vessels [Cin13, Hen11, Sto98, Liu90].
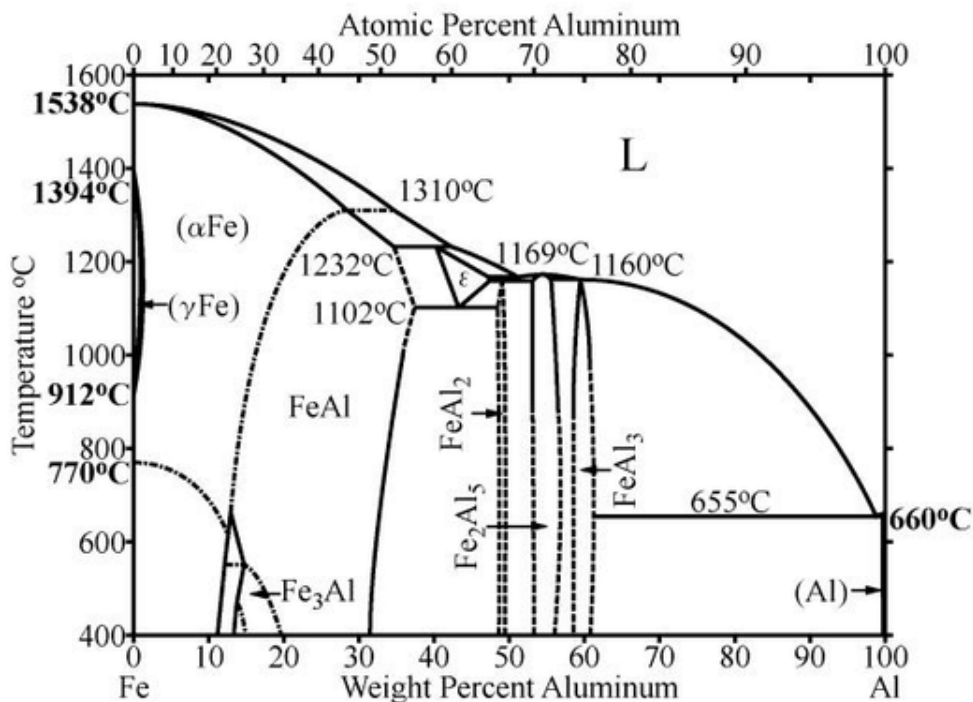

Figure 2.6 *Fe-Al equilibrium phase diagram [Bak92].*

Despite of the excellent high temperature mechanical properties in corrosive environment, the brittle behavior, low fracture resistance and poor ductility limits the use of iron-aluminides as industrial engineering materials [Liu93]. Further enhancement in the

mechanical properties has been attained by the addition of different elements, i.e., Cr, Nb, Hf, Cu, Mo, B, Ta, Ti, Mn, Zr, V [Cin13, McK11, Dee96], to enhance the precipitation or solid solution strengthening effect and ambient temperature ductility. The improvement in high temperature properties is achieved at the cost of reduction in room temperature elongation [Sen16, Cin13, Zam13, Hen11, McK11, Dee96]. Enhancement in the room temperature deformability of intermetallics matrix composites has been achieved by adding soft metals as second phase with upgraded mechanical properties [Kra16, Pit11]. An improvement in the creep resistance have been observed due the dispersion of oxide particles formed during milling process or precipitation of other inclusions [Mor04, Bac03, Var01].
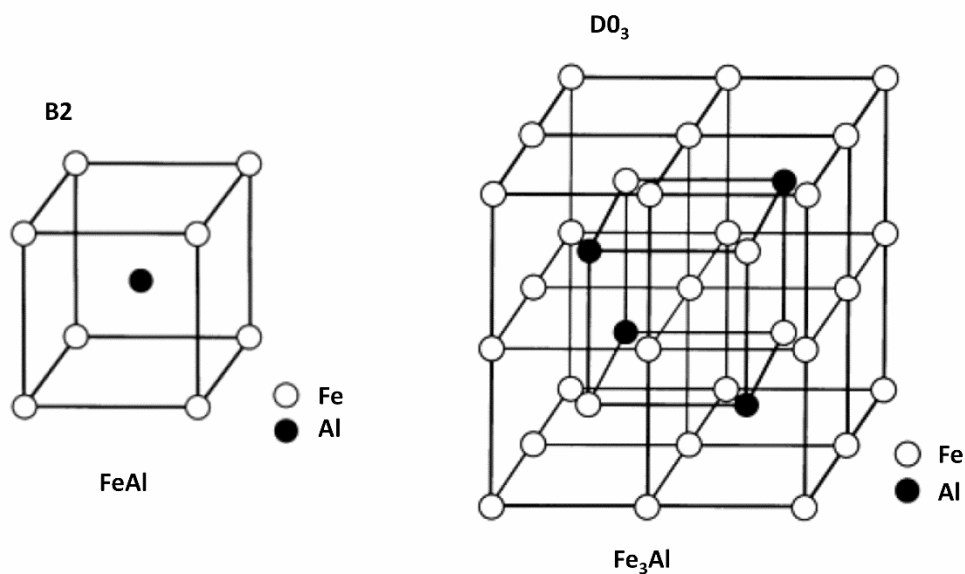

Figure 2.7 *Crystal structures of iron aluminides: FeAl and Fe₃Al [Liu93].*

Beside the composition tailoring by elements addition, grain refinement and the introduction of soft phases in the intermetallic matrix to increase the room temperature ductility of intermetallics, another way to improve the ductility of these materials is the development of intermetallic reinforced lightweight MMCs, which retain inherent ductility from the soft metallic matrix and offer improved high temperature mechanical properties induced by the intermetallic reinforcement [Dub11]. In-situ synthesis of the iron aluminide reinforcements in AMCs has been extensively investigated either by reactive stir casting or by powder metallurgical processing route (P/M processing). Research results indicate the coexistence of $Al_{13}Fe_4$ and Al_5Fe_2 intermetallic phases mostly in core-shell type structures due to the reaction between aluminum and iron at relatively high processing temperatures regardless of processing technique used [Kho15b, Cha13, Lee08, Kal02], while low percentages of iron addition in

aluminum and longer processing time at higher temperature lead only to the formation of $Al_{13}Fe_4$ in the aluminum matrix [Fat15, Gu12, Sto03]. In some cases, the formation of Al_5Fe_2 shells alone around the Fe particles has also been reported even for high processing temperatures and long processing time [Xue15, Wan14]. A series of uniformly dispersed iron aluminides accompanied by alumina particles in AMCs have been produced by the reduction of Fe_2O_3 with aluminum [Dad12, Roy06] by P/M processing and by adding Fe particles in molten aluminum [Lee03a]. AMCs reinforced by ex-situ addition of $Al_{13}Fe_4$ particles using P/M processing route have been investigated for high temperature shear behavior plus strength and ductility using shear punch method [Nem16a] and for hardness, wear, and friction properties as well [Nem16b]. Fe_3Al ex-situ-reinforced AMCs have been synthesized to check the hardness and wear properties [Pan15]. All these works indicate the improvement in mechanical, wear, friction and some functional properties of the aluminum matrix but at the cost of loss in deformability.

2.4.1.3 *Magnesium aluminides*

Mg-Al intermetallics are hard and brittle like other aluminides and considered as reinforcing materials for aluminum and magnesium because of low density, low cost and processing ease. The β-Al_3Mg_2 phase is stable from 38.5 to 40.3 at.% of Mg (Figure 2.8) and arranges 1168 atoms in a huge complex unit cell (cF1168) [Urb04, Bak92, Sam65. The β-phase is a low density (2.25 g/cm^3) complex metallic alloy which offers high temperature strength i.e. ~300 MPa at 573 K [Ste07, Urb04, Gie69]. γ-$Al_{12}Mg_{17}$ phase can be found from 45 to 60.5 at.% Mg at 723 K. The stability range for the γ-phase shrinks with the decrease of temperature and finally at room temperature it is only stable at 60 at.% Mg. This phase contains 58 atoms in its complex cubic unit cell (cI58). $Al_{12}Mg_{17}$ is a low density (2.07 g/cm^3) intermetallic which shows high strength (325 MPa), hardness and corrosion resistance with poor ductility at temperature lower than 523 K [Zol15, Hua12b]. Both β and γ-phases are also designated as complex metallic alloys (CMA) due to the giant complex crystal structure [Zol15, Hua12b, Rag11, Bak92].

Low cost, low density and promising mechanical properties suggest the use of magnesium aluminides as reinforcement materials in metal matrix composites. Therefore, both in-situ and ex-situ incorporation of magnesium aluminide reinforcements have been used to strengthen the aluminum and magnesium matrices. Top of the list is P/M processing technique which can distribute the reinforcement particles uniformly throughout matrix and control the microstructural features due to flexible processing parameters. Different volume fractions of

aluminum powder have been milled with pure magnesium powder followed by hot pressing to synthesize $Al_{12}Mg_{17}$ reinforced Mg-matrix. In-situ creation of $Al_{12}Mg_{17}$ phase have been observed either during milling [Mal16, Cha14, Chu06] or later during consolidation [Par18]. Together with the $Al_{12}Mg_{17}$ phase, the formation of other phases, such as MgO during milling [Cha14] or consolidation [Par18], $MgAl_2O_4$ [Mal16, Chu06], Al_3Mg_2, and Al_2O_3 [Par18], have been reported. The synthesis of finely dispersed aluminides with or without oxides can enhance the mechanical properties at the cost of the reduction in deformability. Extended milling results in the creation of nano-size reinforcing particles and ultra-fine grain matrix which enhances the deformability of composite and vanishes the strain hardening effect [Mal16, Chu06]. In another study, strengthening of AMC rods at the expenses of reduction in the ductility has been noticed due to the creation of Al_3Mg_2 and $Al_{12}Mg_{17}$ intermetallics [Sko14]. Ex-situ addition of Al_3Mg_2 intermetallic (CMA) reinforcement to strengthen the aluminum matrix have been used. Improvement in mechanical and wear properties has been achieved but reduction in the deformability was the side effect [Zol13, Scu09b]. Little has been reported about the co-creation of magnesium aluminides in the form of core-shell structure and its effect on the mechanical properties of the composites with respect to the percentages of different phases present in Al-Mg composites.
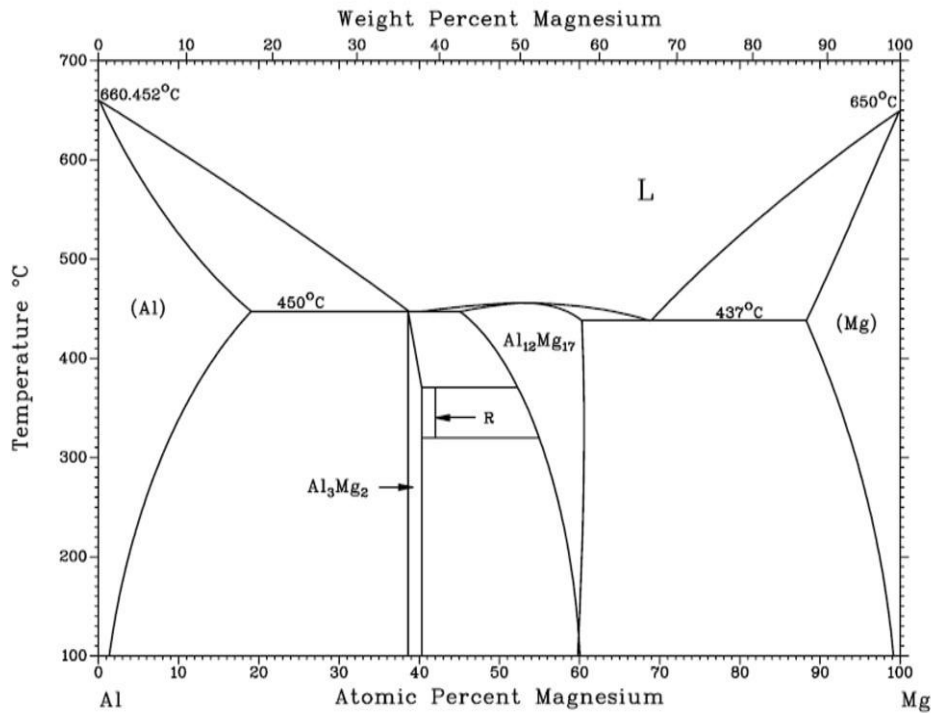

Figure 2.8 *Al-Mg equilibrium phase diagram [Bak92]*

2.5 Strengthening in particle reinforced MMCs

The addition of a hard reinforcement in the soft metallic matrix increases the strength of MMCs in comparison to the unreinforced material. The strength of the composite increases by increasing the volume fraction of the reinforcement and as well as by decreasing the size of the reinforcement particles [Val00, Ram96]. The strengthening mechanism in particulate MMCs (PMMCs) can be categories into direct and indirect strengthening effects. Direct strengthening explains the transfer of applied load from soft matrix to hard and strong reinforcement which shares the stress to strengthen the composite [Cha01, Dav93]. The indirect strengthening is related to the microstructural variations that arise in the matrix due to the addition of reinforcement. Indirect strengthening effects include, dislocation nucleation and multiplication, reinforcement and matrix ligament size reduction and Orowan strengthening [Cha98b, Kra93, Ars88, Vog86]. During processing of MMCs or under service conditions, the difference between the properties (like coefficient of thermal expansion and/or elastic modulus) of the matrix and reinforcement generates dislocations at the interface which improves the strength of PMMCs [Cha01, Cha98b, Vog86]. Microstructural refinement based enhancement in the composite strength is associated to the increment in dislocation movement barriers, for example grain boundaries area, closely spaced and uniformly dispersed submicron particles, matrix-reinforcement interfaces etc. [Cal12, Scu09b].

In addition to the conventional approach for the strengthening of PMMCs, the controlled chemical reaction between matrix and reinforcement and protracted ball milling can be used to introduce the phase transformations and microstructural changes that further increase the strength of PMMCs significantly [Ken14, Sur13b, Kai06, Tan03].

2.5.1 Load transfer strengthening

A composite material under loading condition distributes the applied stress to its matrix and reinforcement. The rule of mixture (RoM) is the simplest method to estimate the strength of composites [Kim00] either using iso-strain conditions [Voi89], where the matrix and reinforcement experience the equal strain under applied load, or iso-stress condition [Reu29], where the matrix and reinforcement face the equal stress. Iso-stress and iso-strain conditions for fiber reinforced composites are shown in Figure 2.9. The Equation 2.1 and 2.2 are widely used to estimate the yield strength of composites under iso-strain (upper-bound) and iso-stress (lower-bound) condition respectively:

$$\sigma_{yc} = V_m\sigma_{ym} + V_r\sigma_{yr} \qquad (Equation\ 2.1)$$

$$\sigma_{yc} = \left(\frac{V_m}{\sigma_{ym}} + \frac{V_r}{\sigma_{yr}} \right)^{-1} \qquad (Equation\ 2.2)$$

Here σ_y stands for the yield strength, *'V'* for volume fraction and the subscripts *'c'*, *'m'* and *'r'* for composite, matrix and reinforcement, respectively.
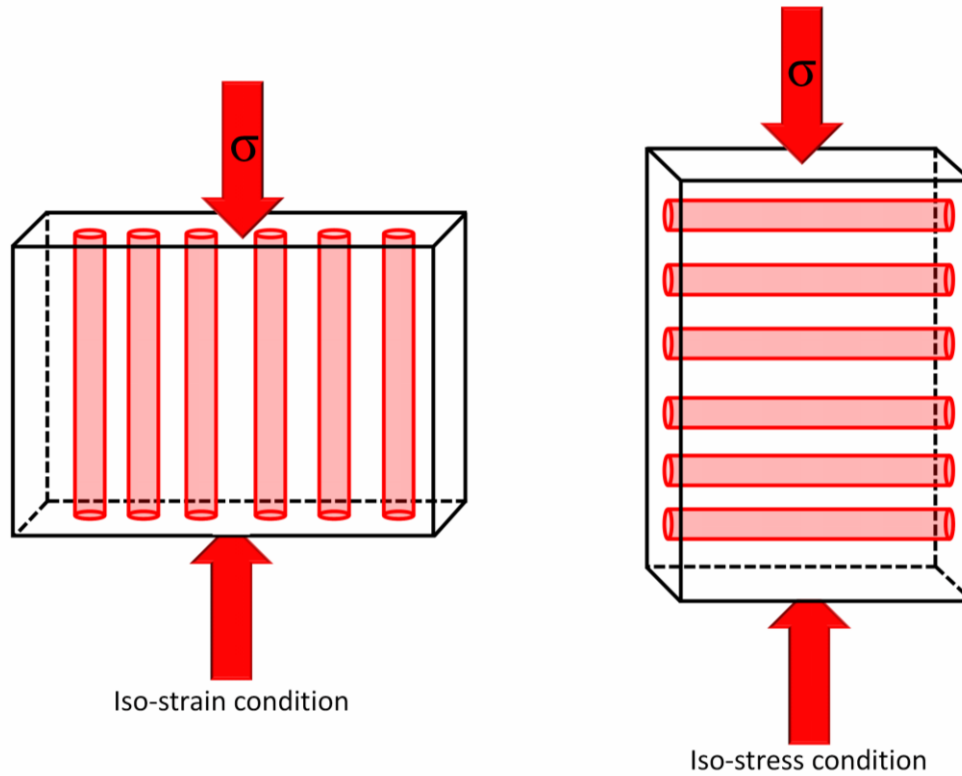

Figure 2.9 *Schematic presentation of iso-strain and iso-stress models (after [Kim00]).*

Particulate MMCs can either follow the iso-stress or is-strain models, depending upon the volume fraction of reinforcement. Usually at high volume fraction of the hard reinforcement, PMMCs data fit to the iso-strain model, while at low reinforcement percentages the composites obey the iso-stress model [Kim0, Kim00]. However, the RoM was found insufficient to estimates the yield strength of PMMCs characterized in several experiment [Ali14, Ali12a, Scu09a, Scu09b] because it does not include the stress fields around the matrix-reinforcement-interface and calculates the composite strength regardless of the reinforcement shape and size [Tay91, Nar86]. An explicit example of the failure of the RoM to predict the yield strength on these grounds for brass matrix composites reinforced with nickel based glassy particles is shown in Figure 2.10. The composites were reinforced using 40 and 60 vol.% of metallic glass particles [Kim12]. One set of the composites prepared by ball milling of the

powder mixtures and subsequently consolidated, while the other set of composites with the same compositions synthesized from powders blended manually. The yield strength data for the ball milled composites (black squares) follow the iso-strain model (dashed line) while for blended composites data (black circles) obey the iso-stress model (dotted line), which indicates the inadequacy of the RoM in prediction of the yield strength of particle reinforced composites [Kim12].
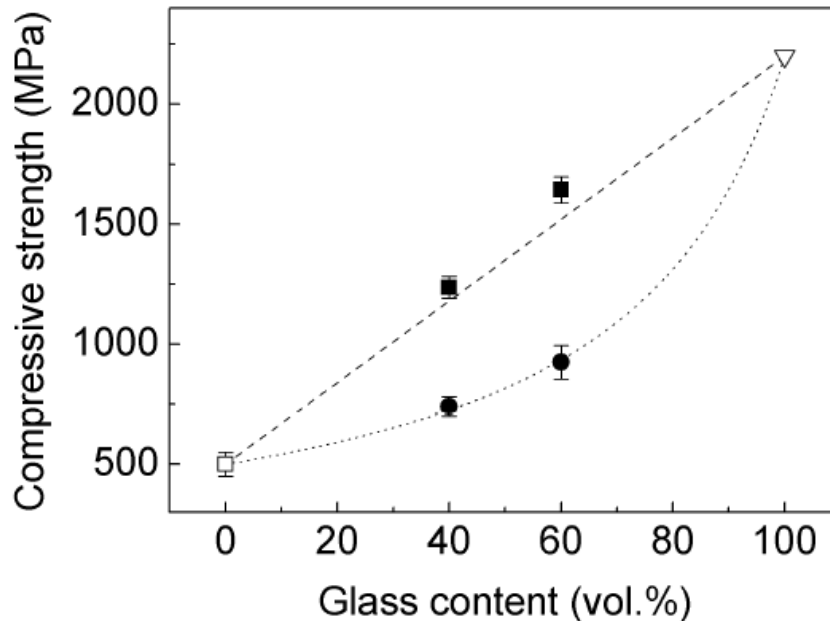

Figure 2.10 *Compressive strength of the nickel based glassy particles reinforced brass matrix composites as a function of reinforcement volume fraction [Kim12].*

The shear log model is an alternative choice to model the yield strength of the composites, which does not include the volume percent of the reinforcement only but also considers the effect of local stress fields in and around the matrix-reinforcement-interface during load transfer from matrix to reinforcement via shear stress [Tay91]. Initially, the shear log model was introduced to calculate the strength of the long-fiber reinforced composites. It considers the reinforcement volume fraction together with the load transfer and stress field contributions along the length *'l'* of the reinforcing fiber (see Figure 2.11) to calculate the composite strength [Cox52]. Afterwards, it was modified to calculate the yield strength of short-fiber reinforced composites. The modification was made to include the additional strengthening arising from both end faces (circular faces with diameter *'d'*) of the short fiber (see Figure 2.11) [Tay91, Nar86].

On the basis of the modified shear-lag model, the following equation can be used to predict the theoretical yield strength (σ_{yc}) of PMMCs. Equation 2.3 takes into account the transfer of load (under applied stress) from soft matrix to hard reinforcing particles rather than to fibrous reinforcement, where σ_{ym} represents the yield strength of un-reinforced matrix, the volume fraction of the particulate reinforcement and matrix are V_p and V_m, respectively, and the particle aspect ratio and shape factor is represented by S [Jay15, Nar87, Nar86].
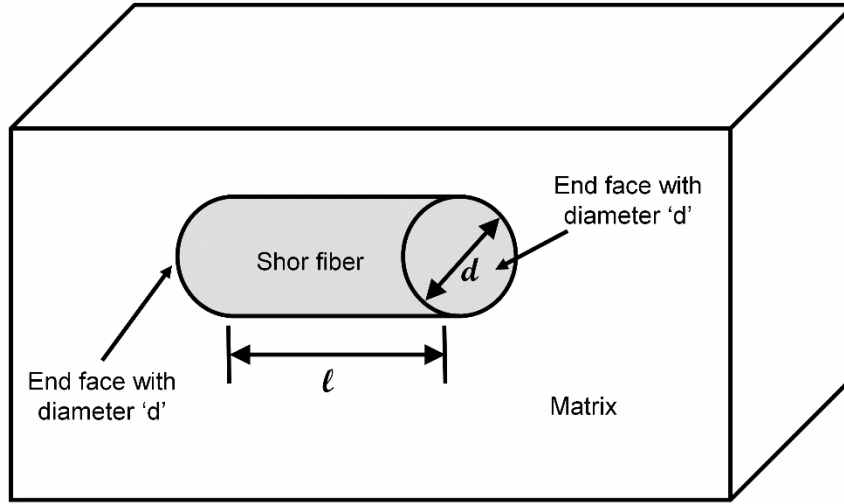

Figure 2.11 *Schematic description of a short fiber (reinforcement) in a matrix (after [Tay91]).*

$$\sigma_{yc} = \sigma_{ym}\{[V_p(1 + S/2)] + V_m\} \qquad (Equation\ 2.3)$$

The Equation 2.3 can be simplified and re-written as Equation 2.4 if '$V_pS/2$' is replaced by f_l which is designated as reinforcement factor associated to the load transfer effect [Ali12a, Scu09b, Ram96].

$$\sigma_{yc} = \sigma_{ym}(1 + f_l) \qquad (Equation\ 2.4)$$

The modified shear lag model underestimates the strength of particulate metal matrix composites because it ignores the indirect strengthening effects such as dislocation strengthening, matrix grain size and reinforcement particle size refinements which may take place during the composite processing [Tan04, Ram96, Gup95]. Another reason for the poor estimation of the strength of PMMC is the reduced aspect ratio of particulate reinforcement in comparison to the fibrous one. The length of the matrix-reinforcement interface decreases with the reduction in reinforcement aspect ratio, which limits the load transfer in terms of shear stress at the interface. Particulate reinforcement creates a three dimensional state of stress at the interface which is a deviation from the assumption of shear lag model [Tay91].

2.5.2 *Dislocation strengthening*

The addition of the reinforcement in the matrix enhances the dislocation density which is a major factor for the increment of the composite strength. Dislocation based strengthening models propose that the reinforcement size is mainly responsible for the enhancement of the composite strength, while the volume fraction has a little effect [Shi92, Ars91, Ars86, Vog86]. The increment in the yield strength of composites generated by the dislocation strengthening ($\Delta\sigma_{dis}$) can be attributed to the accumulative effect of Orowan strengthening ($\Delta\sigma_{or}$), thermal expansion mismatch strengthening ($\Delta\sigma_{th}$) and plastic deformation mismatch strengthening, also known as geometrically necessary dislocation strengthening ($\Delta\sigma_{geo}$) [Jay15, Hum88].

$$\Delta\sigma_{dis} = \sqrt{(\Delta\sigma_{or})^2 + (\Delta\sigma_{th})^2 + \left(\Delta\sigma_{geo}\right)^2} \qquad (Equation\ 2.5)$$

The Orowan strengthening arises due to the interaction of moving dislocations with closely spaced hard reinforcing particles. The non-shear-able hard reinforcement particles pin the moving dislocations and generates the Orowan dislocation loops by bowing the dislocations around them under an applied load. Uniformly dispersed reinforcement of less than 5 micron particle size (particularly nano size reinforcement) considerably rises to the strength of the composite [Jay15, Zha08, Tan04, Gup95, Ars86]. The Orowan strengthening contribution can be written as [Mil91]

$$\Delta\sigma_{or} = \varphi\,\frac{\mu_m b_m}{L} \qquad (Equation\ 2.6)$$

where

$$L = D\left(\frac{\pi}{6V_p}\right)^{1/3} \qquad (Equation\ 2.7)$$

Here, φ is a constant of the order of 2, μ_m is the shear modulus of the matrix, b_m represents the matrix Burger vector, L is the interparticle spacing, D and V_p are the diameter and volume fraction of the reinforcing particles.

The difference between the CTE of the matrix and reinforcement generates thermal stresses during processing, which introduces dislocations at the matrix-reinforcement interface. The stress contribution associated to these dislocations is named as thermal expansion mismatch strengthening and can be written as [Ars91, Ars86, Han77]

$$\Delta\sigma_{th} = \eta\mu_m b_m\sqrt{\rho} \qquad (Equation\ 2.8)$$

where

$$\rho = \frac{12\Delta\alpha\Delta T V_p}{b_m D V_m} \qquad (Equation\ 2.9)$$

Here, η is a constant of the order of 1, ρ is the dislocation density, $\Delta\alpha$ is the difference between the CTE of matrix and reinforcement and ΔT is the difference between processing and room temperature. The thermal mismatch strengthening corresponds to the major portion of the total increment in the composite strengthening observed experimentally [Ars91, Ars88, Ars86] but it does not include the strengthening effect caused by the interface quality due to the presence of oxide layers on reinforcement [And01].

The use of manipulative or forming processes during processing of the composites causes plastic deformation in the composites. Moreover, although the processing or service load is well below the plastic limit of both matrix and reinforcement, even then localized plastic deformation at nano or micro level can occur [Tan04, Bro76]. The plastic flow behavior of reinforcement and matrix is usually different because of the difference between elastic moduli of reinforcement and matrix. Such strain-incompatibility generates the extra dislocations at and around the matrix-reinforcement interface to accommodate the non-uniform plastic deformation of reinforcement and matrix [Jay15, Llo94, Bro76]. The creation of extra dislocations can increase the amount of high-angle grain boundaries in the matrix and thus contribute in the strengthening of the composite [Ali12b, Ali10]. The share of the work hardening in the composite due to plastic deformation mismatch or strain misfit strengthening can be expressed as in Equation 2.10, where β is a geometrical factor of ~0.4 and ε_m represents the plastic strain of the matrix [Bro76]

$$\Delta\sigma_{geo} = \beta\mu_m\sqrt{(V_p\varepsilon_m b_m)/D} \qquad (Equation\ 2.10)$$

Thus, the strength of the composites using the dislocation strengthening model can be estimated using Equation 2.11 [Hum88], which can be further simplified into Equation 2.12 by substituting $\Delta\sigma_{dis}/\sigma_{ym}$ by f_d.

$$\sigma_{yc} = \sigma_{ym} + \Delta\sigma_{dis} \qquad (Equation\ 2.11)$$

$$\sigma_{yc} = \sigma_{ym}(1 + f_d) \qquad (Equation\ 2.12)$$

The creation of additional dislocations during processing further strengthen the composites, which is called indirect strengthening [Ars86, Cha72]. Indirect strengthening is

directly related to the matrix-reinforcement interfaces. Therefore, an increase of the reinforcement volume fraction and reduction of the reinforcement particle size enhances the indirect strengthening due to the increment in interfacial areas [Das14b, Son10, Ram96, Vog86]. The dislocation strengthening model is unable to estimate the strength of composites correctly if the particle size and/or the type of reinforcement is changed [Tan04, And01]. The combined effects of load bearing and dislocation strengthening mechanisms, both by addition and multiplication of the individual effects have been proposed to calculate the strength of composites [Zha08]. Equation 2.13 performs well for low volume fractions of reinforcement but for high volume fractions the predicted values of the composite strength are lower than the ones experimentally measured [Scu09b, Tan04, Ram96]. This indicates that beside the combined multiplicative effect of load bearing and dislocation strengthening as shown below [Ram96], another strengthening mechanism is also active in particulate MMCs [Scu09b]

$$\sigma_{yc} = \sigma_{ym}(1 + f_l)(1 + f_d) \qquad (Equation\ 2.13)$$

2.5.3 Microstructural refinement strengthening

Grain refinement of the pure metals and alloys increases the number of grain boundaries. The grain boundary hinder the dislocation movement and thus increases the yield strength. The Hall-Petch relation explains that the increase in the yield strength of materials due to grain refinement is inversely proportional to the average grain size (diameter) of the material [Cal12, Hal51]. Similarly, matrix grain size and reinforcement particle size refinements both increase the strength of MMCs [Che16, Bal15, Dub11, Hes06, Sto03]. The addition of high volume fractions of reinforcement can separate the matrix into discrete regions. The size of such matrix regions decreases with the increase of reinforcement volume fraction or by decreasing the reinforcement size at the same volume fraction. The size of such matrix segments (known as matrix ligament size, λ) can shrink up to micron level for high volume fractions of reinforcements [Scu09b]. The reduction of the matrix ligament size increases the strength of particulate MMCs [Bal15, Cha14, Cha12, Kim12]. The effect of the matrix ligament refinement is similar to the matrix grain size refinement (Hall-Petch behavior [Hal51]). The matrix grain size refinement increases the density of grain boundary areas, while the reduction of λ enhances the matrix-reinforcement interface area and both can impede the dislocation motion effectively [Scu09b, Hir96, Hal51]. The equation for the strength increase due to matrix ligament size refinement can be written as [Scu09b]

$$\Delta\sigma_s = k/\sqrt{\lambda} \qquad (Equation\ 2.14)$$

where k is a strengthening constant. The strengthening effect of the matrix ligament size refinement can be included in Equation 2.13 to estimate the strength of particulate MMCs as follows

$$\sigma_{yc} = \sigma_{ym}(1 + f_l)(1 + f_d)(1 + f_s) \qquad (Equation\ 2.15)$$

where $f_s = \Delta\sigma_s/\sigma_{ym}$ is a factor related to the strengthening effect of the matrix ligament size refinement [Scu09b]. Equation 2.15 has been successfully used to predict the strength of particulate MMCs and the experimental data are in very good agreement to the model, especially for the high volume fractions of particulate reinforcement [Ali12a, Scu09b].

2.5.4 *Phase transformation strengthening*

Both liquid state and solid state processing techniques for MMCs facilitate the in-situ synthesis of reinforcement [Das14a, Mir01]. In-situ reinforcements are created by establishing a controlled metallurgical reaction between initial components either in the molten or solid states [Sur03, Mir01, Ral97]. In liquid state processing the molten metal reacts with gases and/or solids accompanied by mechanical homogenization; on the other hand, in solid state processing the initial components react either during the mechanical milling/alloying/homogenization stage or later in the high temperature consolidation stage [Ye04, Sur03, Ral97]. Reinforcements produced in-situ are more compatible with the matrix in terms of bonding, are uniformly distributed throughout the matrix and have finer particle size then ex-situ reinforcements, which may also display problems of agglomeration [Ye04]. Solid state atomic diffusion among the initial components of MMCs may lead to the creation of solid solutions or intermetallics. Such in-situ transformations can be used to enhance the mechanical properties of particulate MMCs by producing stronger and more compatible intermetallics at the matrix-reinforcement interface, which in turn may offer improved bonding for the effective load transfer [Yu06, Tan04, Tjo00]. The in-situ reaction not only increases the volume fraction of reinforcement (oxides, intermetallics, etc.), which ultimately participate in the strengthening of MMCs, but also generates volumetric changes in the composite because the densities and crystal structures of the reactants and products are usually different. The volumetric changes associated with the transformation reaction generate strain fields around the reinforcing particles, which may contribute in the enhancement of the composite strength [Gu12, Kai06, Has02a]. Volumetric expansion of the reinforcement during in-situ transformation exert a compressive force at the interface that increases interface bonding and decreases the matrix ligament size (λ) between the reinforcing particles by expanding their

boundaries towards matrix and thus increases the strength of particulate MMCs [Ali14, Tan04, El08]. An incomplete or limited transformation reaction between matrix and reinforcement particles leads to the formation of intermetallic shells around the initial reinforcing particles [Fat15, Xue15, Wan14, Lap10b]. Such reinforcing particles with core-shell-structure are more coherent with the matrix [Ye04], obstruct the crack propagation during loading and thus may provide higher strength and toughness with appreciable compressive deformability [Guo16]. In case of in-situ partial transformation of the reinforcement, Equation 2.15 underestimates the strength values, such as for the incomplete in-situ transformation of quasi-crystalline reinforcement ($Al_{62.5}Cu_{2.5}Fe_{12.5}$) into the Omega phase ($Al_7Cu_2Fe$) in AMCs, for which the model shown in Equation 2.15 shows poor applicability because it does not include the effect of phase-transformation strengthening [Ali14]. Similarly, simple addition of the strengthening factors has been used to predict the strength of AMCs reinforced using core-shell particles but either over- or under-estimation was observed and the deviation of calculated strength values from experimental data were attributed to the reinforcement flocks, structural transformations and presence of nano-size transformed reinforcement particles inside the matrix grain [Kho15a, Lap10a, El08, Lee02].

2.5.5 *Harmonic structural strengthening*

A harmonic structure is a type of bimodal heterogeneous microstructure in which coarse-grain discrete regions are entrapped by a continuous fine-grain phase. Normally, the grain size decreases gradually from the center of discrete coarse-grain region (core) to the surrounding continuous fine-grain phase (shell) [Vaj16a, Hua15, Ame12]. Figure 2.12 displays the schematic illustration of a harmonic structure [Vaj16a].

Severe plastic deformation processes, such as mechanical milling or mechanical alloying, can be used to develop the ultrafine grain metallic materials with homogeneous microstructure [Kai06, Sur01a, Koc97]. Metallic materials with homogenous ultrafine microstructure provide high strength but at the cost of the reduction of ductility [Mir05, Sur03, Upa97]. The inferior ductility not only limits the application of shaping or forming operations but could also lead to in service catastrophic failure of the structural material [Vaj16a, Sur03, Upa97].

Metals and alloys with the heterogeneous distribution of bimodal grain size offer high strength together with adequate plasticity [Dir10, Fan06, Wan02]. Mechanical milling can be used to prepare the fine-grain metallic powders. The fine powders are mixed with un-milled coarse-grained powders and then hot consolidation is used to produce the bulk samples from

the powder mixtures. However, it is difficult to control the distribution of these bimodal powders to get the optimum mechanical properties [Vaj16a, Ame12]. As an alternative way, the low energy ball milling of the coarse-grained powders for extended time followed by hot consolidation could be used to generate materials with harmonic structures [Vaj16ab, Saw14, Fuj06]. Ball milling reduces the grain size at the surface of the powder particles or granules containing coarser grain size in the core. The gradual variation of size from coarser core to finer shell of powder particles / granules of harmonic structure materials leads to improve mechanical properties with considerable plastic deformation in comparison to the conventional homogenous and fine grain materials [Vaj16a, Ame12].
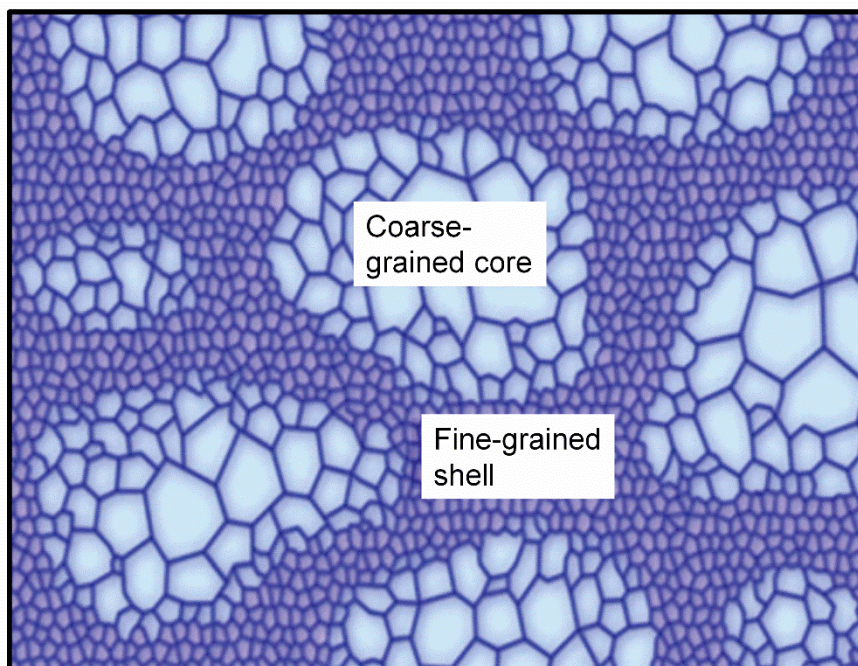

Figure 2.12 *Schematic illustration of harmonic microstructure [Vaj16a].*

Usually, the mechanical properties of PMMCs are improved by increasing the reinforcement volume content or by refining the matrix grains and reinforcement particle size. Uniform dispersion of the reinforcement throughout the matrix, homogeneity of the composite microstructure and quality of the interface plays an important role in the strength enhancement. Such materials are called homogenous microstructures composites [Sur13b, Ger05]. Similar to metals and alloys, the ultrafine grain PMMCs with homogeneous microstructure provide high strength but at the cost of reduction in the ductility [Kai06, Mir05, Sur03, Sur01a, Koc97, Upa97]. The low energy ball milling together with hot pressing can also be used to develop harmonic structure in PMMCs that may offer strength with appreciable ductility.

2.6 Synthesis of particle reinforced MMCs

Metal matrix composites can be synthesized using gaseous, liquid and solid state processing techniques. Gaseous or vapor deposition techniques are usually used to develop either layered composites or to coat fibrous reinforcements in a metallic matrix and then coated fibers are consolidated using diffusion bonding to develop a fibrous MMC [Hag16, Cha06, Kai06]. To make particulate MMCs normally liquid or solid state processes are used. Liquid state processes provide faster production rates than solid state processes and include casting or metal infiltration techniques that are used with or without the application of external pressure [Cha06, Mal97]. Liquid state processing of the MMCs may suffer of the sedimentation and agglomeration of reinforcing particles during the melting, casting and solidification stages because of the density difference between matrix and reinforcement. Inhomogeneous dispersion of the particulates can create reinforcement rich and lean zones in the matrix. The rich zones may have weak bonding due to high concentration of the reinforcement, resulting in poor mechanical properties of the composite. Contrarily, reinforcement lean regions undergo deformation at relatively lower values of applied stress [Ye04, Sur03, Mir01]. To ensure the homogeneous distribution of the reinforcement and improve its wettability with the molten metal, vortex mixing or stir-mixing is used. A sacrificial stirrer that reacts with the molten metal to create and homogenize the in-situ reinforcement can also be used. Too vigorous stirring causes turbulence and consequently entraps gases in the composite while too slow stirring is not sufficient to homogenize the second phase particles in the matrix. The process is not suitable to incorporate submicron particulate reinforcements because of reinforcement agglomeration [Cha06, Ye04, Sur03]. A variant of liquid state processing is spray co-deposition in which a molten metal stream is disintegrated into spray and meanwhile reinforcing powder particles are injected into the spray to produce either bulk MMCs or metal coated reinforcement particles. Hot consolidation of such matrix coated particles is done to create particulate MMCs using another suitable technique such as hot pressing [Cha06, Mal97].

In liquid state processing the molten metal can chemically react with the reinforcement. It is extremely difficult to control the extent of the reaction which can produce detrimental products at the matrix-reinforcement interface [Cha96, Sah91]. In addition, the distribution of the reinforcement and the microstructure of the matrix during solidification is also difficult to control. Solid state processing of MMCs, particularly powder metallurgy is an attractive alternate to tackle such problems. P/M processing includes mixing of different powders followed by their consolidation [Sur13a, Sur03]. Other solid state processes for MMCs

production are roll bonding, friction stir processing and additive manufacturing [Dub11, Cha96]. Roll bonding involves the rolling of different laminates to synthesize the layered composites while friction stir processing is a surface composite development technique in which reinforcing particles are poured in the surface groves of metallic matrix and then homogenized using the friction of a rotating hard tool against the matrix surface [Mis03, Hun93, Man90]. Selective laser melting / sintering is a type of additive manufacturing technique which can produce complex structures by melting / sintering the succeeding layers of powder particles using a laser beam [Dub11, Mir01]. MMCs synthesized by selective laser sintering are porous and need further consolidation steps to reduce the porosity such as iso-static pressing [Dad12, Loh92]. Furthermore, the reinforcing particles tend to agglomerate at the matrix grain boundaries due to the involvement of melting in the process. The process demands high flowability of powders, thus the use is generally restricted to spherical powders only [Sal18, Wei15]. Processes like co-extrusion or diffusion bonding are not commonly used to synthesis the particulate MMCs and forging is normally used for the near-net shaping of MMCs consolidated by hot pressing or extrusion [Cha06, Ral97].

2.6.1 *Powder metallurgy*

Powder metallurgy is a versatile and simple method to synthesis metal matrix composites such as AMCs with desired microstructure and properties. P/M for MMCs involves mixing of matrix and reinforcement powders followed by consolidation [Ger05, Thü93]. The flexible nature of P/M offers the incorporation of a wide range of reinforcement volume fractions, particle shape, size and distribution which is not possible in liquid state processing. Also, the control over processing parameters such as temperature, enables to avoid or manipulate the chemical reaction that may take place at the interface between matrix and reinforcement [Upa97, Thü93]. The blending of initial components can be done both in liquid or dry conditions. The composite mixture of initial powders is consolidated using either hot compaction (axial or isostatic pressing, forging or extrusion) or cold pressing followed by pressure assisted or pressure-less high temperature sintering [Tor03, Har98, Ral97].

P/M processing offers several advantages over other MMCs synthesis techniques (such as liquid state processes) which include manufacturing of near-net-shape product with minimum post consolidation steps which means reduced material loss and low processing costs, development of composites with different phase combinations starting from the same set

of materials, addition of high volume fractions of reinforcement with uniform dispersion [Ger05, Upa97, Thü93].

2.6.2 Ball milling of powder mixtures

Ball milling is an effective and the common way to homogeneously blend the particulate reinforcement within a ductile matrix i.e., aluminum, magnesium, copper, etc. [Har98]. In this process, the mixture of matrix and reinforcement powders and the milling media (hardened balls) are added in a container (also known as grinding vial, jar or bowl) under inert atmosphere (generally Argon). The container is filled and closed under inert environment and then rotated at a predetermined rotational speed (rpm = revolutions per minute). During milling, balls collide with each other and with the wall of the container. The powder particles trapped between the colliding balls face high energy impacts. The repeated impacts cause severe plastic deformation of the milled particles together with their fracturing and cold welding [Sur01a].

The planetary ball mill is a famous device which is widely used for MMCs processing among the others ball mills. In Figure 2.13 a planetary ball mill (Retsch PM 400 used in this work) is shown. A large disk (also known as planetary disc) rotates in one direction and the milling vials attached on it rotate in the opposite direction. The resultant of the centrifugal forces induced by the planetary disc and grinding vial rotations, acts on the grinding media and powders. The motion of the charge (balls and powders) in a vial is indicated by a red dotted path. The charge slides along the inner wall of the vial and then the resultant centrifugal force detach it from the wall and hit across the vial. High speed of the milling media generates high energy impacts between the striking balls and container [Abd14, El01, Sur01a]. Depending upon the milling parameters such as rpm and balls to powder weight ratio (BPR), a significant increase in the local temperature and strain energy of the powder particles facing these high energy impacts can be observed due to rise in the impact frequency and impact energy [Cha01, Abd95].

Ball milling can be used for mechanical milling, mechanical alloying or fabrication of composites mixtures. Mechanical milling is used to refine the size and microstructure of single phase, pre-alloyed or composites powders. Additionally, it can also be used for inducing ordering, disordering or transformation of the phases. Conversely, when powder mixtures of different materials are milled together to obtain a homogeneous alloy through materials transfer then milling process is named mechanical alloying. Ball milling can also be used to synthesize

the composite powders which usually involves the blending of a hard phase and ductile powders to produce a homogenized mixture [Cha01, Abd95].
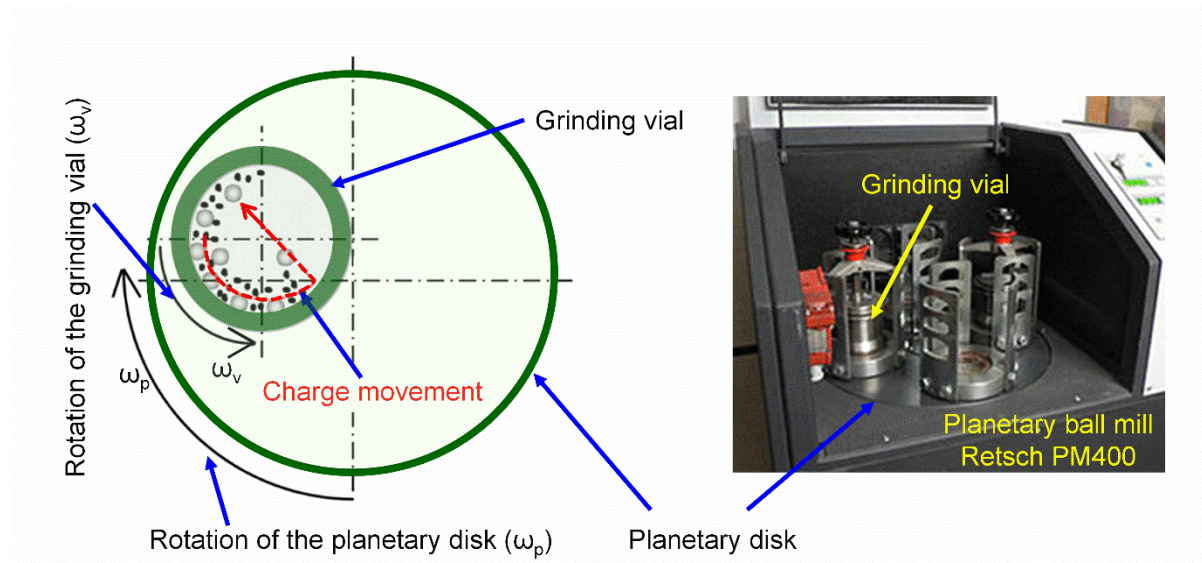

Figure 2.13 *Movement of the planetary disk (ω_p), grinding vial (ω_v) and grinding balls (indicated by red dashed path) (after [Abd14]).*

The structural refinements during *mechanical milling* of a single phase powder proceed through localized plastic strain which generates arrays of dislocations. Recombining and inhalation of the dislocations introduces low angle grain boundaries which partition the grains into nano-meter size subgrains [Val00, Koc97]. Further milling spread this subgrain structure throughout the sample in random orientations [El01, Koc97]. Reduction in the grain size, introduction of disordered structure and increase in defects density (e.g. dislocations, vacancies, grain boundaries and anti-phase boundaries) store energy in the powder particles which can lead the system towards amorphization or the formation of metastable or stable phases depending upon the thermodynamics and transformation kinetics [De11, Zha04, Koc97].

Mechanical alloying is different than mechanical milling. It homogenizes the composition of powder particles to produce an alloy and in addition to that refines their size and microstructure. It starts with the plastic deformation based flattening of ductile particles into flakes followed by cold-welding of the flakes to form a layered structure. Further milling refines the microstructure and reduces the diffusion distances by decreasing the thickness of the layers. Reduced interlayer spacing along with the increased lattice defect density facilitate the interlayer material transfer to do the mechanical allying. Increased temperature due to high

energy milling impacts also expedites the diffusion to get a homogeneous alloy composition with refined structure [Sur13b, Zha04, Sur01a].

Synthesis of composite powder is normally achieved through blending of hard phase powder (reinforcement) within a ductile powder (matrix). Repetitive collisions of the grinding balls with the matrix and reinforcement particles refine the structure by deforming, cold welding, fracturing and fragmentation. [Cor11, Hes07, Koc97]. Powder particles face high impact force during ball milling when trapped between the grinding media. The impact energy causes severe plastic deformation of the powder particles leading to the work hardening and fracture [Cor11, Tan05, Val00, Koc97].

In the early stage of blending, flattening of the ductile particles takes place together with the fragmentation of brittle or hard phase particles. Flattening of the ductile particles increases their surface area and maximizes the reinforcement contact chances with the flattened matrix flakes [Ben90, Ben76]. In the next stage, the fragmented particles get entrapped between the flakes and embedded in the ductile flakes. It may be considered as impregnation of ductile flakes with the reinforcement fragments. The cold welding of the flakes creates composite agglomerates possessing a layered structure. Repeated flattening, cold welding and fracturing of the impregnated particles steadily refines the microstructure. Further milling decreases the interlayer spacing, homogenies the distribution of reinforcement and increases the number of layers in a composite particle, [Ben90, Gil83, Ben74]. Further increase in the milling time can cause fragmentation of the agglomerates into small particles due to increased plastic deformation and strain hardening [Ozk16, Est14, Fog03]. During ball milling cold welding and fracturing mechanisms contest with each other. The dominancy of cold welding leads to the formation of composite agglomerates in the early stage of milling. Later on, frequent collusions of grinding media with the agglomerates generates local deformations and work hardening in the composite particles. Thus, fracturing dominates over cold welding and size of the composite particles decreases [Wu12, Esa07, Zha06].

The milling time affects the morphology of composite powder. Milling of powder at steady state condition (balance between cold-welding and fracturing) leads to the formation of equiaxial or quasi-spherical powder morphologies [Ozk16, Est14, Liu12, Zha05, Fog03]. Shorter milling time is required to achieve the steady state between fracturing and cold welding in high energy ball milling, while low energy milling needs more time to achieve steady state. Thus, low energy milling with extended milling time usually favors the cold-welding which

leads to the formation and growth of the composite agglomerates followed by fracturing, rejoining and spheroidization of composite agglomerates [Liu17, Gan08]. Further increase in milling time performs microstructural refinements in the surface zone of composite agglomerates by reducing the reinforcement particle and matrix grain size. Extended milling can cause fracturing and fragmentation of the composite agglomerates due to strain hardening [Zha15, Kwo14, Gu09]. Figure 2.14 presents the schematic map for the ball milling of a ductile-brittle powder mixture which is ductile powder rich system.
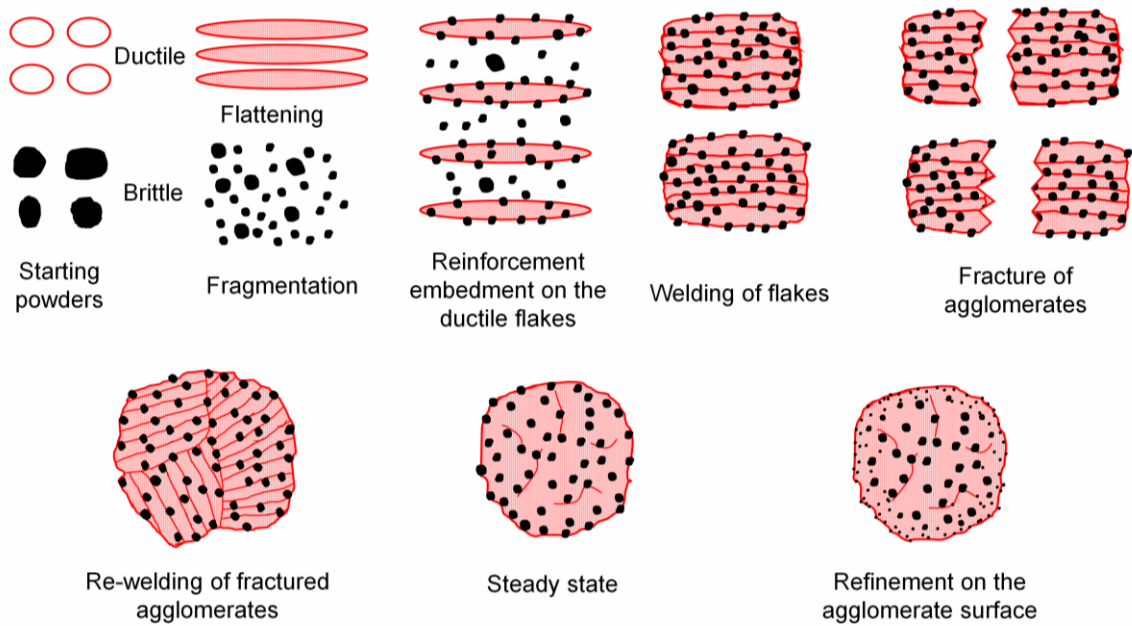

Figure 2.14 *Various stages during ball milling of a ductile-brittle powder mixture (after [Fog03]).*

Milling creates a variety of crystal defects in the particles such as new surfaces, vacancies, stacking faults, disordering, lattice distortion, dislocations, increased number of grain boundaries and interface boundaries [Sur01a, Sur01b]. For example, for structural refinement at the nanometric level, more than 50 % of atoms are connected to the interfaces or grain boundaries [Tjo04]. Refinement of the microstructure (e.g., reduction in particle size and interlamellar spacing) decreases the diffusion distances [Sur13b].

2.6.3 *Powder consolidation*

Powder consolidation is an essential and important step of P/M processing to get the required bulk shape close to the final product with desired density and properties [Ger05, Upa97]. The process includes pouring of powder into a die cavity, compression of the powder by applying pressure using rigid punches, ejection of the green compact from the die cavity

and finally sintering of the green compact by heating it at high temperature to reduce the porosity [Eis98]. Powder compaction and sintering can be done separately and as well as simultaneously. Modern P/M consolidation processes such as hot pressing, spark plasma sintering, hot iso-static pressing and hot extrusion offer the pressing and sintering at the same time.
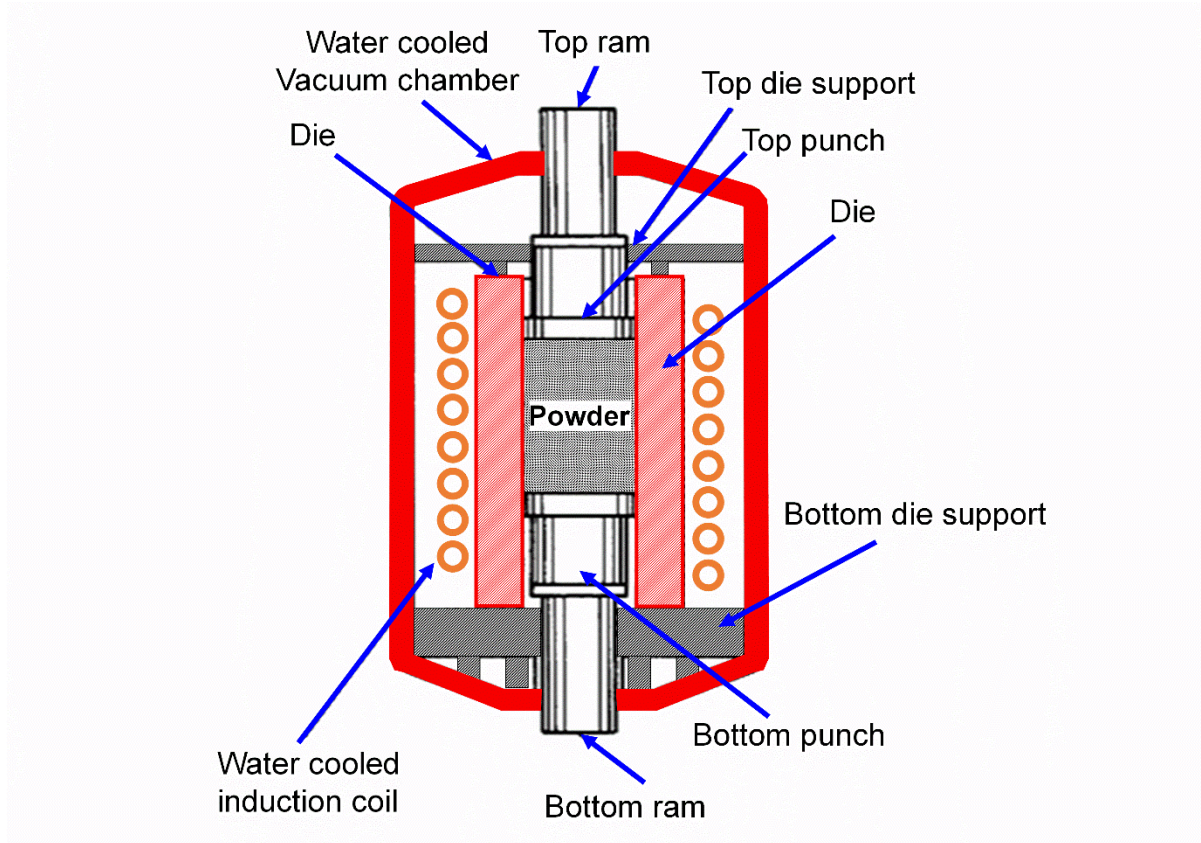

Figure 2.15 *Schematic illustration of an induction heating vacuum hot press (after [Lid66]).*

Hot pressing is the simplest single step uniaxial consolidation process which performs densification of the powder mixture through rearrangement of the powder particles followed by plastic flow due to applied stress in the presence of high temperature. [Upa97, Thü93]. Figure 2.15 shows the schematic arrangement of a hot pressing set-up. Powder is poured into the die cavity and hot pressing chamber is filled with inert gas after its evacuation. Afterwards, the die/mold is heated to a pre-calculated temperature and then a predetermined pressure is applied on the powder. Temperature and pressure are sustained for a fixed time to achieve the high density; this is followed by under pressure cooling of the die to room temperature and ejection of the compact from the mold.

Higher plastic flow during hot pressing due to softer behavior of materials at elevated temperature accompanied by the enhanced diffusion rates enable to achieve the near-full-

density objects in comparison to conventional two-step process, which is cold-pressing and sintering. Processing parameters such as temperature, time, pressure, and consolidation atmosphere determine the mechanical and physical properties of the final compact [Eis98, Thü93].
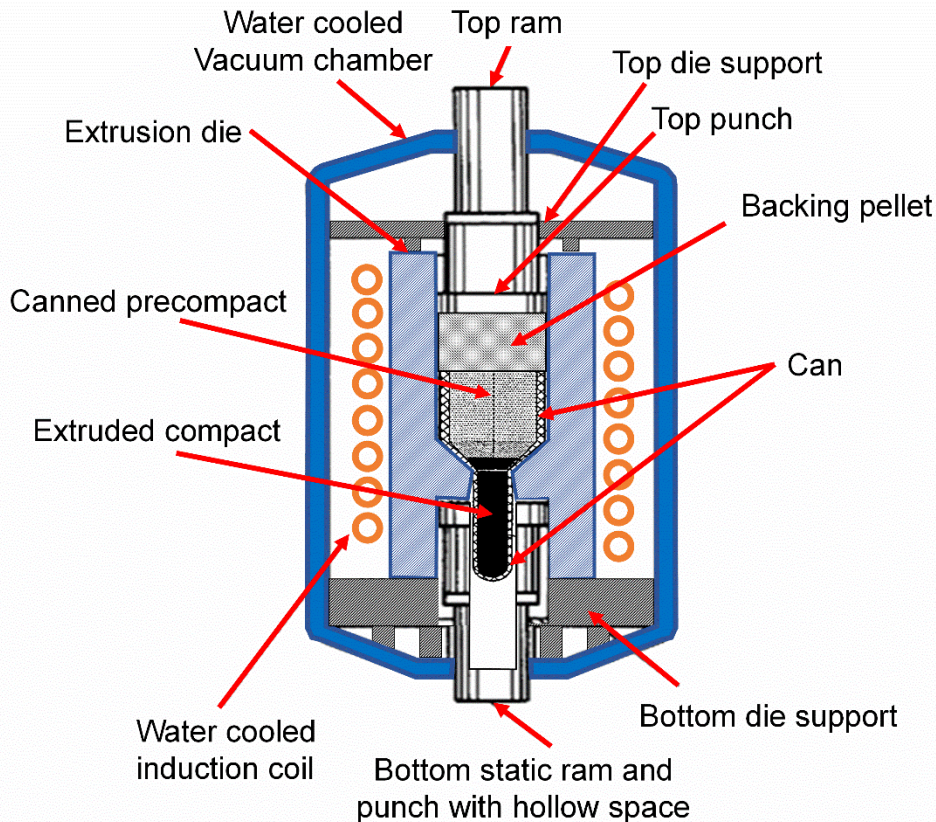

Figure 2.16 *Schematic diagram of hot extrusion process (after[Thü93, Lid66]).*

Hot extrusion is also used to consolidate powders or to enhance the densification of green or hot pressed compacts. A combination of hot pressing and hot mechanical working during hot extrusion exert compressive and shear stresses together on the precompact or powder which helps to get the fully dense products. Canning of the precompact or powder is usually done before performing hot extrusion to avoid contamination from tooling and to reduce the friction between compact and die. After completion of the process the can is removed from the surface of extruded product. The schematic diagram of a simple hot extrusion equipment is shown in Figure 2.16. Among other process parameters such as temperature, extrusion rate, frictional conditions, atmosphere etc., the extrusion ratio (cross-sectional area of precompact divided by the cross-sectional area of extruded compact) is the key parameter to attain the required density [Upa97, Thü93].

Careful optimization of the parameters such as time, temperature and pressure must be done to avoid the un-wanted chemical reactions, grain growth, precipitation, and phase transformations during hot-consolidation processes. In addition to plastic flow of the material, the densification in pressure-assisted sintering proceeds through thermally activated diffusion of material to fill in the porosity. Un-necessary high processing temperature or an extended exposure of the material at high temperature can lead to undesired microstructures and properties of the final product [Eis98, Upa97, Thü93].

2.6.3.1 *Pressure assisted sintering*

In hot consolidation the local stresses arising from the applied load enhance the driving forces for the densification process. According to thermodynamics, a green compact is far away from the equilibrium state, which is single crystal with equilibrium density of defects [Thü93]. Therefore, on providing thermal activation energy the green compact starts to reduce the surface area by increasing particle contact areas and grain growth. The green compact minimizes its free energy to move towards a more stable state by decreasing pore volume, removing unstable phases and non-equilibrium lattice defects (e.g. point defects and dislocations) [Ger05, Eis98].

In the early stage of pressure-less sintering material flow take place due to the Laplace stress σ which is related to the radius of circular contact area between adjacent particles (x), radius of particles (a) and radius of the neck curvature (ρ). Figure 2.17 shows the distribution of the tensile Laplace stress in the neck between two adjacent particles (Equation 2.16 [Thü93])

$$\sigma = \gamma \left(\frac{1}{x} - \frac{1}{\rho} \right) \qquad (Equation\ 2.16)$$

and compressive Laplace stress around closed pores of spherical shape (Equation 2.17 [Thü93]) in the later stages of sintering, where γ is the surface tension and r is the radius of a circular closed pore

$$\sigma = \frac{2\gamma}{r_{pore}} \qquad (Equation\ 2.17)$$

Sintering reduces the Laplace stress at the initial stages by growing the particles contact area and reducing the sharpness of the neck curvature due to atomic diffusion from convex surfaces of the particles to the concave surfaces (neck curvature). In pressure-assisted sintering, such as hot pressing, the external applied load is transmitted through particles to every single

contact between the particles. The superimposition of the transmitted stress on the Laplace stress at the particle contact enhances the effectiveness of the contact stress. Similarly at the later stages of sintering the applied pressure enhances the effect of Laplace stress around an isolated closed pore [Eis98, Ash87].
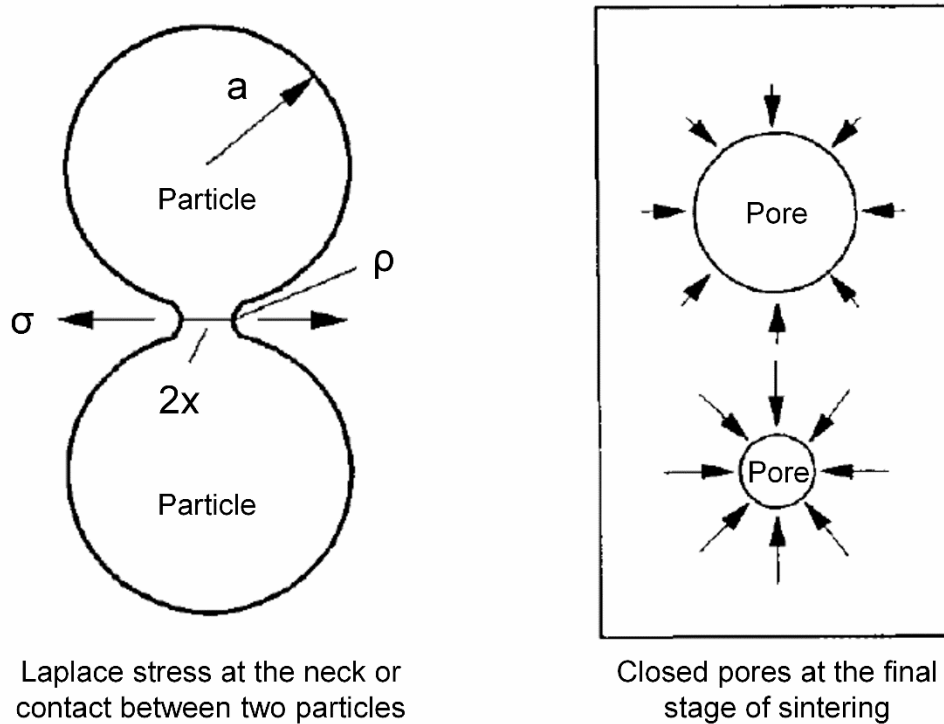

Figure 2.17 *Schematic depiction of the Laplace stress in a neck between two particle and around pores [Thü93].*

In the case of pressureless sintering, the effective pressure on the particle contacts decreases continuously with the growth of particle contact area due to densification. Contrarily, in the case of hot pressing, the effective pressure on the particle contacts get closer to the external applied pressure [Thü93]. Thus in pressure-assisted sintering the Laplace capillary pressure or Laplace stress can be enhanced up to 4 orders of magnitude (from 10^{-2} MPa to 500 MPa) due to the involvement of external pressure. Such high values of local pressure support the mechanisms of material transport [Thü93]. Laplace capillary pressure is the pressure difference at the curved interface between two fluids in a capillary [But06]. It can be calculated using Equation 2.17 and it is equal to the Laplace compressive stress around a closed pore of spherical shape [Gen03, Thü93].

The densification in solid state hot pressing forwards through plastic yielding, dislocation creep (power law creep), diffusional creep (grain boundary or bulk diffusion), and grain

boundary sliding [Eis98, Thü93]. Plastic yielding is the most pressure sensitive mechanism which takes place when particle contact stress and pore surface stress exceed the yield strength of the material. The plastic yielding continues until the material deformation resistance (due to work hardening) balances the effective particle contact stress. The plastic deformation plays its role when the local stress concentrations are high, i.e. during initial densification. Power law creep deformation which occurs due to dislocation climb and glide or dynamic recrystallization is the next sensitive to the applied pressure. The rate of the power law creep based densification increases with the applied pressure [Ger05, Ash87, Len66]. Both power law creep densification and plastic yielding do not depend on the grain or particle size [Thü93, Ash87].

In a stressed grain vacancies flow from tensile zone of grain boundary to compressive zone of grain boundary due to vacancy gradient. Thus, atoms diffuse in opposite direction wither through crystal lattice (Nabaroo-Herrning) or grain boundary (Colbe creep). The densification rate through diffusional creep increases linearly with pressure and strongly depends on the grain size (inversely proportional to the square-root of grain size). Therefore its contribution can be enhanced using small grain size or fine powder particles [Thü93, Ger89, Ash87].

Chapter 3. Sample preparation and characterization

In this work aluminum-magnesium and aluminum-Fe_3Al composites were produced using powder metallurgy. The composites were investigated for microstructural evolutions due to structural refinements and phase transformations during processing. The effect of the microstructural changes on the mechanical properties of the composites were examined.

3.1 Powder blending

A Retsch PM 400 planetary ball mill (Figure 3.1) was used to homogenize the powder mixtures and to refine the macrostructure of the particles. The initial powders along with hardened steel balls of 10 mm diameter were loaded in hardened steel milling vials. Each milling vial of capacity 250 ml, equipped with flexible O-ring for sealing purposes, was charged with 30 g of powder mixtures accompanied by 300 g of grinding media (ball to powder weight ratio = 10:1). In order to minimize air contamination during milling, the filling, sealing and opening of milling vials and any successive sampling or handling of the composite powder mixtures were performed under purified argon atmosphere (less than 1 ppm of oxygen and H_2O) in a Braun MB 150B-G glovebox. Milling was stopped after every 15 minutes for an interval of 15 minutes to avoid any excessive temperature rise during the process.

Figure 3.1 *Images of Retsch PM400 planetary ball mill [You15]*

Commercially available aluminum powder (Alfa Aesar GmbH & Co KG) with D(50) = 3μm and magnesium powder with D(50) = 30 μm were used to synthesize the Al-Mg composites. The mixtures consisting of Al with different volume fractions of magnesium (*V=*

46

10, 20, 40, 60, 80 and 90 vol.%) were blended by ball milling for 1 hour at 100 rpm. Similar blending parameters, equipment, atmosphere and aluminum powder were used to prepare the powder mixtures for the aluminum-Fe$_3$Al composites. Different amounts (V= 10, 20, 25, 40, 60 and 80 vol.%) of Fe$_3$Al powder {D(50) = 10μm} were mixed with the aluminum powder.

In order to generate the Al-Fe$_3$Al composites with harmonic structures, powder mixtures consisting of the aluminum and 20 vol.% Fe$_3$Al particles were ball milled for different periods (t_m = 1, 5, 10, 20, 30, 40 and 50 hours). The other milling parameters, equipment and environment were kept same as has been previously described.

3.2 Powder consolidation

The blended composite powder mixtures were consolidated into pellets of cylindrical shape (10 mm height and 10 mm diameter) using hot pressing. An electro-hydraulic uniaxial pressing machine with a maximum load capacity of 350kN, shown in Figure 3.2, made by WEBER PWV 30 EDS (Germany) was used for this purpose.
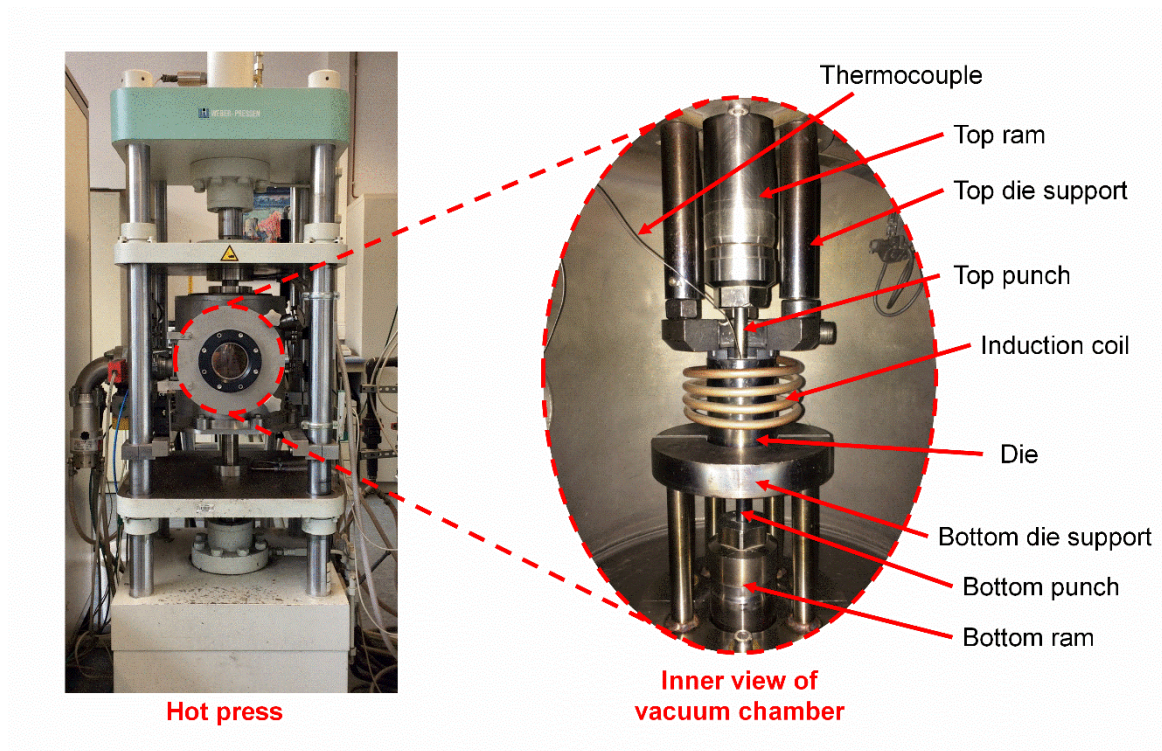

Figure 3.2 *Hot press machine used in this work along a view of its vacuum chamber.*

After cleaning the die cavity and both compression punches, a thin layer of boron nitride was sprayed to reduce the friction effects. Afterwards, the powder mixture was poured into the die cavity and, after tapping, the top punch was lowered to close the die. Then, the vacuum

chamber was evacuated to 1×10^{-3} Pa followed by the application of the desired compaction load and argon filling in the chamber up to 40×10^3 Pa to create an inert environment inside the chamber during hot pressing. The compaction setup was heated up to the pre-fixed temperature (selected on the basis of the DSC experiments) using an induction coil and the temperature was continuously measured by a Pr / Rh Pt thermocouple, which was inserted in the dedicated cavity of the die. After finishing the hot pressing cycle (compaction, heating, cooling, releasing pressure) the pellet was ejected from the die. The uniaxial compaction pressure and dwelling time for all consolidation experiments were 640 MPa and 10 minutes respectively.

Hot pressing of the aluminum-magnesium composites was performed at 673 K. Besides the hot pressing of the Al-Mg powder mixture, few additional aluminum-magnesium bi-layer composites containing 50 volume percent of magnesium were also produced by hot pressing the layers of aluminum and magnesium powders together at 573, 623 and 673 K.

The Al-Fe$_3$Al composite mixtures were hot pressed at 743 and 903 K (except AMCs with $V = 10$ and 25 vol.% which were consolidated at 903 K only) to examine the strengthening effect induced by the in-situ phase transformation which takes place due to the chemical reaction between the initial components. The AMCs hot pressed at 743 and 903 K are designated as *non-transformed* and *transformed* composites, respectively. For comparison, single-phase Fe$_3$Al and unreinforced pure aluminum matrix were hot pressed at 903 and 743 K. In order to analyze the phase sequence induced by the Al-Fe$_3$Al reaction, composites consisting of Al matrix and a single millimeter-sized Fe$_3$Al particle were synthesized as follows: (i) the Fe$_3$Al powder was hot pressed at 903 K to obtain a 2 mm-thick pellet, (ii) millimeter-sized particles were produced from the pellet, (iii) the macro-particles were mixed with Al powder and hot pressed at 823, 873 and 903 K.

Powder mixtures consisting of pure aluminum with 20 vol.% of Fe$_3$Al particles ball milled for different milling periods ($t_m = 1, 5, 10, 20, 30, 40$ and 50 h) were consolidated at room temperature and 743 K to synthesize the harmonic structured composites.

3.3 Structural and thermal characterization

The blended powder mixtures and the consolidated composites were characterized using X-ray diffraction and scanning electron microscopes to examine the size, shape, phase distribution and microstructural features. The thermal stability was examined by differential scanning calorimetry.

3.3.1 X-ray diffraction

A laboratory X-ray diffractometer D3290 PANalytical X'pert PRO with Co-$K\alpha$ radiation ($\lambda = 0.179$ nm) in reflection mode was used for the phase identification and structural analysis of the blended powders and hot pressed composites. The diffractometer was operated at a voltage of 40 kV and 40 mA current and the intensities of the diffracted X-rays were recorded between 20 and 120 degrees of 2θ values. The step size $\Delta(2\theta) = 0.013°$ was used with an acquisition time of 2 seconds per step. The powder samples were fixed on PVC holder using an acetone diluted resin. Both holder and resin did not interfere in the scanning range of current experiment [Boe01].

3.3.2 Scanning electron microscopy

In this work two different scanning electron microscopes were used to analyze the microstructural features of powders and consolidated composite samples. Secondary electrons and back scattered electrons can be used to take the SEM images which contain the topographical and chemical compositional based contrast information respectively.

The morphology and size of the milled powders were investigated using a Hitachi TM-1000 table top scanning electron microscope. Ten to fifteen SEM micrographs were analyzed for every specimen using the software 'ImagJ' and the cumulative size distribution curves (cumulative frequency percent as a function of the particle size range [Ger05]) were used to calculate the population based D(50) size of the milled powders.

A high resolution Gemini LEO 1530 scanning electron microscope manufactured by Carl Zeiss AG (Germany) with Schottky type FEG-source was used to analyze the microstructural features of the composites and mounted and polished powder blends. An energy dispersive X-ray spectrometer (EDX: Quantax400) with Si(Li) detector and the QUANTAX evaluation software of Bruker AXS were used to get the chemical composition details of the different areas through point or line scans and also to acquire the elemental distribution area maps. The experiments were performed at a working distance of 10-20 mm using 60-120 μm aperture size with 15-20 kV voltage and 7 nA beam current. The image analyzer software 'ImagJ' was used to estimate the volume fraction of the phases present in the composites from the SEM micrographs. Ten to fifty SEM images were analyzed for every composite. The matrix ligament size ($\lambda = L/N$, where N is the number of matrix region intercepts on the test line of length L [Und85]) characterizing the composites was calculated from the arithmetic mean of seventy measurements by superimposing random lines on seven SEM micrographs.

3.3.3 Differential scanning calorimetry

A computer controlled differential scanning calorimeter Netzsch DSC 404 with Netzsch proteus thermal analysis software was used to investigate the thermal stability of the cold-pressed Al-Fe$_3$Al composites. Ten to twenty milligrams of the sample were charged in the sample holder (alumina crucible covered with alumina lid), then the specimen chamber is evacuated for ten minutes to reach evacuation level of 0.1 Pa and afterwards filled with argon gas; the experiments were performed under a continuous flow of argon (100 ml/min) to avoid the oxidation.

Isochronal DSC scans were conducted up to 903 K at heating and cooling rates of 20 K/min. Two heating and cooling cycles were applied to each sample. By considering the second DSC run as baseline and subtracting it from first DSC run the accurate behavior of the sample under analysis can be gathered and the effect of the equipment specific shift of the base line can be subtracted from the behavior of the sample. The onset temperature (T_x) of the exothermic transformation event along with its peak temperature (T_p) and the enthalpy of the transformation (ΔH) were calculated from the DSC peaks.

3.4 Oxygen content measurement

The amount of oxygen in the powders of pure aluminum, Fe$_3$Al and Al-20 vol.% Fe$_3$Al powder mixtures blended for 20, 40 and 50 hours was evaluated to estimate the extent of contamination during milling of the powder mixtures. A Leco ON-836 analyzer was used to determine the oxygen contents. The equipment was calibrated using standard procedure and standard nickel capsule sample to subtract the background effect or interference that may arise from the sample holder or carrier helium gas. After calibration, 40 milligrams of the sample were sealed in the nickel capsule and then placed in the sample holder that consist of a graphite crucible positioned in an impulse furnace. The sample reacts with the graphite crucible due to impulse heating and releases its oxygen in the form of CO_2 and CO as a result of the carbon assisted reduction reaction. The carrier gas (helium) sweeps the liberated gases from the sample chamber and passes through a series of infrared detectors. The processor receives the signal from the infrared detectors and uses a built-in software to calculate and display the oxygen content of the sample.

3.5 *Physical and mechanical properties characterization*

3.5.1 *Density measurements*

The Archimedes method was used to calculate the density of the consolidated samples. The mass of the samples was recorded in air and then in distilled water. Air bubbles were removed from the surface of the immersed sample before measuring its weight. The density of the consolidated sample was determined by using a Sartorius density measurement set YDK-01(0D) through following equation

$$\rho_s = \frac{m_a(\rho_w - \rho_a)}{m_a - m_w}$$

$$(Equation\ 3.1)$$

Here, ρ and m represent the density and mass while the subscripts a, s and w indicate air, consolidated sample and distilled water respectively.

To calculate the relative density of the consolidated samples, the experimental density measured by the Archimedes method is divided by the theoretical density, which is determined using the rule of mixture (RoM). For the non-transformed Al-Fe$_3$Al composites the theoretical density was calculated from the initial reinforcement content, whereas for the transformed Al-Fe$_3$Al composites it was determined using the vol.% of the phases that have been experimentally observed by SEM.

3.5.2 *Compressive testing*

All consolidated composite, unreinforced aluminum and pure Fe$_3$Al samples were tested at room temperature under quasistatic compressive loading at a strain rate of $1\times10^{-4}\,s^{-1}$ to access the mechanical properties, such as strength (yield and compressive) along with strain (elastic and plastic) using an INSTRON 8562 universal testing machine. Compression test samples of 6 mm height and 3 mm diameter were prepared from the hot pressed specimens of 10 mm height and 10 mm diameter (see Figure 3.3) by wire cutting. The dimensions of the compression test samples (length to diameter ratio of 2:1 for cylindrical samples) are in accordance with the ASTM standard for compression testing [AST03]. Before testing, the curved longitudinal surface of the compression test samples were polished using emery paper and the flat ends were grinded and polished to make them parallel to each other and perpendicular to the longitudinal surface. Plates of tungsten carbide steel lubricated with MoS$_2$ grease were used for the compression tests and the strain was measured directly on the surface of sample using a laser extensometer of Fiedler Optoelektronik GmbH (Germany). A minimum

of four specimens for each composite were tested in order to ensure the reproducibility of the results.

For the highly-deformable pure Al samples, non-transformed Al-Fe$_3$Al composites with V = 20 and 40 vol.% hot pressed at 743 K (V indicates the initial vol% of Fe$_3$Al), and all AMCs with harmonic structure (except for the 50 h milled AMC) the compression tests were intentionally stopped at 20% strain.
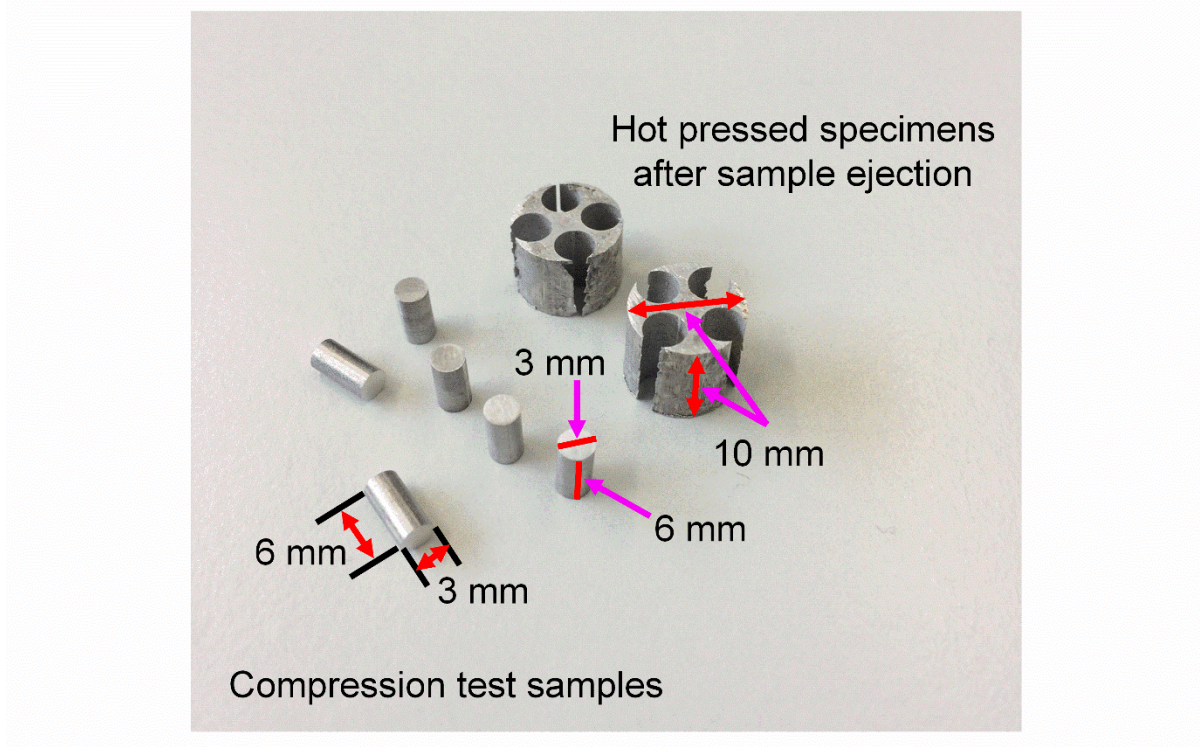

Figure 3.3 *Compression test samples and consolidated pellets after the ejection of compression test samples by wire cutting.*

Chapter 4. Microstructure and mechanical behavior of Al-Mg composites synthesized by reactive sintering

Interfacial reactions between the components of composite materials lead to phase transformations and microstructural changes which may affect the properties of the composites depending upon the nature of the reaction products, their bonding with the surrounding phases, and the volumetric changes involved in the transformation [Kai06, Has02a]. The enhancement of the mechanical properties of quasicrystal reinforced aluminum matrix composites induced by phase transformations has been observed [Ali14, Ken14, Lap10a , Tan03]. In the light of previous studies, the aluminum-magnesium composite system was selected to investigate the effect of the in-situ phase transformations on the microstructure and mechanical properties. For that purpose, Al-Mg powder blends with different volume percent of Mg (V= 10, 20, 40, 60, 80, 90 vol.%) were hot pressed at 673 K and then characterized to examine the changes in the microstructure and mechanical properties using techniques described in Chapter 3. The key factors behind the selection of the Al-Mg composite system are their low densities, high specific strength and stiffness, and the simplicity of the Al-Mg system, as their equilibrium phase diagram shows only two intermetallics β-Al_3Mg_2 and γ-$Al_{12}Mg_{17}$ at room temperature for the entire composition range [Bak92].

The first part of this chapter explains the phase evolutions and microstructural changes in the Al-Mg composites induced by the in-situ reaction which takes place at the interface between aluminum and magnesium during hot consolidation of the composites. The amount of the in-situ phases is discussed as a function of initial volume fraction of magnesium. In the second part the mechanical behavior of the composites is elaborated and the improvement of the mechanical properties of the composites is discussed in the context of in-situ phase transformations and resulting microstructural modifications.

4.1 Phase analysis and microstructural characterization

Figure 4.1(a) shows the XRD patterns for the Al-Mg powder mixtures after 1 h of blending by ball milling. The patterns indicate the presence of pure aluminum and magnesium only, which illustrates the absence of any reaction during the mechanically-induced mixing process carried out in the present milling conditions. Aluminum and magnesium react during hot consolidation of the powder mixtures at 673 K to create the β-Al_3Mg_2 and γ-$Al_{12}Mg_{17}$

intermetallics, as shown in Figure 4.1(b). The XRD patterns for the consolidated composites with an initial content of 10 and 20 vol.% Mg ($V = 10$ and 20) exhibit the presence of Al_3Mg_2 along with residual aluminum, whereas $Al_{12}Mg_{17}$ and magnesium are not observed. The composites with $V = 40$ and 60 contains both the intermetallics Al_3Mg_2 and $Al_{12}Mg_{17}$ accompanied by residual magnesium and aluminum. On the other hand, the composites $V = 80$ and 90 show only the presence of $Al_{12}Mg_{17}$ and magnesium, while the Al_3Mg_2 and aluminum phases are not observed. The creation of the Al_3Mg_2 and $Al_{12}Mg_{17}$ intermetallics during high temperature processing of aluminum and magnesium composites is in compliance with the reported results [Zha17a, För15, Kit15, Li15, Sko14].
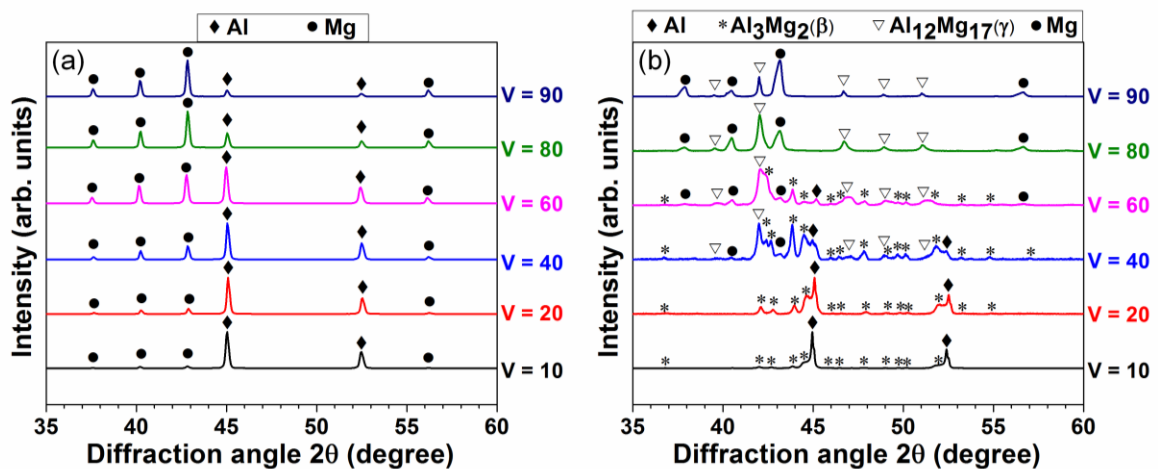

Figure 4.1 *XRD patterns (Co Kα radiation) of Al-Mg (a) powder mixtures milled for 1 h and (b) composites hot pressed at 673 K. (V = 10, 20, 40, 60, 80 and 90 initial vol.% of Mg)*

The SEM images and EDX elemental maps for the consolidated composites are displayed in Figure 4.2, 4.3 and 4.4. The composites with $V = 10$ and 20 show a core-shell microstructure that consists of a Mg core enclosed by a two consecutive shells of $Al_{12}Mg_{17}$ and Al_3Mg_2 which are finally covered by a rather continuous residual aluminum (Figure 4.2). The formation of multiphase in-situ core-shell microstructures has been reported in several composite systems [Guo16, Kho15a, Xue15, Wan14, Qi13, Lap10b, Lee03b] and can be attributed to the incomplete transformation reactions under the provided processing parameters, like temperature and pressure [Sha17]. In the composite with $V = 40$, the continuity of the aluminum phase has been disrupted by the substantial growth of the intermetallics, which can be attributed to the higher initial volume percent of magnesium. Here, the Al_3Mg_2 phase is continuous throughout the microstructure, the magnesium cores are surrounded by the $Al_{12}Mg_{17}$ phase and only a limited amount of isolated Al is observed.
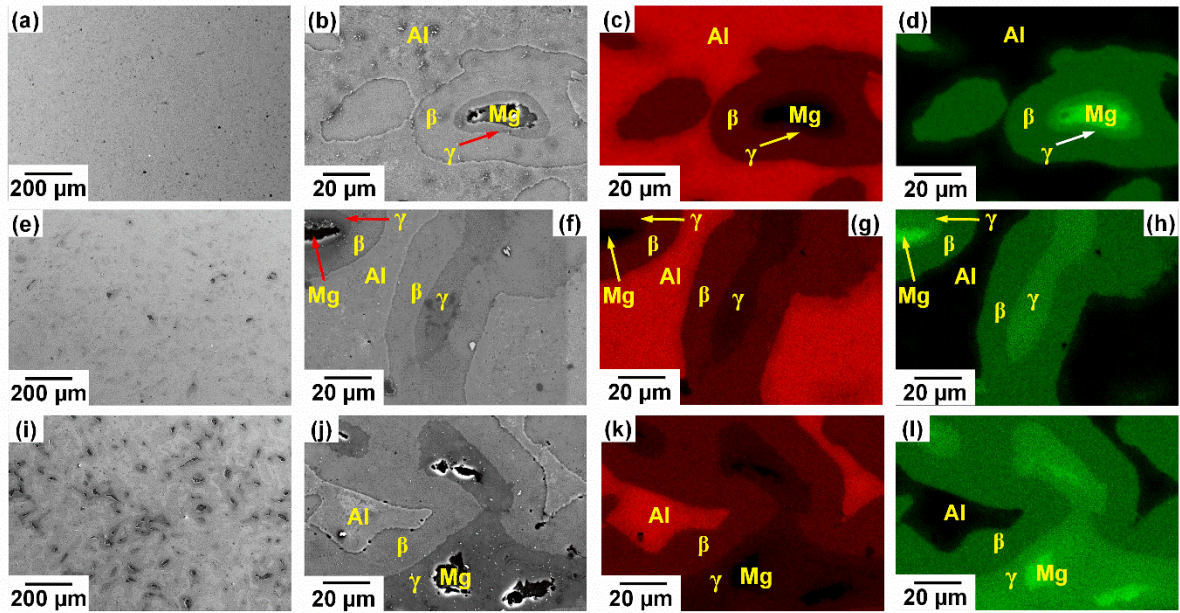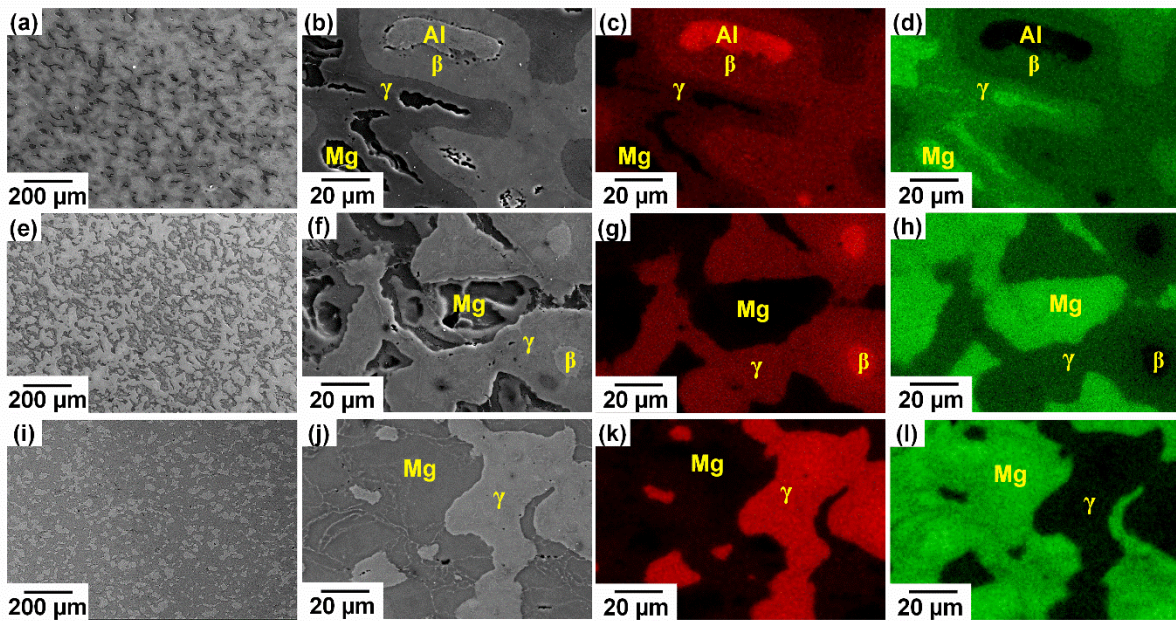
Figure 4.2 *SEM images and EDX elemental maps of Al (red) and Mg (green) distribution for the Al-Mg composites hot pressed at 673 K with initial Mg content (**a, b, c, d**) 10, (**e, f, g, h**) 20 and (**i, j, k, l**) 40 vol.%.*

Figure 4.3 *SEM images and EDX elemental maps of Al (red) and Mg (green) distribution for the Al-Mg composites hot pressed at 673 K with initial Mg content (**a, b, c, d**) 60, (**e, f, g, h**) 80 and (**i, j, k, l**) 90 vol.%.*

In the composite $V = 60$ (Figure 4.3), the size of the isolated aluminum regions further decreases, while the size of magnesium cores increases and both Al_3Mg_2 and $Al_{12}Mg_{17}$ intermetallic phases are rather continuous throughout the microstructure, where the amount of $Al_{12}Mg_{17}$ phase appears to be higher than the Al_3Mg_2. Conversely, in the composite $V = 80$,

pure aluminum is not found and the Al_3Mg_2 phase appears as cores encapsulated by the $Al_{12}Mg_{17}$ phase, which is further covered by a continuous residual magnesium phase. The microstructure of the composite $V = 90$ consists of islands of $Al_{12}Mg_{17}$ phase surrounded by residual magnesium. Phase identification in the composites is supported by the EDX elemental concentration profiles shown in Figure 4.4, which are in good agreement with the XRD results in Figure 4.1(b).
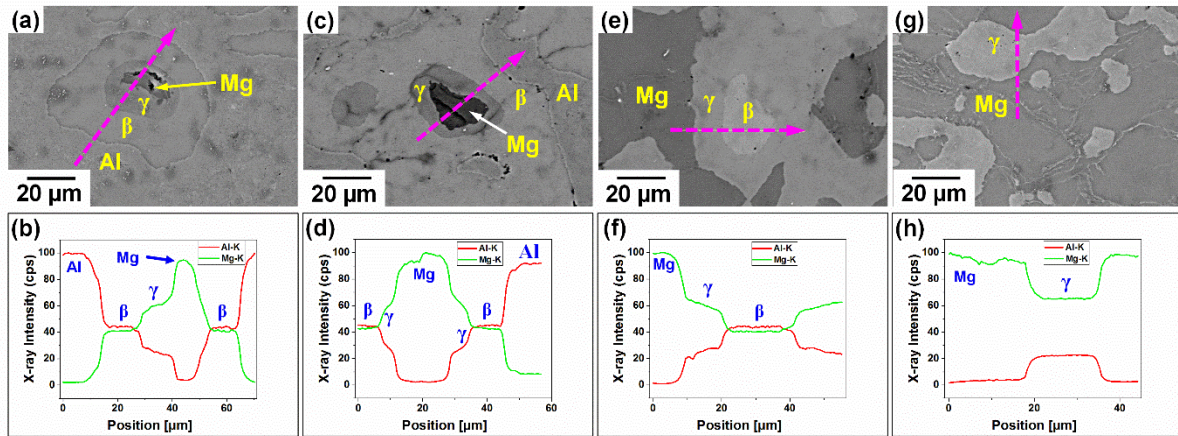

Figure 4.4 *SEM images and EDX elemental concentration profiles for the composites hot pressed at 673 K with initial magnesium content (**a, b**) 10, (**c, d**) 40, (**e, f**) 80 and (**g, h**) 90 vol.%. The dashed red arrows represent the scanned EDX line.*

Figure 4.5 illustrates the volume percentages of the different phases in the consolidated composites, estimated from the SEM images, as a function of the initial volume content of magnesium (V). The quantity of Al_3Mg_2 progressively increases from ~15 vol.% for $V = 10$ to ~55 vol.% for $V = 40$. Afterwards, it gradually declines to ~1.5 vol.% for $V = 80$ and finally it is not present anymore in the composite with $V = 90$. The amount of $Al_{12}Mg_{17}$ slowly rises to ~12 vol.% for $V = 40$, then sharply increases to 50 and 53 vol.% for $V = 60$ and 80, respectively, and finally decreases to about 25 vol.% for $V = 90$. The amount of Aluminum decreases continuously from ~85% for $V = 10$ to ~3% for $V = 60$ and then it diminishes to zero in the composites $V = 80$ and 90. The quantity of residual magnesium for $V = 40$ is ~2 vol.% and then it steadily increases to ~75 vol.% for $V = 90$. Figure 4.5 divides the consolidated composites into two sections separated by vertical lines on the basis of volume profiles intersections. At about $V = 55$ the volume profiles of aluminum and magnesium are equal. Additionally, the volume profiles of $Al_{12}Mg_{17}$ and Al_3Mg_2 also intersect at the same point. This suggests that the microstructure of the composites from $V = 10$ to 55 consist of aluminum as major soft phase along with Al_3Mg_2 and $Al_{12}Mg_{17}$ as dominant reinforcements, whereas for $V > 55$ magnesium

becomes the main soft phase predominantly reinforced by $Al_{12}Mg_{17}$, except for the composite with $V = 60$, where both $Al_{12}Mg_{17}$ and Al_3Mg_2 are present in high percentages.
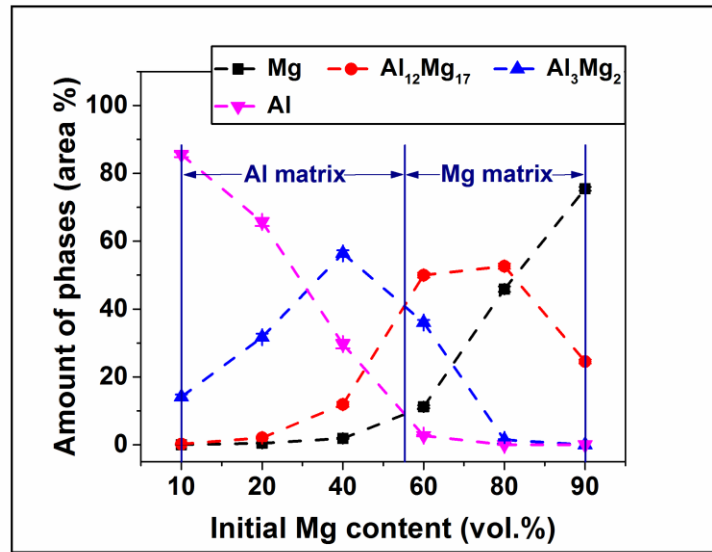

Figure 4.5 *Variation of the amounts of the different phases present in the Al-Mg composites hot pressed at 673 K.*

4.2 Sequence of phase formation during reaction of Al and Mg

In order to further examine the phase formation induced by the reaction between Al and Mg, aluminum and magnesium bilayer specimens were produced by hot pressing at different temperatures (573, 623 and 673 K). The corresponding SEM images and EDX elemental concentration profiles across the interface between Al and Mg layers are shown in Figure 4.6. In a homogenous composite, phase transformations occurring at an Al-Mg interface may have an influence on the diffusion and reaction fields arising from its neighboring similar interfaces. The synthesis of the bilayer composites helps to analyze the sequence of intermetallics formation at the Al-Mg interface in the absence of any reactional caused by the neighboring interfaces. The Al-Mg bilayer composite hot pressed at 573 K does not display any reaction product (Figure 4.6(a-c)). Because the diffusion coefficient of aluminum is higher than that of magnesium [Azi18, Bre12, Wan08], it is plausible to assume that at higher processing temperature (623 K) the aluminum atoms diffuse into the magnesium layer and form $Al_{12}Mg_{17}$ as the first reaction product (Figure 4.6(d-f)). The Al_3Mg_2 phase may then be generated by additional diffusion of aluminum into the $Al_{12}Mg_{17}$ intermetallic and by the diffusion of magnesium into the Al matrix [Afg16, Liu15]. At this stage, the reaction is rather discontinuous and a rough layer of $Al_{12}Mg_{17}$ and Al_3Mg_2 intermetallics is formed at the Al-Mg interface. The interfacial layer is composed of a 2.5 ± 1 μm thick $Al_{12}Mg_{17}$ layer next to magnesium and a 4

± 2.5 μm thick Al_3Mg_2 layer next to the aluminum. The existence and position of both intermetallic layers at the Al-Mg interface observed here is in accordance with previous studies [Lee13, Pan12, Die11, Su97]. Further increase in the temperature to 673 K smoothens the interface and enhances the widths of the intermetallic layers [Neg12] to 5 ± 1 μm thick $Al_{12}Mg_{17}$ and 14 ± 1 μm thick Al_3Mg_2. The limited growth of the $Al_{12}Mg_{17}$ layer can be attributed to its smaller inter-diffusion coefficient value in comparison to Al_3Mg_2 [Liu15, Nji01].

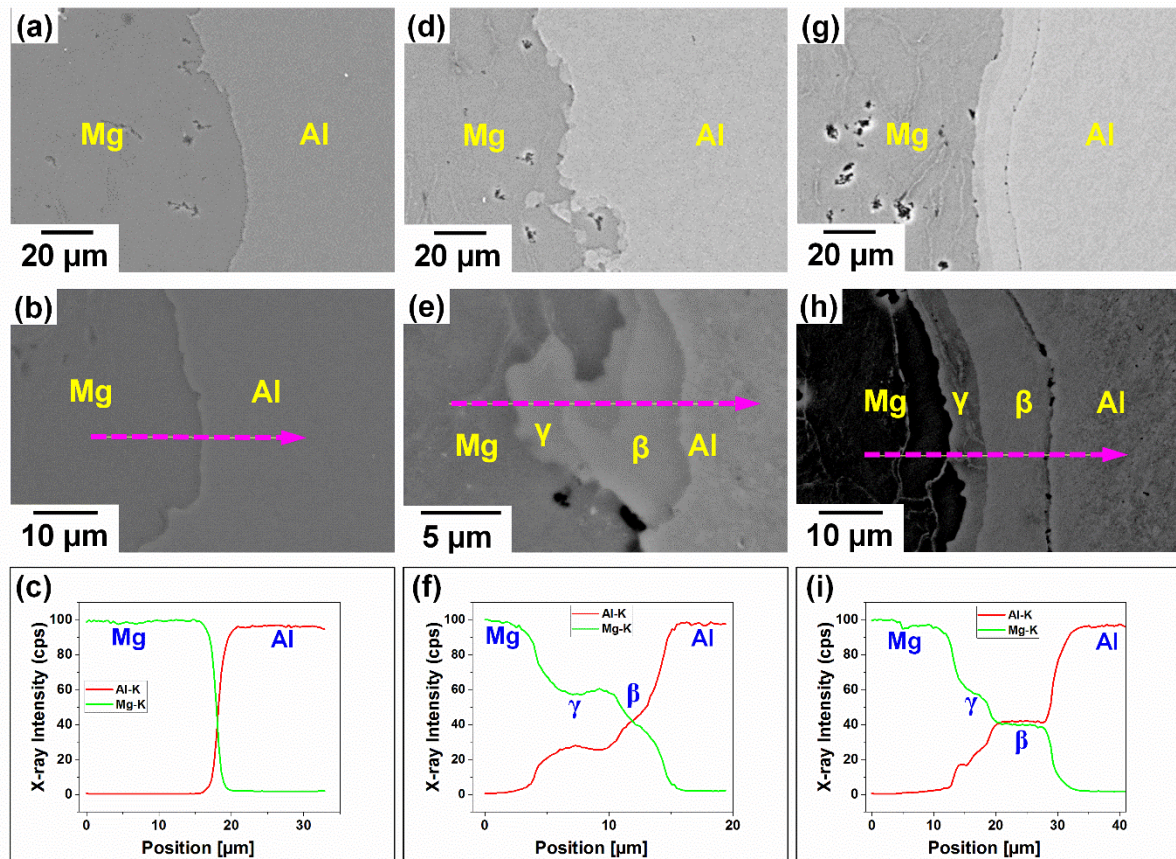***Figure 4.6*** *SEM micrographs and EDX elemental concentration profiles for the bilayer Al-Mg composites hot pressed at (**a, b, c**) 573, (**d, e, f**) 623 and (**g, h, i**) 673 K. The dashed red arrows represent the scanned EDX line.*

A closer look at the interface of the bilayer hot pressed at 623 K (Figure 4.7(a)) reveals additional features characterizing the surface of the aluminum layer. Every area on the aluminum surface undergoing the reaction with Mg is concave, whereas the intermetallics are hump shaped islands with similar morphology throughout the specimen. As already mentioned, the diffusion coefficient of aluminum is one to two orders of magnitude higher than that of magnesium [Bre12, Fun72,]. The aluminum atoms diffuse through the interface with a higher flux than that of magnesium and when the composition of the intermetallic phase γ-$Al_{12}Mg_{17}$

is locally reached, it nucleates and progressively grows into the magnesium layer [Afg16, Bre12, Pan12]. The preferential formation of the intermetallic phases at the concave zones of the aluminum surface indicates that stoichiometric concentration of aluminum atoms to form the intermetallics is reached faster in the concave zone than at the convex or straight zones. In order to analyze this aspect, Figure 4.7(b) shows schematically the linear paths of the diffusion of aluminum atoms in the Al-Mg bilayer. The diffusion line density in the concave zones is larger than that in the convex zones. As a result, the stoichiometric concentration in the concave zones is reached faster than in any other zone.
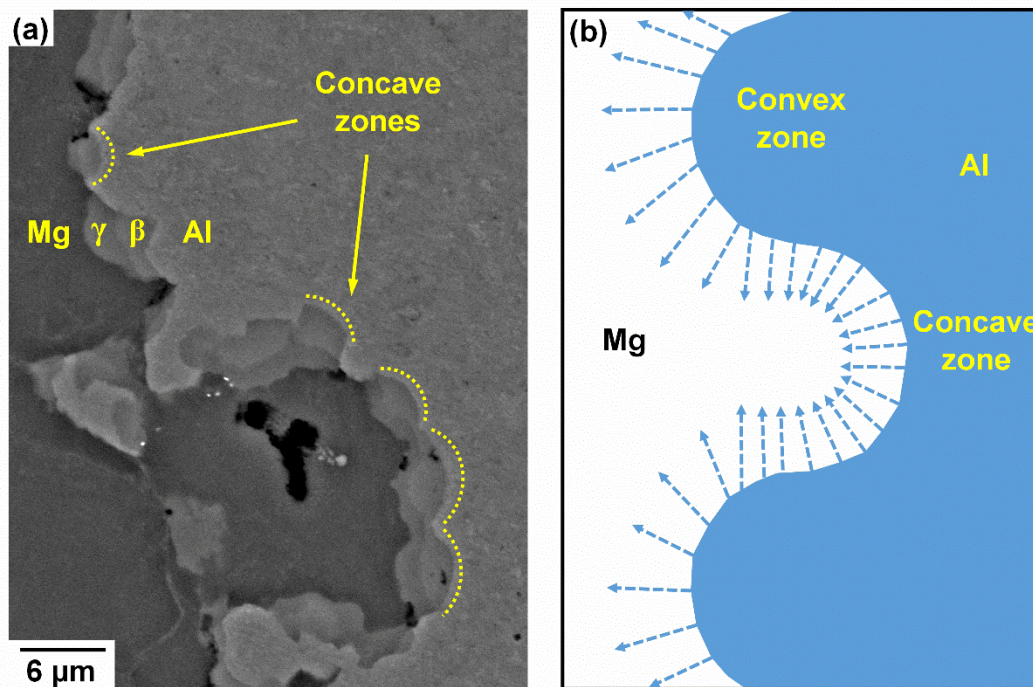

Figure 4.7 (a) *SEM image of the Al-Mg interface in the bilayer composite hot pressed at 623 K showing the preferential formation of the intermetallic phases at the concave zones of the aluminum surface. **(b)** Schematic representation of the linear paths of the diffusion of aluminum atoms in the Al-Mg bilayer.*

The bilayer composite hot pressed at 673 K (Figure 4.8(a)) shows thicker layers of intermetallics. The Arrhenius diffusion equation predicts higher atomic and vacancy mobility at higher temperatures [Lai87], which in turns explains the larger thickness of the intermetallic phases compared with composite sample hot pressed at 623 K. An oxide layer is present along the aluminum layer facing the edge of the β-Al$_3$Mg$_2$. This oxide layer represents the initial contact surface between the aluminum and magnesium particles [Bre12] and its existence near aluminum indicates that the phase transformations occur within the magnesium region [Neg12] [Bre12]. The presence of the boundaries of the pre-existing magnesium particle in the γ-

$Al_{12}Mg_{17}$ phase supports this conclusion. The interfaces between Mg and γ-$Al_{12}Mg_{17}$ and between γ-$Al_{12}Mg_{17}$ and β-Al_3Mg_2 do not show porosity, while the interface between β-Al_3Mg_2 and Al exhibits porosity that can be designated as Kirkendall's porosity [Svo17]; this aspect can be ascribed to the higher mobility of aluminum atoms in comparison to magnesium and to the coalescence of vacancies towards aluminum [Azi18, Bha10, Bre12].
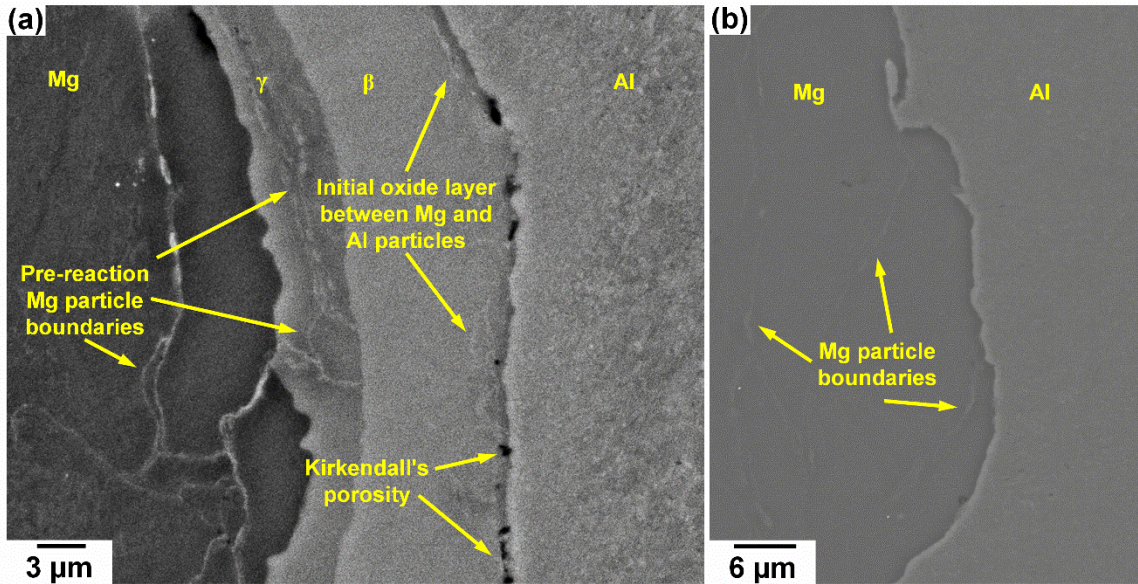

Figure 4.8 *SEM images of the Al-Mg interface in the bilayer composite hot pressed at (**a**) 623 and (**b**) 473 K.*

4.3 Mechanical properties

Figure 4.9(a) and (b) display the room temperature compression stress-strain curves for the composites and the summary of the corresponding mechanical data. The yield strength (0.2% offset) of the composites increases from 126 ± 7 MPa for the material with $V = 10$ to 562 ± 23 MPa for the composite $V = 60$ and then decreases to 207 ± 20 MPa for the composite $V = 90$. Similarly, the compressive strength (maximum stress that a material can stand with under compression loading [AST03]) increases from 238 ± 7 to 562 ± 23 MPa for the composites with $V = 10$ and 60, respectively, and afterwards, it decreases to 385 ± 20 MPa for the composites with $V = 90$. Conversely, the plastic deformability of the composites drastically decreases from 17 ± 0.2 % to 1.2 ± 0.1 % for the composites with $V = 20$ and 60 then it increases again to 11 ± 0.3 % for the composite $V = 90$. The composite with $V = 10$ does not show failure up to 20% strain where the test was stopped. The yield strength of the composites cannot be directly correlated to the initial volume percent of magnesium, as shown in Figure 4.9(c). The in-situ transformed Al_3Mg_2 and $Al_{12}Mg_{17}$ intermetallics play the role of reinforcement in the

composites. Therefore, the yield strength data are plotted in Figure 4.9(d) against the cumulative amount of both intermetallics along with the strength values predicted by the iso-stress (red dashed line) and iso-strain (blue dot-dashed line) models of the rule of mixture (RoM) [Scu08, Kim00, Cha87]. The yield strength of the composites increases with increasing the total amount of intermetallics. The values of strength are closer to the iso-stress model, which assumes that matrix and reinforcement experience the same stress during deformation, while the iso-strain model, which assumes that all components of a composite undergo the same strain during deformation [Cha87], overestimates the values.
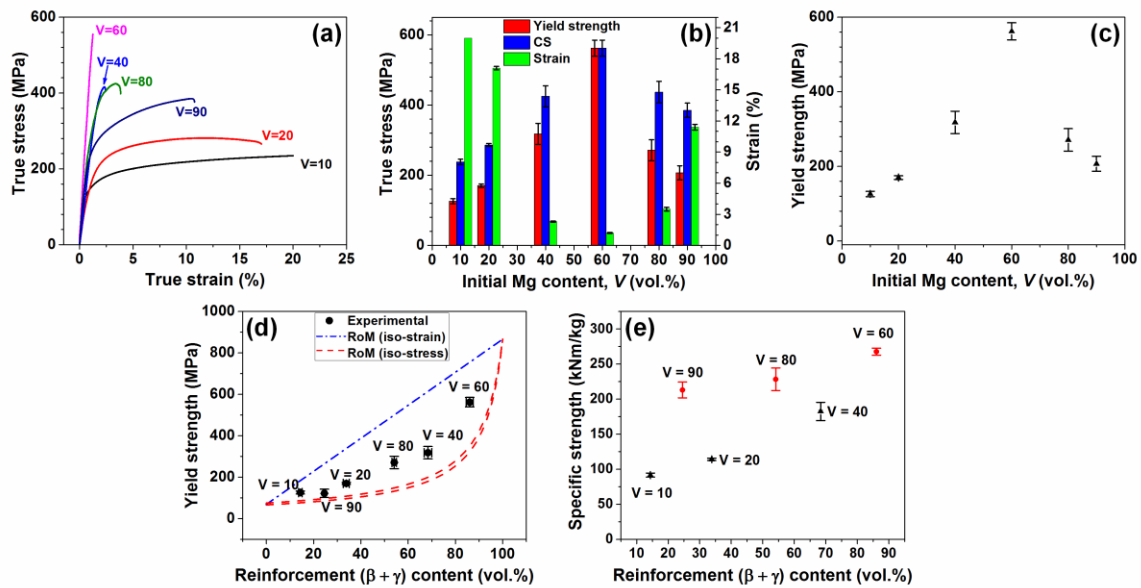

***Figure 4.9 (a)** Room temperature compression stress-strain curves for the composites with V = 10, 20, 40, 60, 80, and 90 vol.% Mg hot pressed at 673 K and **(b)** summary of the mechanical data. **(c)** Yield strength of the composites as a function of the initial Mg content. **(d)** Experimental yield strength of the composites as a function of the cumulative amount of β-Al₃Mg₂ and γ-Al₁₂Mg₁₇ and values calculated using the iso-stress and iso-strain models. The red dashed curves in **(d)** correspond to the iso-stress models with Mg (lower curve) and Al (upper curve) matrices. The yield strength for the 100 vol.% Al₃Mg₂ + Al₁₂Mg₁₇ in **(d)** is calculated from their hardness values given in Refs.[Sin16, Zol13]. **(e)** Specific strength (compressive strength divided by the density) of the composites as a function of the amount of β-Al₃Mg₂ + γ-Al₁₂Mg₁₇.*

Under compressive loading the reinforcement particles move in the loading direction to get closer to each other if the volume fraction of reinforcement is high and the distance between the reinforcement particles is small [Kim01]. In such cases the reinforcement particles may undergo deformation due to load transfer and the strength of composite follows the iso-strain model [Kim01]. On the other hand, a smaller volume fractions of reinforcement leads to larger distance between reinforcement particles and, in such cases, deformation takes place mainly in

the matrix. The iso-stress model describe the strength behavior of this type of composites [Kim12, Kim01, Li99]. Therefore, the deviation of the yield strength data for the composites with $V = 40$, 60 and 80 could be attributed to the high volume fraction of reinforcement and complex microstructure. The iso-stress behavior for aluminum matrix composites and the deviation of the yield strength from it have been observed in previous studies [Sha17, Wan15b, Scu08, Li99].

Finally, Figure 4.9(e) shows the specific strength (compressive strength divided by the density) of the composites vs. the cumulative volume percent of the β-Al_3Mg_2 and γ-$Al_{12}Mg_{17}$ reinforcement. The specific strength of the composites with aluminum as a major soft phase is represented by black triangles, while in the case of magnesium as main phase red circles are used. The specific strength of pure aluminum (55 kN m kg^{-1} [Scu09b]) increases to 90 and 180 kN m kg^{-1} by adding only 10 and 40 vol.% of magnesium as a result of the creation of approximately 14 and 67 vol.% intermetallics. Similarly, the specific strength of the composites with magnesium as the main soft phase, containing 25 ($V = 90$) and 85 vol.% ($V = 60$) of intermetallics increases from 210 to 270 kN m kg^{-1}, respectively.

The research work presented in this chapter describes that reactive hot consolidation of Al-Mg powder mixtures has been used to synthesize lightweight composites reinforced with β-Al_3Mg_2 and γ-$Al_{12}Mg_{17}$ intermetallics formed in-situ during consolidation. The formation of core-shell microstructures are observed in the Al-rich composites, where the Mg cores are surrounded by a double-shell of β-Al_3Mg_2 and γ-$Al_{12}Mg_{17}$ intermetallic phases. In the Mg-rich composites, aluminum has been fully consumed except in the composite $V = 60$. Microstructural examinations of a bilayer composites suggests that γ-$Al_{12}Mg_{17}$ is the first reaction product that originates at the interface between Al and Mg followed by the formation of the β-Al_3Mg_2 phase.

The mechanical behavior of the composites has been examined using room-temperature compression tests. The formation of the intermetallic phases increases the yield and compressive strengths of the composites, but decreases their plastic deformation. The strengthening effect depends on the amount of intermetallics formed during the consolidation step and, as a result, the yield strength of the composites follow iso-stress model when the data are plotted as a function of the cumulative volume percent of the intermetallic reinforcement.

Chapter 5. Microstructural strengthening by phase transformation in Al-Fe₃Al composites

To extend the concept of phase transformation induced strengthening of lightweight metal matrix composites, presented for Al-Mg composites in Chapter 4, another aluminum matrix composites system reinforced with Fe_3Al intermetallic particles was analyzed. Fe_3Al and other iron-aluminides are potential substitutes for ceramics and more expensive metallic reinforcements in AMCs [Nem16b, Cha13] because of their remarkable properties such as low cost, high strength, good resistance to corrosive environments along with good fatigue, creep and wear properties [Sto98, Dee96]. AMCs containing different volume fractions of Fe_3Al particles (varying from 10 to 80 vol.%) were synthesized by powder metallurgy and characterized using the techniques presented in Chapter 3.

The focus of the current chapter is thus to investigate the effectiveness of the interfacial reaction as a strengthening method for the Al-Fe_3Al composites. To achieve this aim, transformed and non-transformed composites have been produced by hot pressing of Al-Fe_3Al powder blends at 743 and 903 K, respectively. Phases and microstructures of the consolidated composites have been studied in detail and presented in the first part of this chapter. Subsequently, phase evolution sequence incepted by the Al-F_3Al reaction is explicitly discussed. The observed reaction takes place at interface of millimeter sized Fe_3Al particle imbedded in aluminum matrix, when heated up to 903 K. The (micro)structural modifications originated by the transformation have been correlated with the observed variations of the mechanical properties in the last section of this chapter. The major part of this research has been published in Ref [Sha17].

5.1 *Phase analysis and microstructural characterization*

Figure 5.1(a) and (b) display the XRD patterns of the non-transformed and transformed AMCs hot pressed at 743 and 903 K, respectively, along with the patterns of the unreinforced Al matrix ($V = 0$) and single-phase Fe_3Al intermetallic ($V = 100$). The patterns of the AMCs in Figure 5.1(a) show the presence of the D0₃-type Fe_3Al and f.c.c.-aluminum only, which indicates that no reaction between matrix and reinforcement takes place during consolidation of the composites at 743 K. Hot pressing of the materials at 903 K leads to the formation of

additional intermetallic phases due to the interfacial reaction between aluminum and Fe₃Al, as shown in Figure 5.1(b).
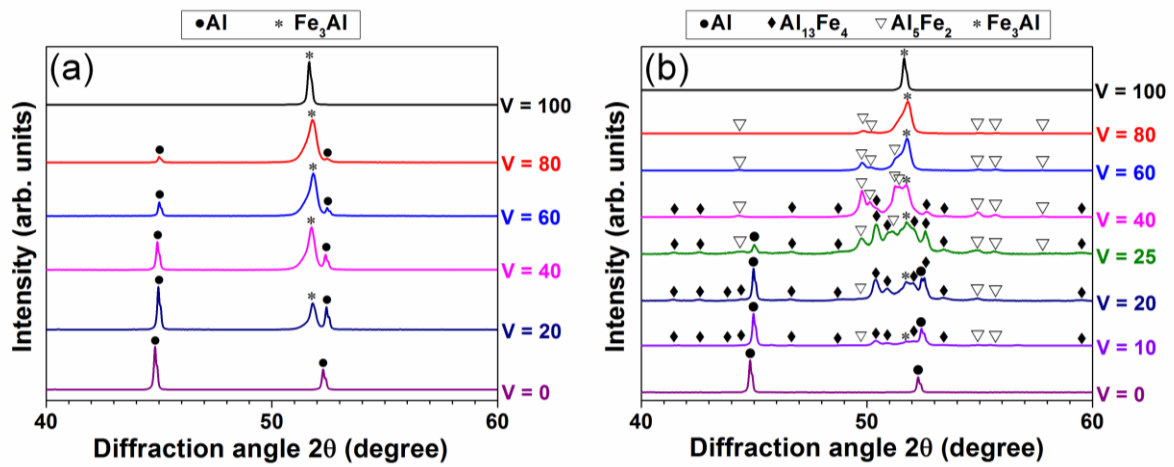

Figure 5.1 *XRD patterns (Co Kα radiation) of pure aluminum (V = 0), single-phase Fe₃Al intermetallic (V = 100) and Al-Fe₃Al composites **(a)** non-transformed hot pressed at 743 K and **(b)** transformed hot pressed at 903 K. Here 'V' indicates the initial volume percent of Fe₃Al.*

Figure 5.2 *SEM images and EDX elemental maps of Al (red) and Fe (green) distribution for the non-transformed AMCs hot pressed at 743 K with initial Fe₃Al content **(a-d)** 20, **(e-h)** 40, **(i-l)** 60 and **(m-p)** 80 vol.%.*

The XRD patterns for the transformed composites with 10 and 20 vol.% of initial Fe_3Al ($V = 10$ and 20) reveal the presence of monoclinic $Al_{13}Fe_4$ phase and a small amount of orthorhombic Al_5Fe_2 along with residual aluminum and Fe_3Al. The formation of Al_5Fe_2 and $Al_{13}Fe_4$ is in agreement with previous reports on intermetallic in-situ formation in the Al-Fe system [Lee03a, Csa88].
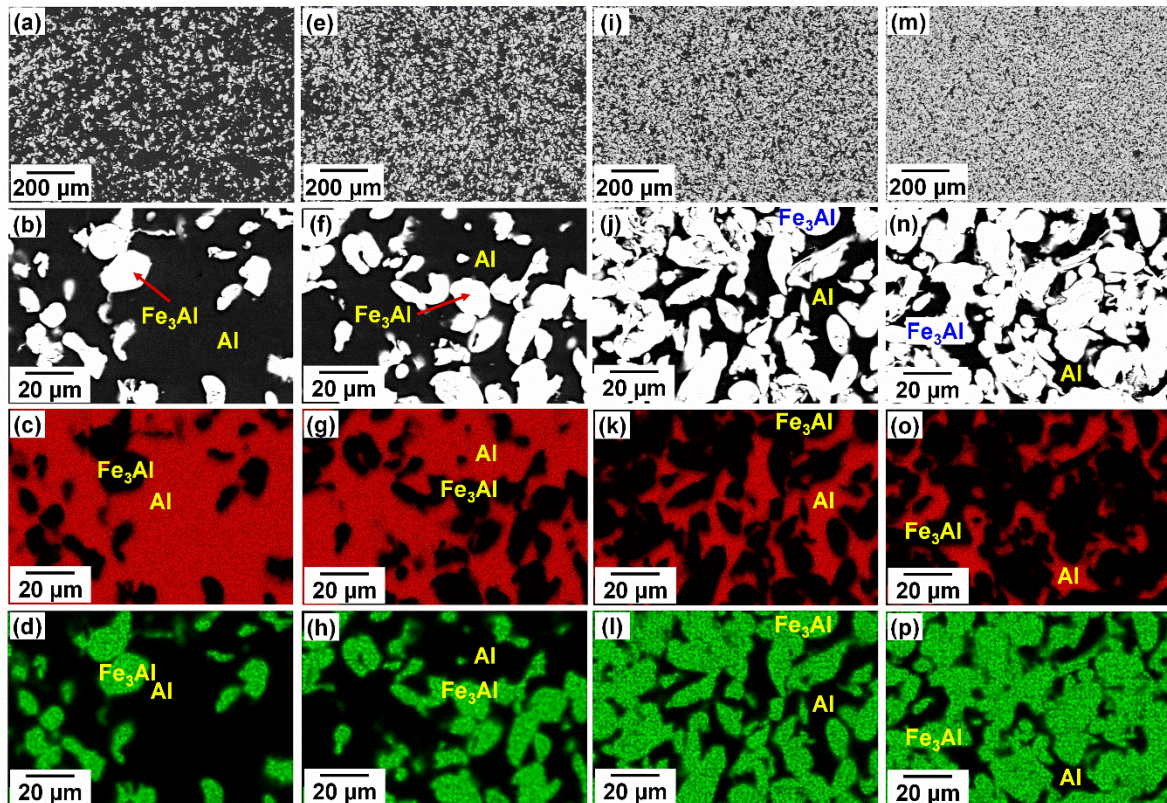

Figure 5.3 *SEM images and EDX elemental maps of Al (red) and Fe (green) distribution for the transformed AMCs hot pressed at 903 K with initial Fe₃Al content (a-d) 10, (e-h) 20 and (i-l) 25 vol.%.*

In the transformed samples with $V = 25$ and 40 the amount of Al_5Fe_2 increases significantly while the intermetallics $Al_{13}Fe_4$ and Fe_3Al are also present. The transformed composite with $V = 25$ retains a small amount of aluminum whereas no residual Al is visible in composite with $V = 40$, suggesting that the Al matrix has been partially utilized by the matrix-reinforcement reaction by increasing the initial volume fraction of Fe_3Al and it has been

entirely consumed in the transformed composite with $V = 40$. The XRD patterns for the transformed composites with $V = 60$ and 80 show only the diffraction peaks of Al_5Fe_2 and Fe_3Al, whereas the $Al_{13}Fe_4$ phase is not observed.
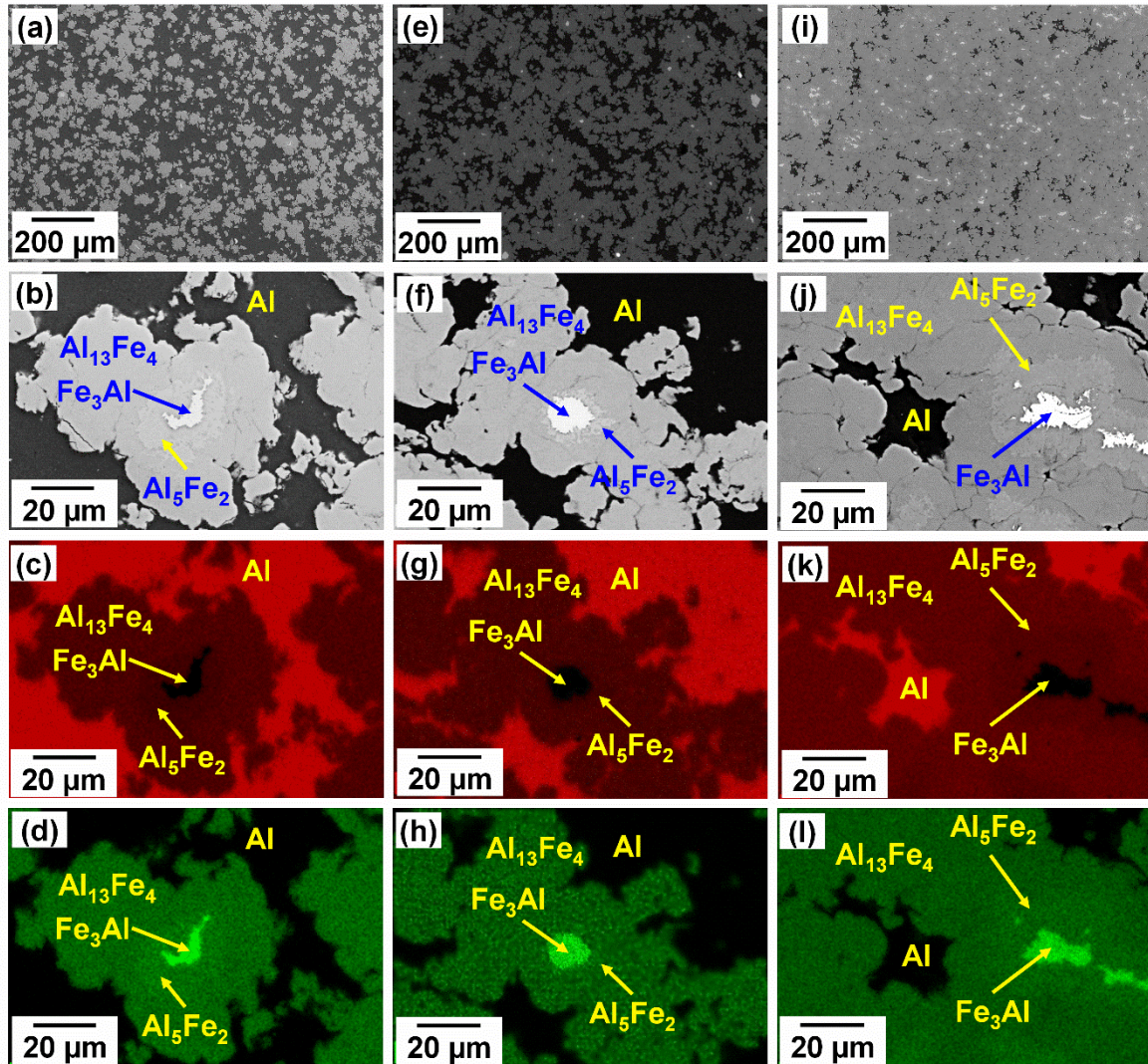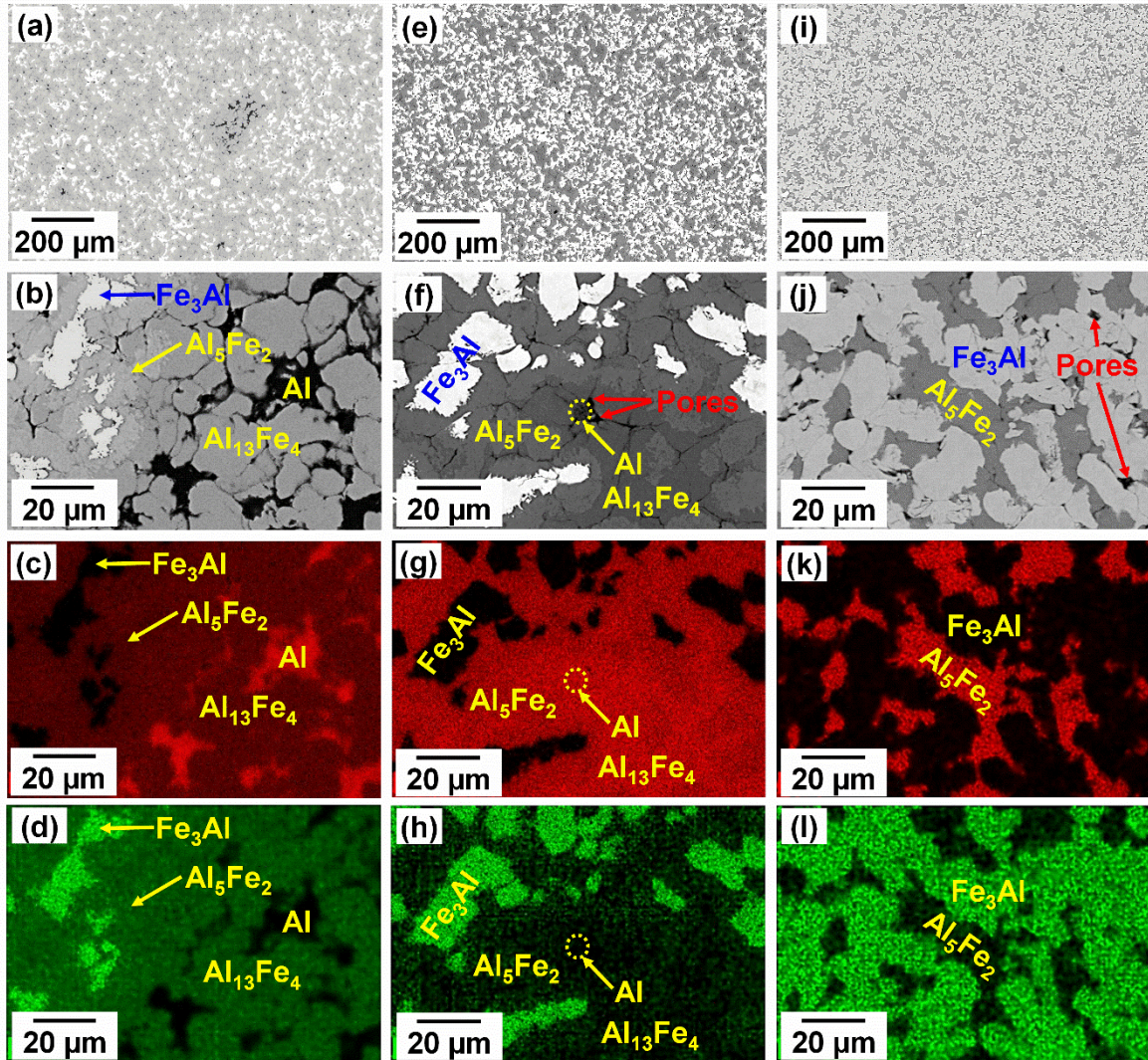

Figure 5.4 *SEM images and EDX elemental maps of Al (red) and Fe (green) distribution for the transformed AMCs hot pressed at 903 K with initial Fe₃Al content **(a-d)** 40, **(e-h)** 60 and **(i-l)** 80 vol.%.*

The SEM images and EDX elemental maps of the non-transformed AMCs, presented in Figure 5.2, show the uniform distribution of the Fe₃Al particles in the aluminum matrix. EDX analysis displays only the initial components (aluminum and Fe₃Al), corroborating the XRD results shown in Figure 5.1(a). The microstructure of the transformed composites is also rather homogeneous. The SEM micrographs and EDX elemental distribution maps for the transformed composites are shown in Figure 5.3 and 5.4. EDX elemental concentration profiles of the transformed composites obtained by line scans are displayed in Figure 5.5 and 5.6. The

elemental area maps and concentration profiles confirm the presence of the reaction products around the Fe_3Al particles in the form of core-shell structures. In the transformed specimens with $V = 10$ and 20, the Fe_3Al core is surrounded by Al_5Fe_2, which is itself covered by $Al_{13}Fe_4$ and, finally, aluminum is present at the outermost boundary of this multiphase microstructure. With increasing amount of initial Fe_3Al reinforcement to $V = 25$, Al is limited to isolated regions, which gradually shrink in the composites with $V = 40$ and 60. The corresponding XRD patterns of these composites ($V = 40$ and 60) in Figure 5.1(b) do not show residual Al; this is most likely due to the extremely small amount of Al below the detection limit of the device. In the transformed composite with $V = 80$ only Al_5Fe_2 and residual Fe_3Al are present, confirming the XRD results shown in Figure 5.1(b).
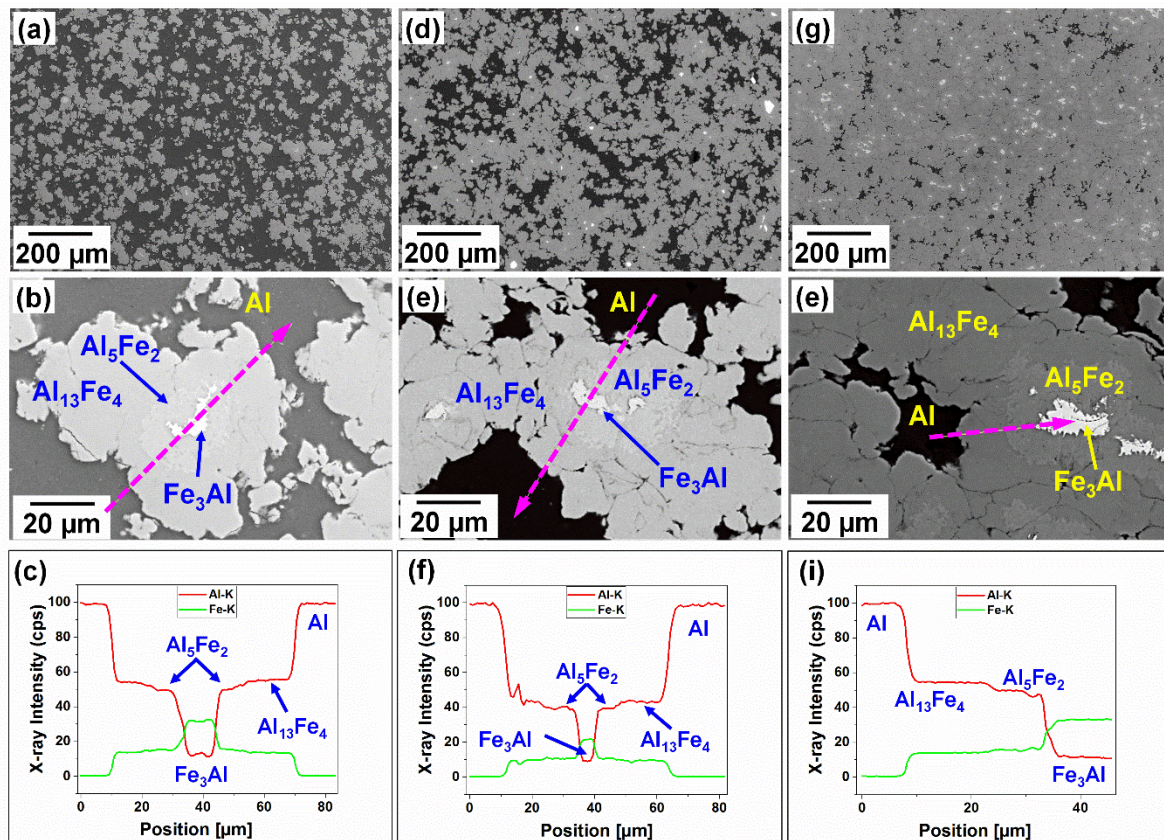

Figure 5.5 *SEM images and EDX elemental concentration profiles for the transformed composites hot pressed at 903 K with initial Fe₃Al content (**a, b, c**) 10, (**d, e, f**) 20 and (**g, h, i**) 25 vol.%. The dashed red arrows represent the scanned EDX line.*

The in-situ formation of core-shell structures in iron or iron-aluminide reinforced AMCs has been already observed [Lag16, Xue15, Wan14]. In these studies, it has been reported that the reaction between matrix and reinforcement leads to the formation of a single shell around the initial reinforcement core; in contrast to the present study, where the formation of a

doubleshell-reinforcement (i.e. Al_5Fe_2 and $Al_{13}Fe_4$ around Fe_3Al) is observed. This behavior can be ascribed to the different starting materials used in the current work and, consequently, to the different reaction paths, which most likely do not allow the reaction to reach completion in the present consolidation conditions of temperature and pressure.
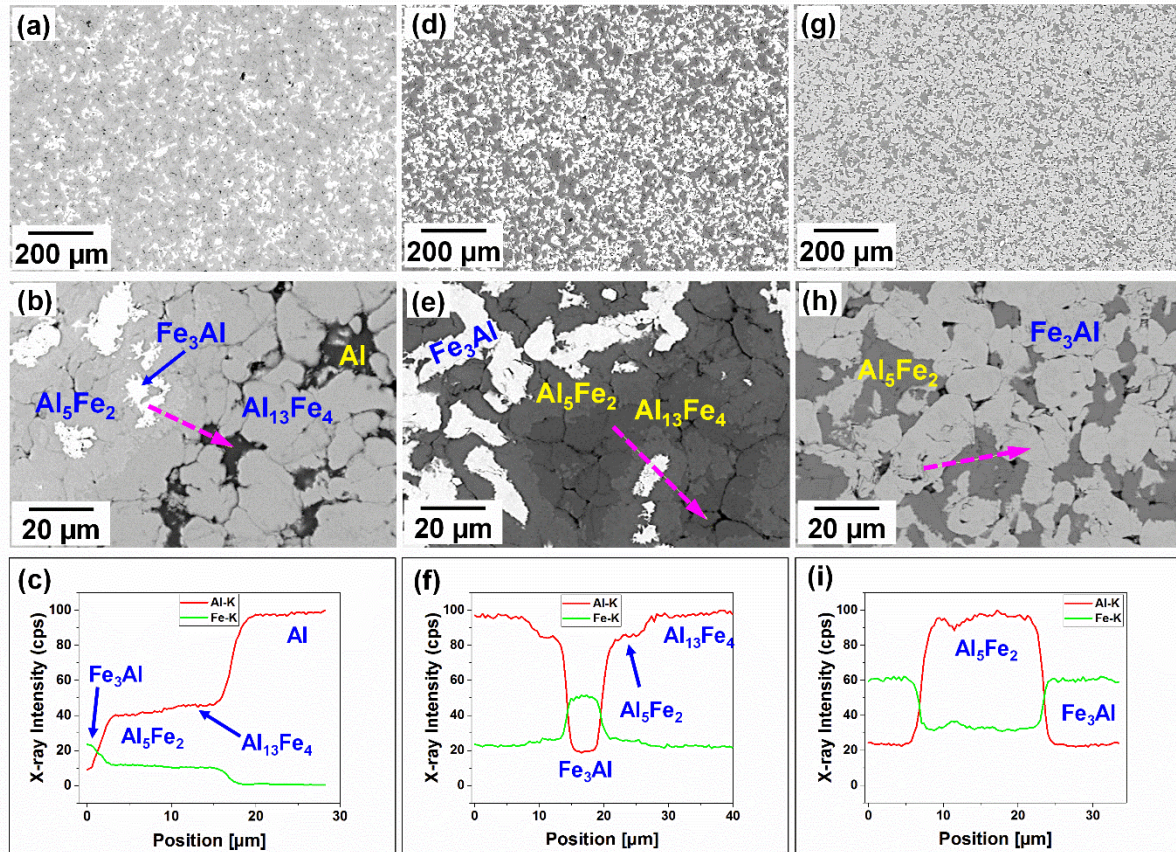

Figure 5.6 *SEM images and EDX elemental concentration profiles for the transformed composites hot pressed at 903 K with initial Fe₃Al content (**a, b, c**) 40, (**d, e, f**) 60 and (**g, h, i**) 80 vol.%. The dashed purple arrows represent the scanned EDX line.*

The volume fraction of the different phases (evaluated from the SEM micrographs) present in the transformed AMCs is shown in Figure 5.7(a) as a function of the initial Fe_3Al content V. The amount of Al_5Fe_2 is negligible (0.3 vol.%) in the transformed composite with $V = 10$, afterwards it progressively increases from ~10 vol.% for $V = 20$ to about 50 vol.% in the composite with $V = 40$ and then it gradually decreases to 30 vol.% for $V = 80$. The quantity of $Al_{13}Fe_4$ is ~ 40 vol.% at $V = 10$, reaches a maximum value (58 vol.%) for $V = 20$ and then it progressively decreases to 0 vol.% for $V = 80$. The amount of Al gradually decreases from 60 to 7 vol.% with increasing V from 10 to 25 then subsequently decreases to ~2 vol.% at $V = 60$ and steadily reaches 0 vol.% for $V = 80$. In contrast, the amount of Fe_3Al slowly increases from 0.5 to 1.12 vol.% with increasing the initial reinforcement content V from 10 to 25 vol.%. Later

it increases progressively to 88 vol.% with increasing the initial reinforcement content *V* from 20 to 100. The discrepancy between expected and experimentally observed Fe₃Al content for the single-phase Fe₃Al phase can be ascribed to the high porosity of this specimen (Figure 5.7(b)). The vol.% profiles of pure aluminum and Fe₃Al in Figure 5.7(a) intersect at about *V* = 30, which suggests that Al act as major soft phase for the transformed AMCs from *V* = 0 to 30 and, hereafter, the Fe₃Al phase acts as soft matrix up to *V* = 100. This partition is indicated by the vertical straight lines in Figure 5.7(a).
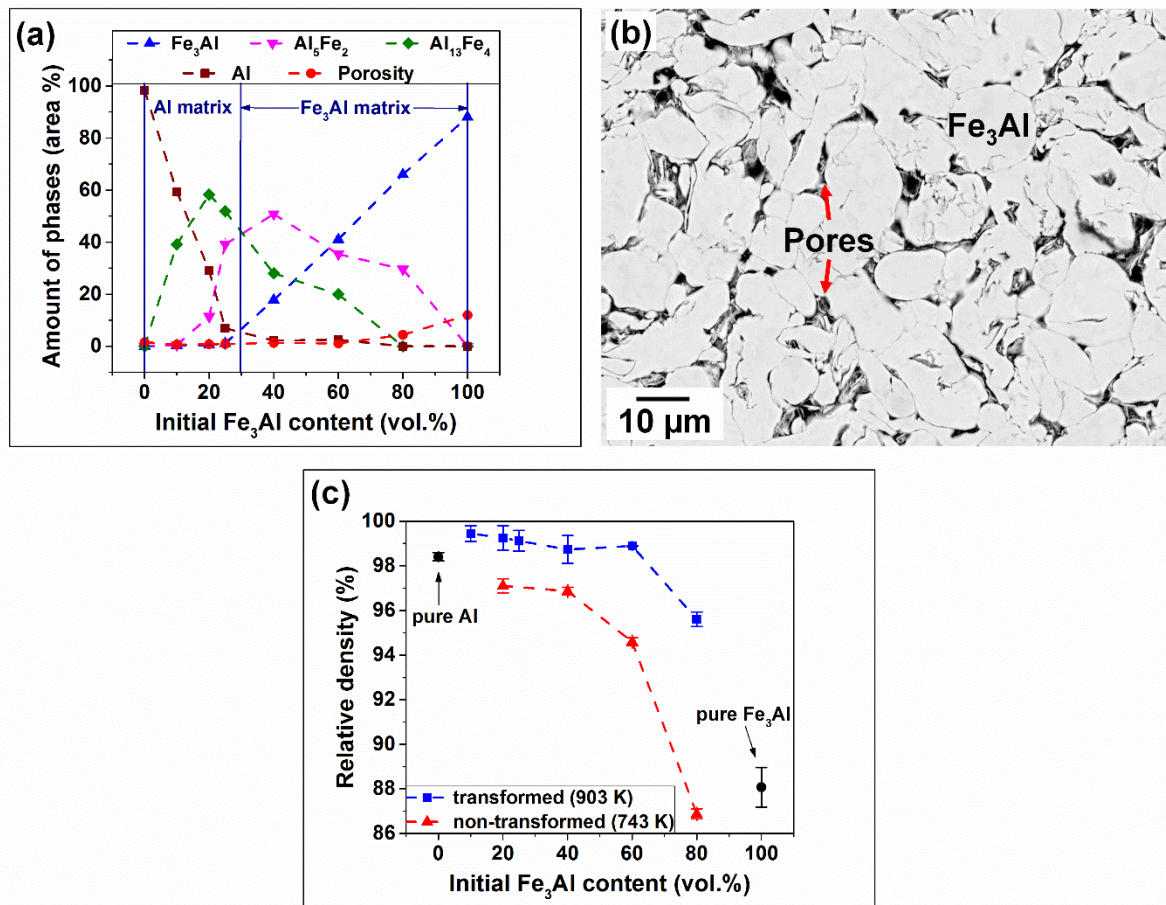

Figure 5.7(a) *Variation of the amounts of the different phases present in the transformed composites hot pressed at 903 K. **(b)** SEM image for Fe₃Al hot pressed at 903 K revealing high porosity. **(c)** Relative density values of transformed and non-transformed composites as a function of the initial volume percent of Fe₃Al reinforcement.*

Figure 5.7(c) displays the relative density of the composites consolidated at 743 and 903 K. To calculate the relative density, the experimental density measured by the Archimedes method is divided by the theoretical density. For the non-transformed composites (743 K), the theoretical density was calculated from the initial Fe₃Al content, whereas for the transformed composites (903 K) it was determined using the vol.% of the phases that have been experimentally observed in the transformed AMCs (Figure 5.7(a)). The relative density of the

69

pure Fe_3Al is $88 \pm 1\%$, which confirms the large porosity visible in Figure 5.7(b), while the density of the unreinforced pure Al is $98.4 \pm 0.2\%$. This indicates that the hot pressing temperature used for consolidating the single-phase Fe_3Al is too low to achieve highly-dense specimens. The relative density of the non-transformed composites decreases from 98 ± 0.1 to $87 \pm 0.2\%$ with increasing the Fe_3Al content. This behavior can be ascribed to the difficulty of sintering the composites with increasing amount of Fe_3Al-Fe_3Al interfaces observed for large reinforcement contents. The transformed AMCs with $V = 20$, 40 and 60 all display values of relative density exceeding 98.5%, implying that for these compositions the transformation occurring during sintering (along with the higher hot pressing temperature) leads to materials with improved density compared with the non-transformed composites. Finally, the relative density decreases to $95.6 \pm 0.3\%$ for the material with $V = 80$, most likely because of the larger amount of hard-to sinter Fe_3Al-Fe_3Al interfaces.

Figure 5.8 *SEM micrographs and EDX elemental concentration profiles for the composites consisting of the Al matrix and mm-sized Fe₃Al particles hot pressed at (**a, b, c**) 823, (**d, e, f**) 873 and (**g, h, i**) 903 K. The dashed purple arrows represent the scanned EDX line.*

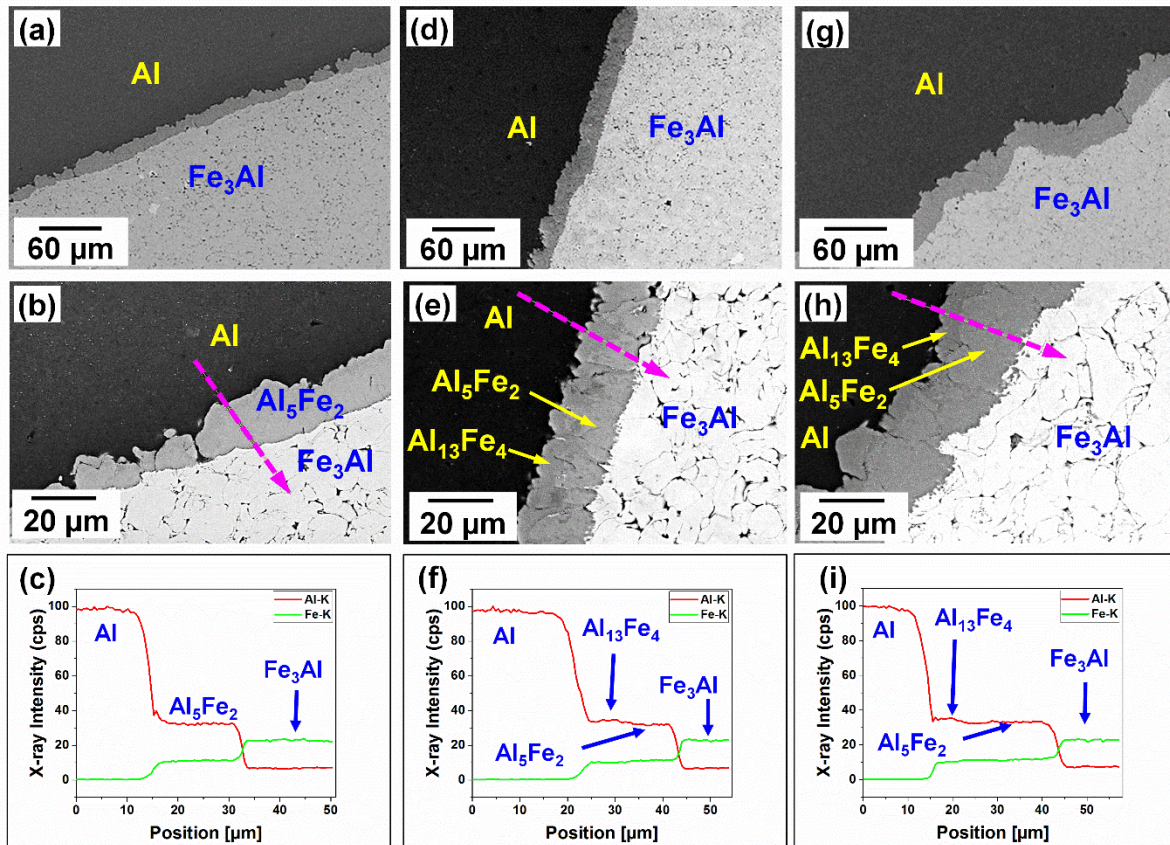Figure 5.8 shows the SEM micrographs and EDX elemental concentration profiles of the composites consisting of the Al matrix and a single mm-sized Fe_3Al particle produced by hot

pressing at 823, 873 and 903 K (see Chapter 3). The presence of a single Fe_3Al particle permits to analyze the phase sequence resulting from the $Al-Fe_3Al$ reaction without the interference of the diffusion and reaction fields from additional particles. The microstructure of the composites consists of the starting Al and Fe_3Al phases along with a thin layer at the Al- Fe_3Al interface due to the reaction between matrix and reinforcement. The thickness of the interfacial reaction layer initially increases from 15 ± 1 µm for the sample hot pressed at 823 K to 29 ± 4 µm for hot pressing at 873 K and it only slightly increases to 31 ± 2 µm for the sample synthesized at 903 K, which suggests that the reaction slows down when the thickness of the reaction layer is about 30 µm. The concentration profiles reveal that the first phase formed is the Al_5Fe_2 phase at 823 K (Figure 5.8(c)). $Al_{13}Fe_4$ is formed at higher temperatures between the Al matrix and the Al_5Fe_2 phase formed at 823 K (Figure 5.8(f) and (i)).
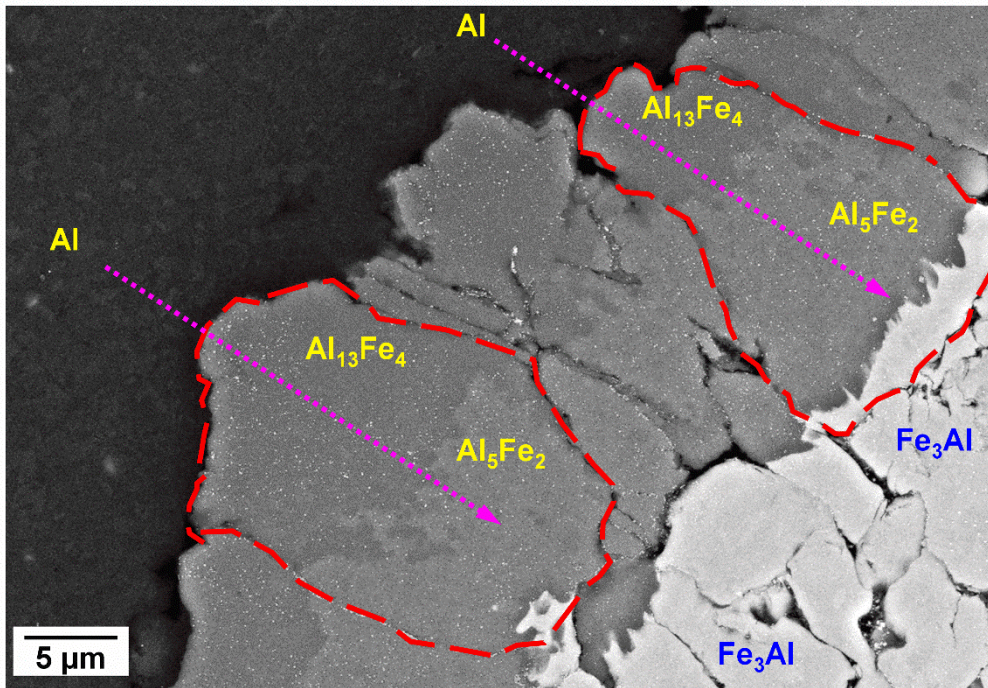
Figure 5.9 *SEM micrograph for the composite with a single mm-sized Fe_3Al particle hot pressed at 903 K showing the formation of the Al_5Fe_2 and $Al_{13}Fe_4$ phases within the original Fe_3Al particles. The dotted purple arrows represent the direction of Al diffusion.*

The formation of Al_5Fe_2 and $Al_{13}Fe_4$ takes place exclusively within the original Fe_3Al particles, as shown in Figure 5.9, where the particle boundaries (indicated by the red dashed contours) enclose the Fe_3Al, Al_5Fe_2 and $Al_{13}Fe_4$ phases and no Fe-containing phases are observed within the Al matrix. Therefore, Al diffuses into the Fe_3Al particles to form Al-rich Fe-Al phases, whereas no Fe diffusion occurs towards the Al matrix. The almost constant layer thickness of about 30 µm for hot pressing at temperatures ≥873 K can be correlated with the

decreased driving force for Al diffusion resulting from the reduced composition gradient. This can also explain the incomplete Al-Fe$_3$Al reaction in the present consolidation conditions and the formation of the double-shell structure observed in Figure 5.3 to 5.6, where the distance between the isolated areas of residual Al generally exceeds 30 μm.

A schematic description of the different phases present in the current AMCs is given in Figure 5.10(a)-(g)). A non-transformed AMC with $V = 20$ displaying exclusively the initial phases is shown in Figure 5.10(a). When the same composite is consolidated at 903 K, the reaction has fully consumed Fe$_3$Al to form Al$_{13}$Fe$_4$ and Al$_5$Fe$_2$ (Figure 5.10(b,c)). Only small traces of residual Fe$_3$Al (0.5 ± 0.1 vol.%) were rarely observed (Fig. 3(b,c)). The composites with $V = 40$ and 60 show the presence of Fe$_3$Al, Al$_5$Fe$_2$ and Al$_{13}$Fe$_4$ in the form of core shell structures (Figure 5.10(d) - (f)), while the amount of Al is negligible (~2 vol.%) and only occasionally was observed by SEM (Figure 5.10(e) and (f)). In case of the transformed material with $V = 80$, only Fe$_3$Al and Al$_5$Fe$_2$ are present because Al has been entirely consumed to form Al$_{13}$Fe$_4$, which most likely further transforms into Al$_5$Fe$_2$ due to higher Fe concentration of the composite (Figure 5.10(g)).
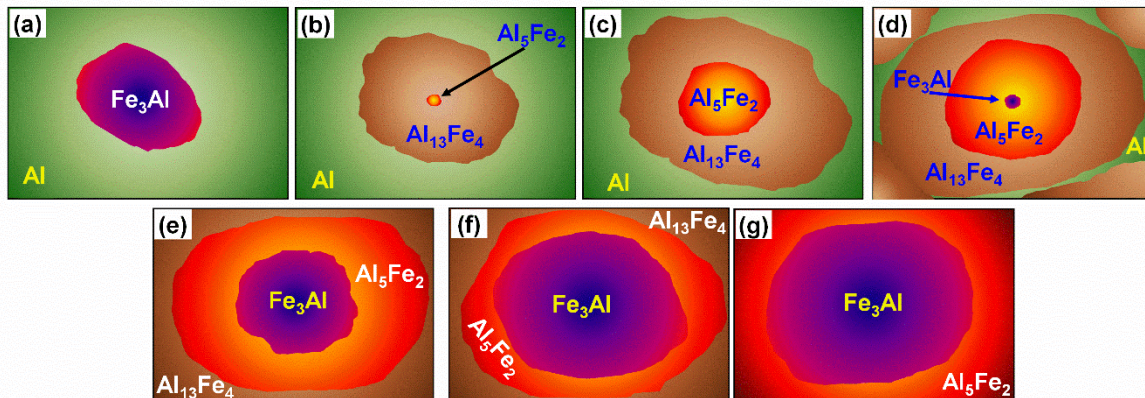
Figure 5.10 *Schematic representation of the composites with initial Fe₃Al content (a) 20 vol.% hot pressed at 743 K, (b) 10, (c) 20, (d) 25, (e) 40, (f) 60, and (g) 80 vol.% hot pressed at 903 K.*

5.2 *Effect of interfacial reaction on the mechanical behavior*

The room-temperature stress-strain curves under compression for the non-transformed and transformed composites are shown in Figure 5.11(a) and (b) and the corresponding mechanical data are summarized in Figure 5.11(c-e). The yield strength (0.2% offset) for the non-transformed AMCs increases from 66 ± 7 MPa for the unreinforced Al matrix ($V = 0$) to 360 ± 10 MPa for the composite with $V = 80$ (Figure 5.11(c)). The compressive strength (the

highest compressive stress that the material is able to bear [AST03]) also increases with increasing Fe_3Al up to 490 ± 20 MPa for $V = 80$ (Figure 5.11(d)). The AMCs with $V = 20$ and 40 did not show failure up to 20% strain, where the test was stopped (Figure 5.11(e)). Despite the high porosity of the specimen, the yield and compressive strengths of the pure Fe_3Al ($V = 100$) reach values of 690 ± 10 and 990 ± 30 MPa, respectively, along with $11 \pm 1\%$ strain. In the transformed composites (Figure 5.11(b)), both yield and compressive strengths are drastically increased after the phase transformation, while the plastic deformability is generally reduced compared with the non-transformed AMCs. The yield strength of these materials first increases with the increase of initial Fe_3Al up to $V = 40$ and afterward it gradually decreases (Figure 5.12(b)).
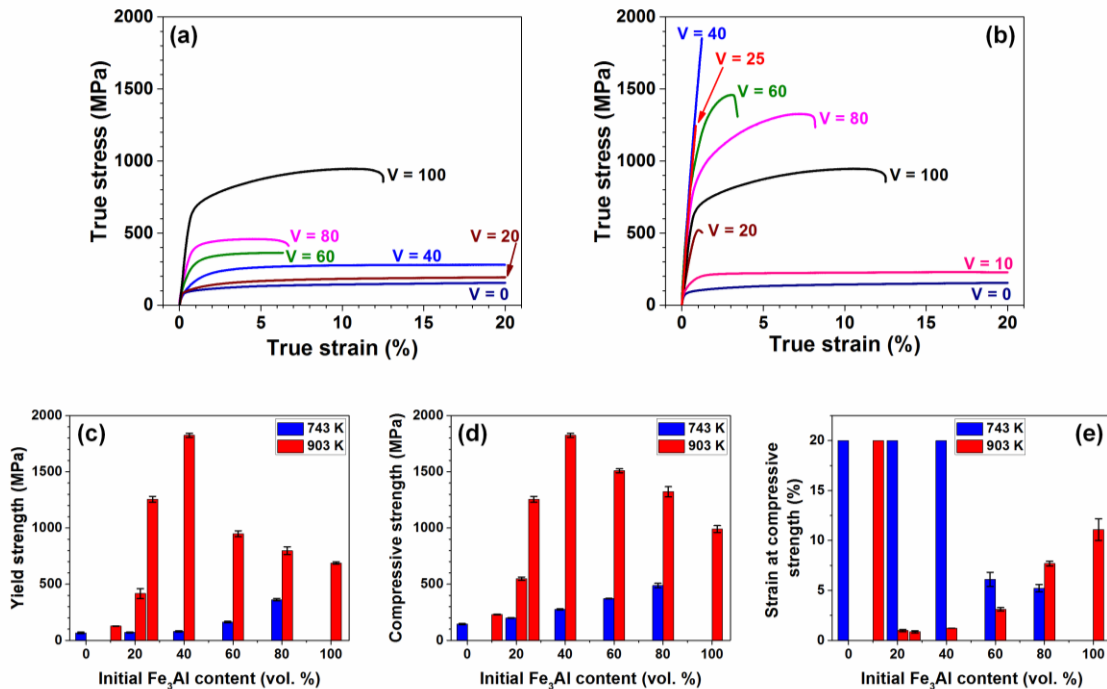

Figure 5.11 *Room temperature compression stress-strain curves for (**a**) non-transformed AMCs hot pressed at 743 K and (**b**) transformed composites hot pressed at 903 K along with pure aluminum and pure Fe₃Al (V indicates the initial volume percent of Fe₃Al). Summary of the mechanical data for transformed and non-transformed composites: (**c**) yield strength, (**d**) compressive strength and (**e**) strain at compressive strength*

On the other hand, plastic deformation increases by increasing the initial amount of Fe_3Al from $V = 25$ to 100. The maximum value of yield strength, which in this case coincides with the compressive strength, is 1820 ± 18 MPa in the transformed composite with $V = 40$, whereas the transformed material with $V = 10$ shows the minimum values of yield (127 ± 1 MPa) and compressive (230 ± 2 MPa) strengths. These results are in line with the compressive strength reported for AMCs reinforced with iron-aluminides. For example, 270 MPa strength was

observed for Al-1 vol.% Fe composite prepared by cold pressing and then sintering in nitrogen environment [Xue15]. This value increases to 461 MPa for Al-20 vol.% Fe composite prepared by cold pressing, sintering and subsequent hot extrusion [Wan14], 550 MPa for 15 mass % Fe-Al composite prepared by powder metallurgy processing [Fat15], 700 MPa for 20 vol.% Al-Al_5Fe_2 composite [Kra16], and, finally, to 1130 MPa for 10 at. % Fe-Al composite prepared by mechanical milling followed by spark plasma sintering [Gu12]. Although a direct comparison with the present results is not possible because of the different phases and microstructure involved, this indicates that the mechanical behavior of the Al-FeAl composites can be tuned within a wide range of strength depending on the initial volume fraction of reinforcement as well as on the reaction between matrix and reinforcement and final phases and microstructures.
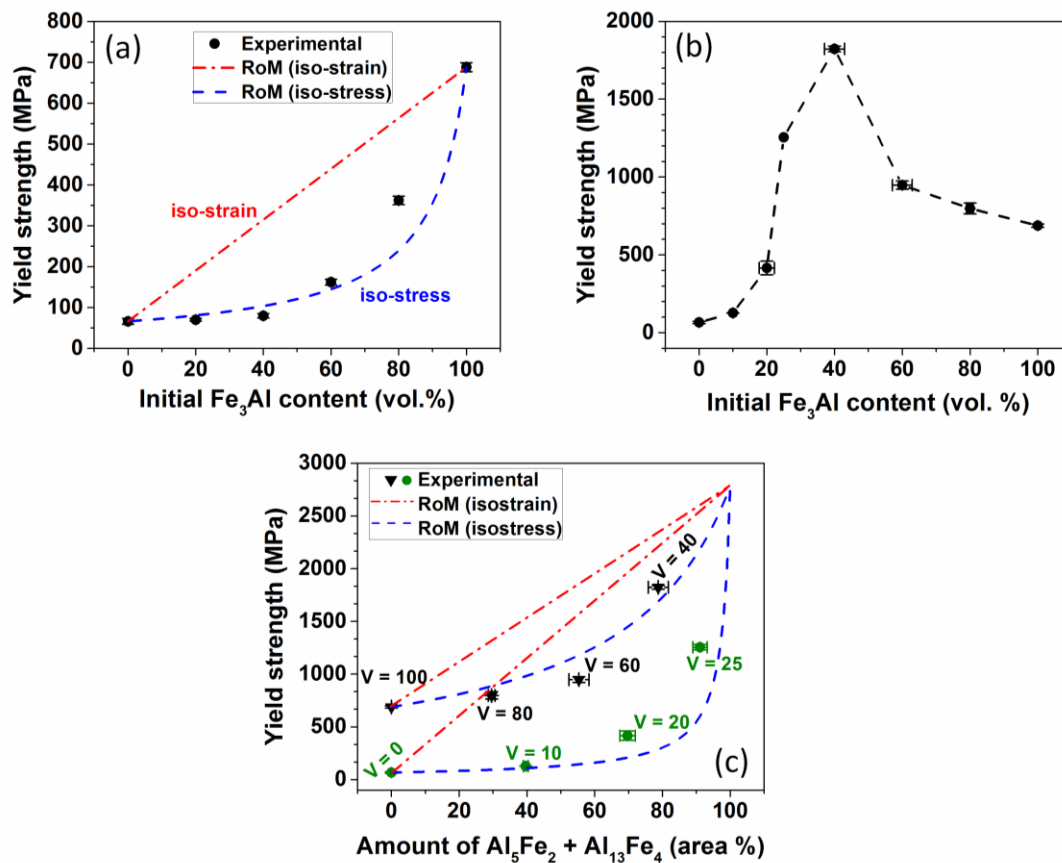
Figure 5.12 *Yield strength as a function of the initial Fe₃Al content for the (**a**) non-transformed and (**b**) transformed composites. (**c**) Yield strength of the transformed composites as a function of the cumulative amount of Al₅Fe₂ and Al₁₃Fe₄. V indicates the initial volume fraction of Fe₃Al. The yield strength for the 100% Al₅Fe₂+Al₁₃Fe₄ in (**c**) is calculated from their hardness given in Ref: [Eck10].*

The yield strength of the non-transformed AMCs (square data points) is shown in Figure 5.12(a) along with the values predicted by the RoM according to the iso-stress (dashed blue

line) and iso-strain (dot-dashed red line) models [Scu08, Cha87] (please refer to Equation 2.1 & 2.2 in Chapter 2 for iso-strain and iso-stress models). The iso-strain model, which assumes that matrix and reinforcement experience the same strain during deformation [Cha87], overestimates the yield strength of the non-transformed AMCs. In contrast, the yield strength for these composites is in good agreement with the iso-stress model (matrix and reinforcement experience the same stress [Cha87]) except in the case of the AMC with $V = 80$, for which the strength is higher than expected. The iso-strain model describes well the strength of composites with large volume fraction of reinforcement, where the distance between the reinforcing particles is small [Kim01]. In this case, the reinforcing particles come closer to each other in the loading direction and then they may undergo deformation due to load transfer [Kim00]. In contrast, the iso-stress model performs well for composites with small volume fraction of reinforcement (i.e. with longer distances between the reinforcing particles), where the deformation mainly occurs in the soft matrix [Kim01, Kim00, Li99]. This can explain the deviation of the yield strength of the AMC with $V = 80$ from the iso-stress towards the values predicted by the iso-strain model. Similar results have been observed for Al-based matrix composites reinforced with Al-Ti intermetallics [Wan15a] and metallic glasses [Scu08], which also follow the iso-stress model, in accordance with the conclusions of Li et al. [Li99].

Due to the phase and microstructure changes, the yield strength of the transformed composites neither follows the iso-stress nor the iso-strain model when considering the initial amount of Fe₃Al (Figure 5.12(b)). When the experimental data are plotted vs. the cumulative amount of Al₁₃Fe₄ and Al₅Fe₂ (Figure 5.12(c)), the data can be grouped according to the main soft phase (i.e. Al or Fe₃Al matrix) present in the material (see Figure 5.7(a)) and the strength of the composites can be again fitted using the iso-stress model. The black triangular data points represent the samples with no or very limited amount of Fe₃Al after the transformation reaction. Here, Al is the soft matrix. For example, in the transformed composite with $V = 20$ the amount of Al is ~30%, while Fe₃Al is only about 0.5%. Although this composite has an amount of Al₁₃Fe₄ + Al₅Fe₂ of ~70%, the presence of the very soft Al matrix induces lower yield strength than the transformed composites with $V = 40$, 60 and 80. Similarly, the transformed composite with $V = 25$ contains ~80% of Al₁₃Fe₄ + Al₅Fe₂ with 1% of F$_e$3Al but due to the presence only 7 % aluminum in the shape of isolated islands its strength is also quite lower than the transformed composites with $V = 40$, 60 and 80. On the other hand, for the composites with no or negligible amount of Al ($V \geq 40$; round green data points in Figure 5.12(c)), Fe₃Al is the soft matrix that dictates the mechanical behavior of the composites.

The investigations and the findings reported in Chapter 5 describe that addition of Fe_3Al reinforcement in aluminum matrix using P/M process generates homogeneous microstructure in transformed and non-transformed composites. At higher temperature aluminum atoms diffuse into Fe_3Al particles to create first reaction product Al_5Fe_2. Further increase in the temperature produces $Al_{13}Fe_4$ between aluminum matrix and Al_5Fe_2 phase. In the Al-rich composites, a double-shell-reinforcement with Al_5Fe_2 and $Al_{13}Fe_4$ intermetallics surrounding the Fe_3Al phase is formed, while the Al matrix is progressively consumed with increasing the reinforcement content. Conversely, in the reinforcement-rich composites only Al_5Fe_2 and residual Fe_3Al are present. Yield and compressive strength of the non-transformed composites increase from 70-360 MPa and 200-500 MPa, respectively by increasing Fe_3Al amount while in-situ phase transformation enhances these values to 130-1800 MPa and 550-1800 MPa for the transformed materials. The transformed composite with 80 vol% of initial Fe_3Al reinforcement displays the best compromise between strength and plasticity: yield and compressive strengths exceed that of the corresponding non-transformed composite by a factor of about 2.5, while retaining appreciable plastic deformation of 7%. The yield strength of both transformed and non-transformed composites follows the iso-stress model when the characteristic structural features (i.e. strengthening phases and matrix) are taken into account.

Chapter 6. Strengthening of Al-Fe₃Al composites by the generation of harmonic structures

The incorporation of a hard phase in a soft metallic matrix improves the strength of a composite due to the higher load bearing ability of the reinforcement [Kai06, Dav93]. Furthermore, dislocations multiplication and their reduced mobility due to the microstructural variations caused by the reinforcement addition enhance the composite strength [Ars91, Mil91]. The strength of composites increases by increasing the reinforcement content, through reinforcement size reduction and microstructural refinements that are commonly achieved by ball milling [Sur13b, Cha01]. Beside these conventional techniques of composite strengthening, unconventional methods like in-situ phase transformation and generation of harmonic microstructures can also be used. Harmonic structures are a type of heterogeneous bimodal microstructure which offers strength with appreciable retained plastic deformation. It consists of coarse-grained cores embedded in a continuous network of fine-grained matrix. Soft cores contribute in the retained deformability, while the fine-grained continuous network brings the strength [Hua15].

Strengthening of composites by increasing the reinforcement content as well as through in-situ phase transformations has been discussed in Chapters 3 and 4. The present chapter deals with the strengthening of Fe₃Al reinforced AMCs through the generation of harmonic microstructures using ball milling and hot pressing. The effect of ball milling time on the size, shape, distribution and microstructure of the Al-Fe₃Al powder mixtures is analyzed accompanied by the thermal stability of the cold pressed composites obtained from the milled powders. The second part elaborates the microstructural features and phase distributions of the hot pressed composites that contain harmonic structures. The third part presents the mechanical properties of the composites and, finally, the chapter correlates the different features of the harmonic microstructure with the strength of the composites. A model able to predict the strength of particulate reinforced composites containing harmonic structures is proposed. A major portion of this research work has been published in ref: [Sha18].

6.1 Ball milling of Al-Fe₃Al powder mixtures

In order to generate Al-Fe₃Al composites with harmonic structures, powder mixtures consisting of pure aluminum [D(50) = 3 μm, Figure 6.1(a)] and 20 vol.% of Fe₃Al particles

[D(50) = 10 μm, Figure 6.1(b)] were ball milled for different periods (t_m = 1, 5, 10, 20, 30, 40 and 50 h). The SEM image of the Al-Fe₃Al powder mixture milled for 1 h (Figure 6.1(c)) shows that only a limited amount of powder clusters, consisting of Fe₃Al particles trapped by aluminum, are formed at this stage. The increase of milling time to 5 h leads to the formation of larger clusters with a maximum size of about 140 μm along with comparatively less agglomerated aluminum and Fe₃Al particles (Figure 6.1(d)). Clusters consisting exclusively of Fe₃Al particles are not observed.

Figure 6.2(a–e) display the SEM micrographs for the powder mixtures milled for t_m = 10, 20, 30, 40 and 50 h. After 10 h, only Al-Fe₃Al clusters are visible and non-agglomerated aluminum or Fe₃Al particles are not present anymore. The average size of these macro-particles increases with increasing milling time, while the particle size distribution become progressively narrower (Figure 6.2(f) and Table 6.1).
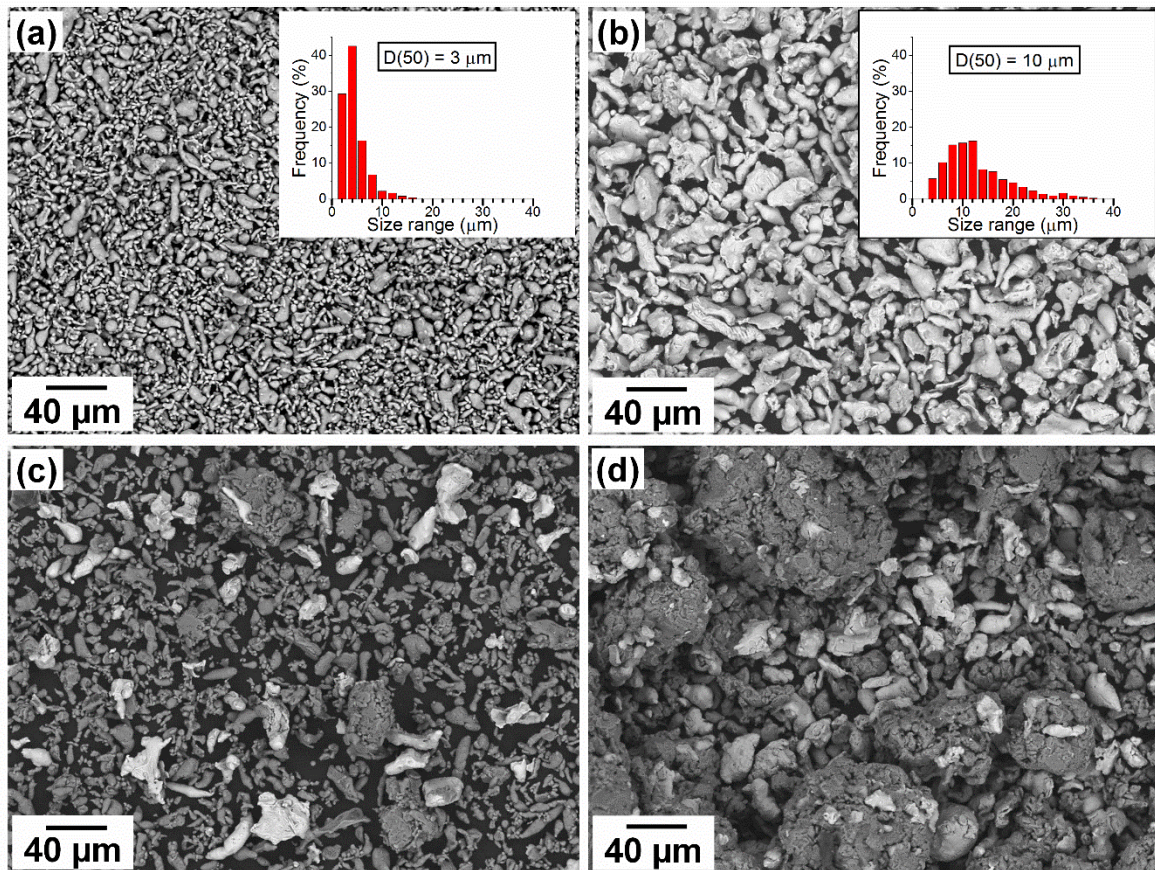

Figure 6.1 *Initial particle morphology. SEM micrographs and corresponding particle size distribution of (**a**) pure aluminum and (**b**) Fe₃Al. Particle morphology for the Al-Fe₃Al powder mixtures milled for (**c**) 1 and (**d**) 5 h.*
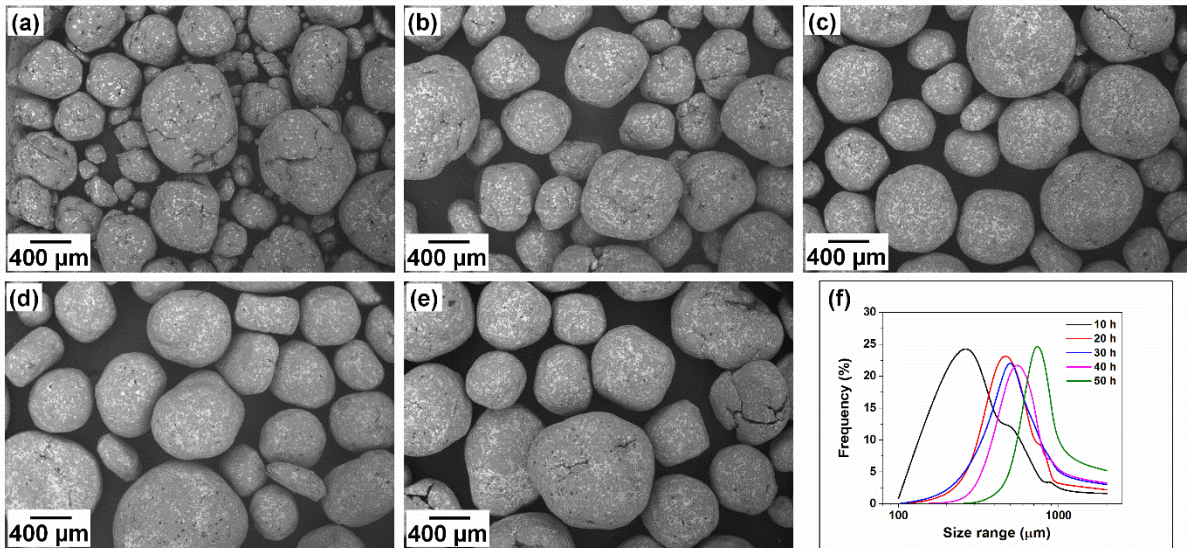
Figure 6.2 *Effect of ball milling on particle size. SEM micrographs of the Al-Fe₃Al powder mixtures milled for (a) 10, (b) 20, (c) 30, (d) 40 and (e) 50 h. (f) Particle size distributions of the powders milled for different periods.*

Table 6.1 *Effect of milling time on particle size, shell thickness and transformation temperature for the Al-Fe₃Al powder mixtures.*

Milling time (h)	Particle size D(50) (μm)	Shell thickness (μm)	Transformation temperature (K)
1	---	---	769
10	300	8 ± 0.6	747
20	490	15 ± 1.3	730
30	510	21 ± 0.8	722
40	570	27 ± 1.5	712
50	800	33 ± 1.6	702

The characteristic microstructure of the macro-particles is reported in Figure 6.3, which shows the SEM images of the polished cross-section of the milled powders as a function of the milling time for $t_m \geq 10$. Every macro-particle displays a core consisting of relatively large Fe₃Al particles embedded in the Al matrix, which is surrounded by a shell made of Al and small, mostly sub-micron, Fe₃Al particles. In the core, the dispersion of Fe₃Al is fairly homogeneous and the presence of submicron Fe₃Al particles is rare. This indicates that after the formation of the macro-particles at $t_m = 10$ h the microstructural refining induced by ball milling is limited to their surface. Here, the Fe₃Al particles are progressively fragmented by the action of the milling media and the thickness of the shell increases with increasing the

milling time (Table 6.1). The preferential microstructural refinement limited to the surface of the particles is a necessary prerequisite for the generation of harmonic structures during subsequent powder consolidation [Saw14].
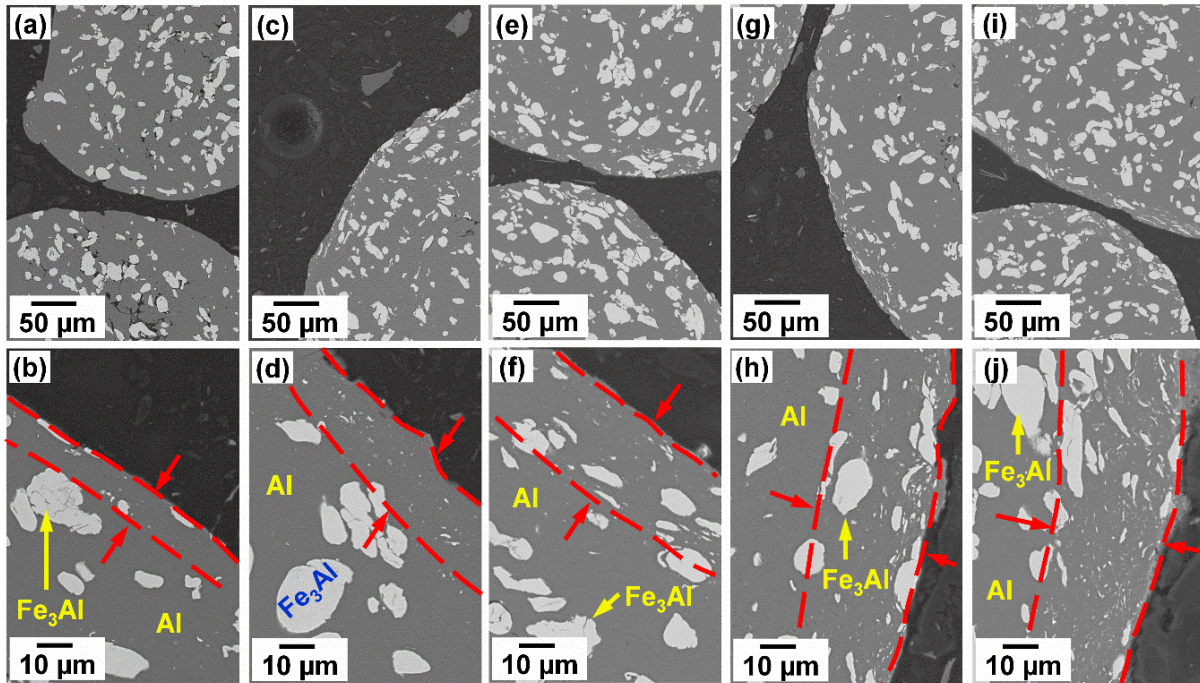
Figure 6.3 *Effect of ball milling on particle microstructure. SEM images of the polished cross-section of the Al-Fe₃Al powder mixtures milled for (**a**, **b**) 10, (**c**, **d**) 20, (**e**, **f**) 30, (**g**, **h**) 40 and (**i**, **j**) 50 h revealing the formation of a refined microstructure on the particle surface.*

Figure 6.4 *Thermal stability of the milled powders. DSC scans (heating rate 20 K/min) of the Al-Fe₃Al powder mixtures milled for 1, 10, 20, 30, 40 and 50 h.*

The combination of Al and Fe$_3$Al phases in the present composites are not in a stable configuration and, when heated to high temperatures, they react to form Al$_5$Fe$_2$ and Al$_{13}$Fe$_4$ intermetallics [Sha17]. The knowledge of the influence of milling on the thermal stability of the Al-Fe$_3$Al mixtures is thus a prerequisite for pr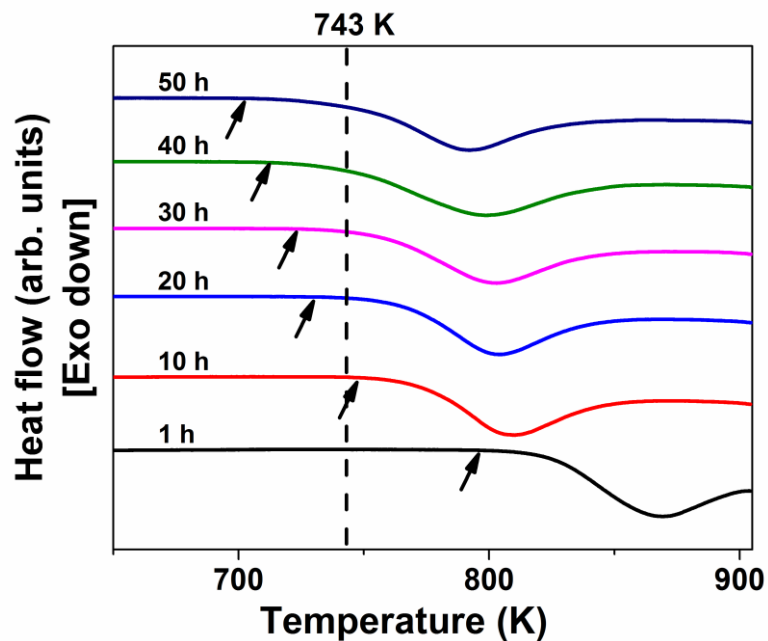operly controlling the subsequent consolidation step. To address this aspect, we performed DSC experiments on cold-pressed specimens obtained from powders mixtures milled from 1 to 50 h. Cold pressing ensures the formation of interfaces between the macro-particles, allowing atomic diffusion and, consequently, the phase transformation during heating, while preserving the as-milled microstructure.

Figure 6.4 displays the DSC scans of the cold-pressed composites. In the temperature range investigated here, the DSC curves exhibit one exothermic peak, indicative of a phase transformation. It has been reported that during heating of aluminum-Fe$_3$Al composites, aluminum diffuses into Fe$_3$Al particles and creates Al$_5$Fe$_2$ as first intermetallic reaction product at low sintering temperatures [Sha17]. Here, the formation of Al$_5$Fe$_2$ is shifted toward lower temperatures with increasing milling time, as shown by the change of the onset temperature of the transformation T_x (i.e. the temperature at which the heat flow signal diverge from the baseline [Sal13]) marked by arrows in Figure 6.4. The increase of milling time from 1 to 50 h decreases T_x by ~67 K (Table 6.1).
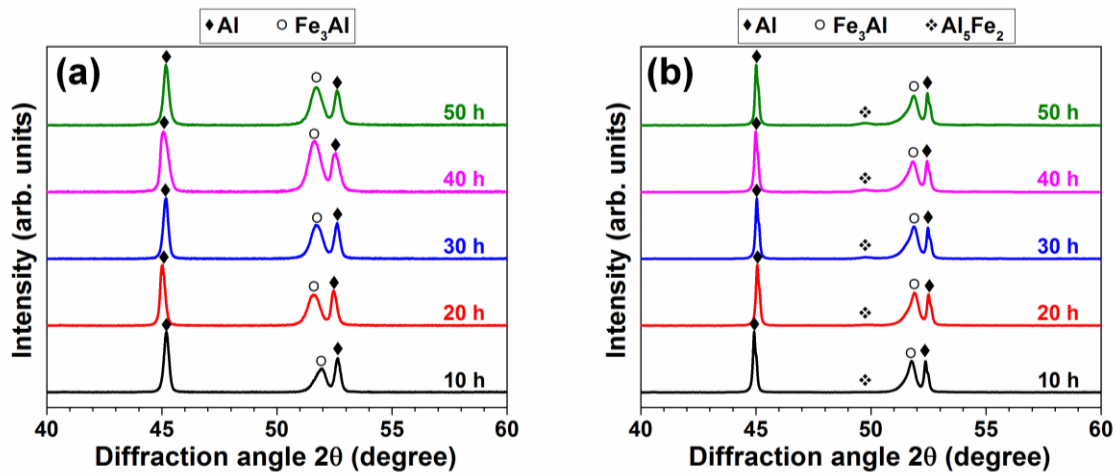
Figure 6.5 *Effect of ball milling on phase formation in the particulate precursors and bulk composites. XRD patterns (λ = 0.179 nm) for (**a**) the ball-milled Al-Fe₃Al powder mixtures and (**b**) bulk composite specimens synthesized by hot pressing of the milled powders.*

The decrease of the transformation temperature can be ascribed to the energy accumulated in the milled powder. During milling, powder particles are subjected to high-energy impacts when trapped between the milling media [Sur01a]. The energy transferred to

the particles at the impacts leads to work-hardening and fracture. Additionally, milling generates a variety of crystal defects, including dislocations, vacancies and stacking faults as well as new surfaces and grain boundaries [Sur13b, Sur01a, Sur01b]. As a results, a significant amount of enthalpy, which can reach values of about 40% of the heat of fusion [Eck11], can be stored in the milled material. The stored enthalpy is then released during heating at high temperatures due to defect recovery and grain growth [Hel11], which can in turn remarkably decrease the characteristic temperature of a reaction [Lu97, Sch90, Sch89], as observed here.
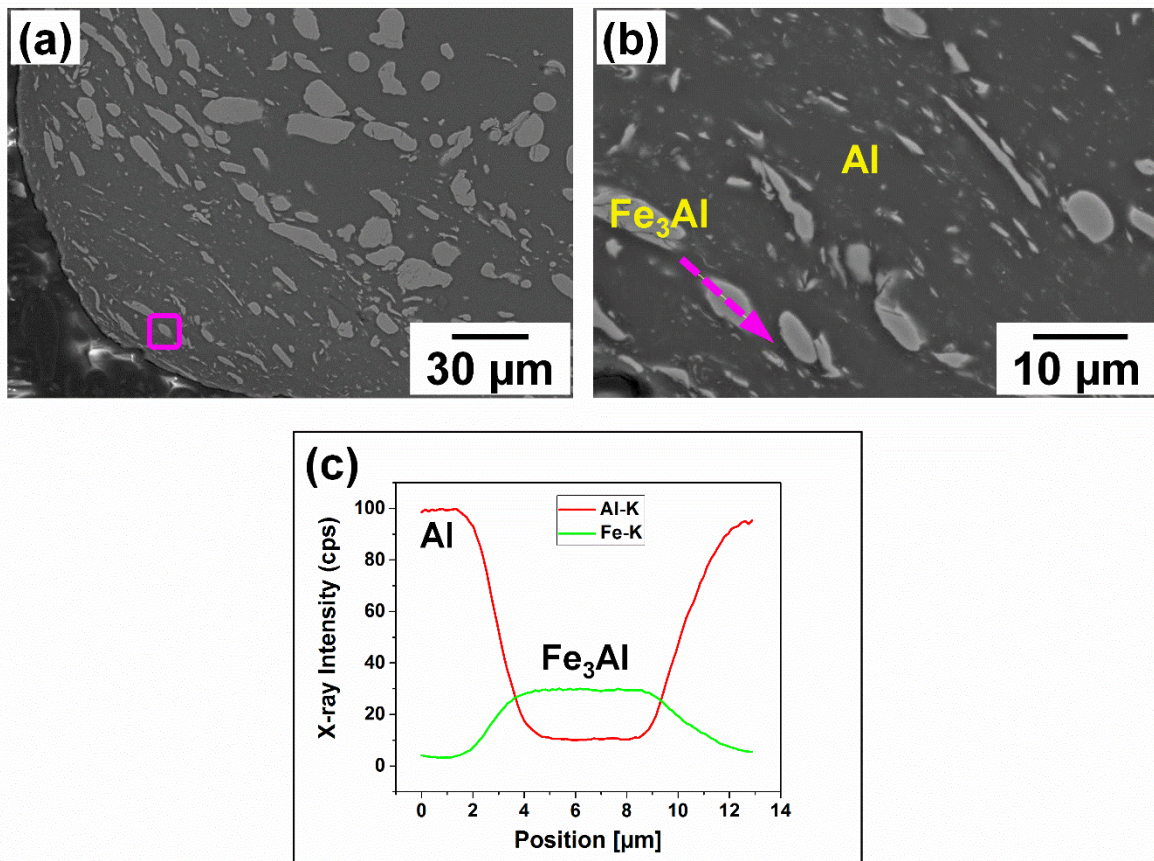
Figure 6.6 *Compositional analysis of matrix-reinforcement interface. SEM images (**a,b**) and EDX elemental concentration profiles (**c**) for the Al-Fe₃Al powder mixture milled for 50 h. The area shown in (**b**) corresponds to the purple box in (**a**). The dashed purple arrow in (**b**) represents the scanned EDX line.*

Figure 6.5 displays the XRD patterns for the powder mixtures milled for different times. The patterns exclusively show the presence of Al and D03-type Fe₃Al phases, which indicates that no new phases are generated during milling. The patterns exhibit peak broadening with the increase of milling time from 10 to 50 h for both aluminum and Fe₃Al peaks, which can be attributed to the reduction of the reinforcement and matrix particle size (especially in the shells

of the composite macro-particles, Figure 6.3) and to the increase in defect density and lattice strain [Mos12, Hua97, Koc97, Cul78].

The absence of a mechanically-induced reaction between Al matrix and Fe_3Al reinforcement is corroborated by the SEM micrographs and EDX elemental concentration profiles of the powder milled for 50 h displayed in Figure 6.6(a-c): no additional phases, beside Al and Fe_3Al, are detected, not even in the shell of the macro-particles which is presumably at a higher energy level due to the reduced size and presence of a high defect density.

6.2 Bulk composites by hot-pressing of milled Al- Fe₃Al powders

The XRD patterns for the hot-pressed AMCs (Figure 6.5(b)) reveal the presence of aluminum and Fe_3Al in all samples. In addition, the AMCs show that a small amount of orthorhombic Al_5Fe_2 phase is also formed. The peak intensity of the Al_5Fe_2 phase slightly increases with the increase of milling time, suggesting that an increasing amount of Al_5Fe_2 is formed. This behavior can be ascribed to the diminished temperature Tx (where the Al_5Fe_2 phase starts to form) displayed in Figure 6.4, which becomes progressively lower than the hot pressing temperature (743 K).

Figure 6.7 and 6.8 show the SEM images and EDX elemental concentration profiles for the AMCs produced by hot pressing of the composite powders milled for $t_m = 1, 10, 20, 30, 40$ and 50 h. The bulk specimens exhibit a harmonic-type microstructure with features resembling the parent milled macro-particles: macro-areas consisting of large and relatively undeformed Fe_3Al particles embedded into the Al matrix that are surrounded by an interface where the size of the Fe_3Al particles is reduced. EDX analysis indicates that Al_5Fe_2 is not formed in the AMC synthesized from the powder milled for 1 h. On the other hand, the AMCs consolidated from the powders milled for $t_m \geq 10$ h show the formation of the Al_5Fe_2 phase at the interface between Fe_3Al and aluminum matrix, confirming the results from XRD in Figure 6.5(b). The Al_5Fe_2 phase is typically formed at the interface between the parent macro-particles. This behavior can be attributed to the effect of milling, which is localized here to the surface of the particles (Figure 6.3). As a result, the microstructure of the surface is considerably refined and supposedly has a higher defect density than the core of the macro-particles. During hot pressing, the higher enthalpy stored in the surface would, therefore, locally induce the formation of the Al_5Fe_2 phase at lower temperatures compared with the less defective cores, explaining the present results. As a result of the increased shell thickness in the parent particles (Figure 6.3), the thickness of the refined interface in the composites increases with milling time

and reaches a maximum of about 50 μm after milling for 50 h. In contrast to the other specimens, the refined interface between macro-areas is not continuous in the 50 h AMC and pores with size of 5–10 μm size are observed. This is reflected in the lower relative density of this sample ($96.7 \pm 0.4\%$) compared with the composites synthesized from the powders milled for $t_m < 50$ h ($98.8 \pm 0.5\%$).

Figure 6.7 *Microstructure of the bulk composites. SEM images and EDX elemental concentration profiles for the AMCs synthesized by hot pressing of the powder mixtures milled for (**a–d**) 1, (**e–h**) 10 and (**i–l**) 20 h. The dashed purple arrows represent the scanned EDX lines.*
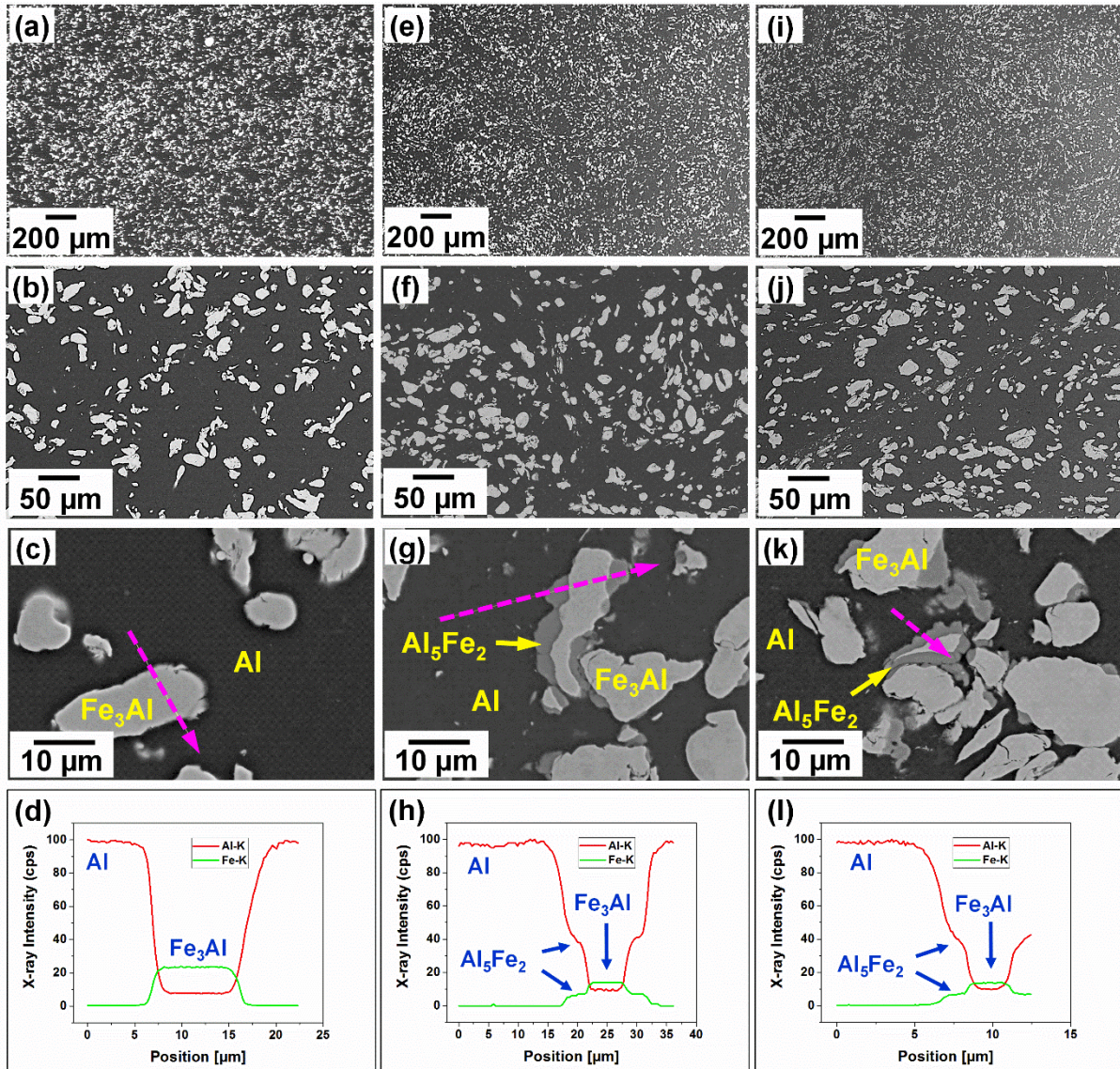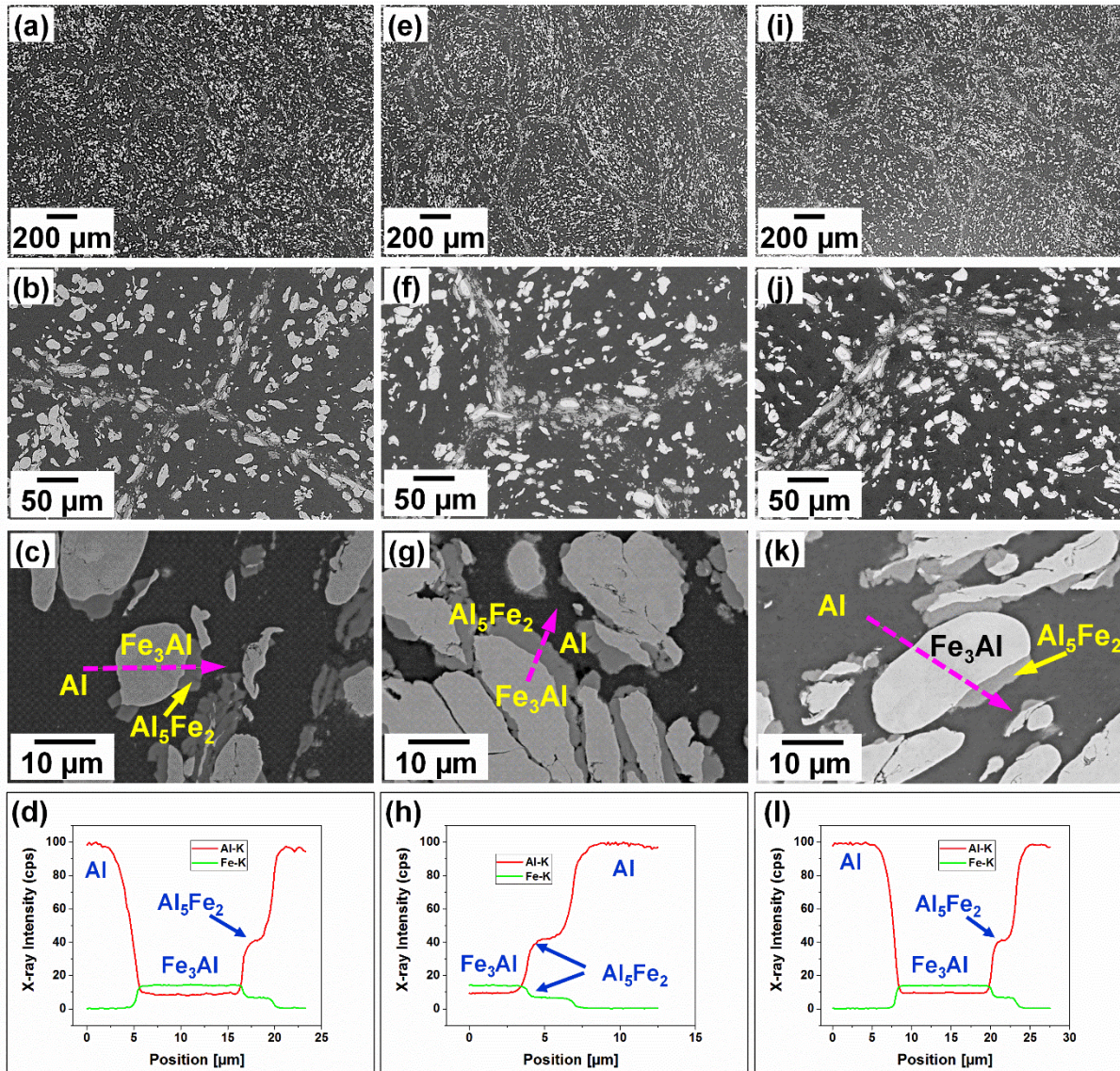
Figure 6.8 *Microstructure of the bulk composites. SEM images and EDX elemental concentration profiles for the AMCs synthesized by hot pressing of the powder mixtures milled for (**a–d**) 30, (**e–h**) 40 and (**i–l**) 50 h. The dashed purple arrows represent the scanned EDX lines.*

The amount of phases characterizing the different composites evaluated by SEM is shown in Figure 6.9. The volume fraction of Al_5Fe_2 increases with increasing milling time (along with the thickness of the shells of the parent macro-particles) and, accordingly, the volume fraction of aluminum and Fe_3Al decreases. The volume fraction of Al_5Fe_2 is highest in the 50 h AMC (15 ± 1 vol.%); this may explain the large residual porosity in this specimen as a result of the consolidation temperature used, being too low to properly sinter FeAl-rich samples [Mas16].
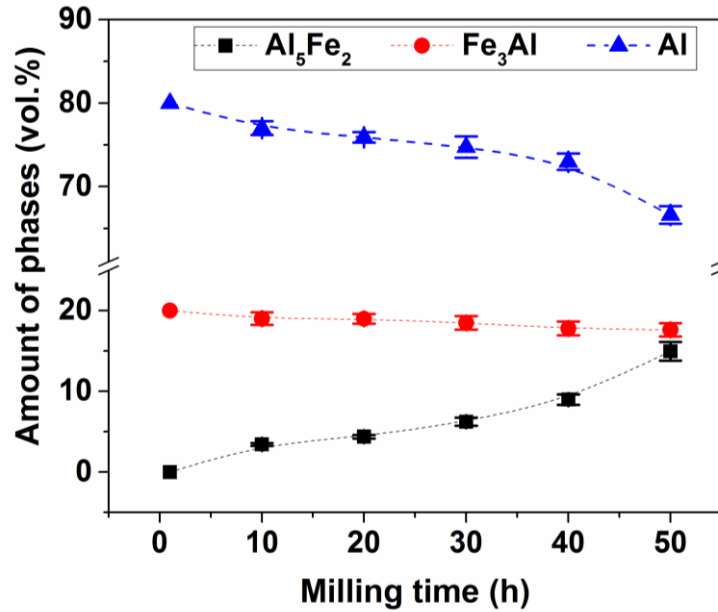
Figure 6.9 *Effect of ball milling on amounts of phases in the bulk composites. Volume percent of the different phases characterizing the hot-pressed composites as function of the milling time showing the progressive formation of the Al₅Fe₂ phase.*
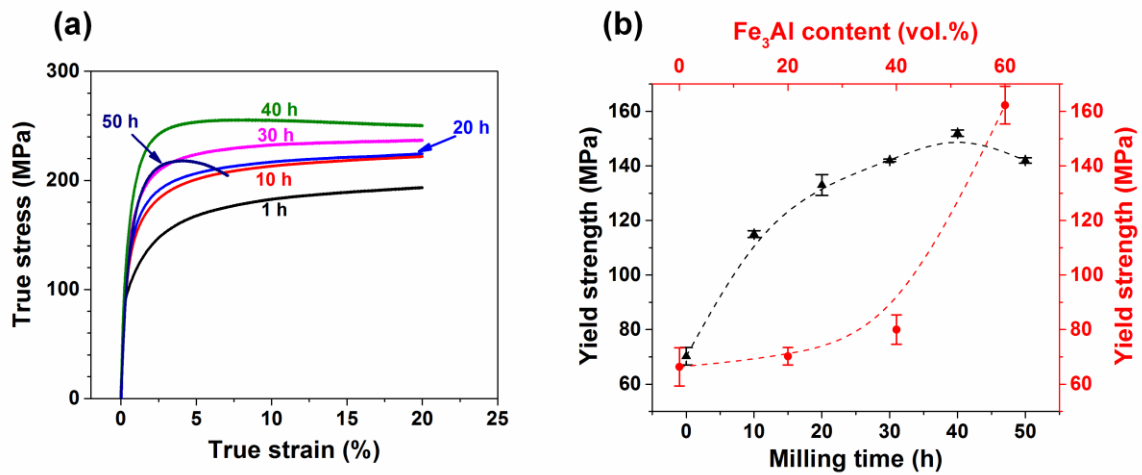
Figure 6.10 *Effect of milling on mechanical properties. (**a**) Room temperature compressive stress-strain curves for hot-pressed AMCs obtained from the powder mixture (Al + 20 vol.% Fe₃Al) milled for 1, 10, 20, 30, 40, and 50 h. (**b**) Yield strength of the bulk Al-Fe₃Al composites (initial Fe₃Al content of 20 vol.%) as a function of the milling time (black triangular points) and of the Al-Fe₃Al composites synthesized from 1 h milled powder mixtures (see chapter 5) as a function of Fe₃Al content (red circles).*

6.3 *Mechanical properties of hot-pressed Al- Fe₃Al composites*

The mechanical behavior of the AMCs consolidated from the powders milled for 1 to 50 h were investigated by using room temperature compression tests. The stress-strain curves are shown in Figure 6.10 along with the corresponding yield strength (0.2% offset). The strengthening effect induced by milling is quite remarkable: the yield strength of the composites increases from 70 ± 3 MPa for the 1 h AMC to 152 ± 1 MPa for the 40 h AMC and then it decreases to 142 ± 1 MPa for the 50 h AMC, most likely because of the higher residual porosity of this sample. The strength of the 40 h AMC is only 10 MPa lower than the composite reinforced with 60 vol.% of Fe_3Al (see chapter 5) fabricated from powder mixtures milled for only 1 h (red data points in Figure 6.10(b)). Given that the total amount of reinforcement ($Fe_3Al + Al_5Fe_2$) in the 40 h AMC is only 27 vol.% (Figure 6.9), the observed strengthening can be ascribed to the microstructural changes induced by milling the powder mixtures.
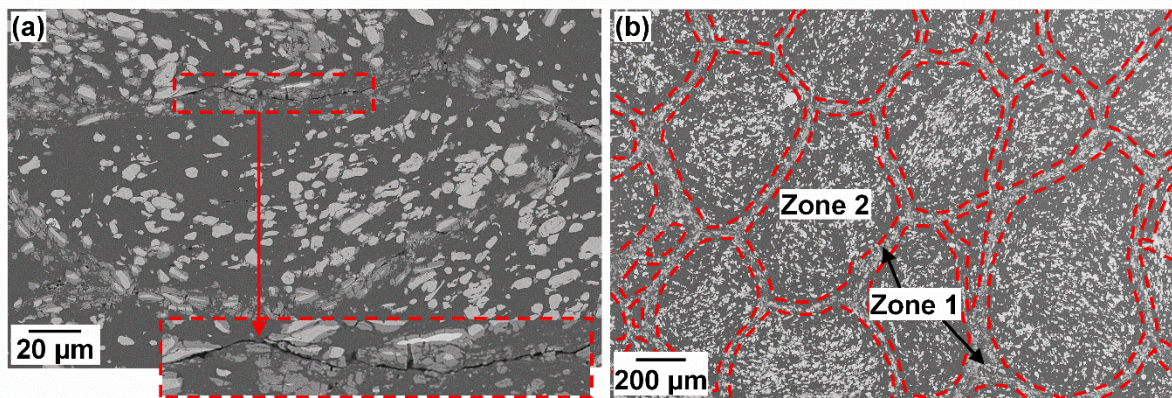
Figure 6.11 Microstructural features of the harmonic composites. (a) SEM images after compression test of the AMC synthesized from the powder milled for 50 h revealing preferential crack formation along the Al₅Fe₂-rich refined matrix. (b) Representative micrograph of the harmonic structures generated in the bulk Al-Fe₃Al composites consisting of a continuous matrix with refined reinforcement (zone 1) that encloses macro-regions with coarser and rather homogeneously distributed reinforcing particles (zone 2).

All composites and pure aluminum samples show no less than 20% strain, where the compression test was stopped, except for the 50 h AMC, which displays fracture at about 7% strain. Again, the reduced plastic deformation can be attributed to the residual porosity along with the large volume fraction of brittle Al_5Fe_2 formed during hot pressing at the interfaces of the macro-particles. The brittleness of these areas is illustrated in Figure 6.11(a): cracks preferentially form and propagate through the Al_5Fe_2-rich boundaries between the parent macro-particles.

The amount of oxygen, evaluated by carrier gas hot extraction method was found to be 0.495 ± 0.011 wt.% in the pure Al powder and 0.692 ± 0.005 wt.% in the Fe3Al particles, which gives a value of 0.570 ± 0.012 wt.% in the initial Al-Fe3Al powder mixture. The oxygen content slightly increases to 0.607 ± 0.006 wt.%, 0.627 ± 0.009 wt.% and 0.616 ± 0.020 wt.% in the composite powders milled for 20, 40 and 50 h, respectively. The strengthening contribution resulting from oxide formation can, therefore, be neglected.

6.4 Correlations between harmonic structure and mechanical behavior

The strength of composites reinforced with small volume fractions of reinforcement, where the distance between the reinforcing particles is large, can be well described by the lower bound of the rule of mixtures (RoM), the iso-stress model, which assumes that the matrix and reinforcement experience the same stress [Scu08, Kim01, Kim00, Cha87] as:

$$\sigma_c = \left(\frac{V_r}{\sigma_r} + \frac{V_m}{\sigma_m} \right)^{-1} \qquad (Equation\ 6.1)$$

where V is the volume fraction, σ is the strength and the subscripts c, r and m indicate the composite, the reinforcement and the matrix, respectively. Indeed, the variation of the yield strength for the Al-Fe₃Al composites with the Fe₃Al particles uniformly distributed in the aluminum matrix is in good agreement with the trend predicted by the iso-stress model [Sha17]. On the other hand, the strength of the present composites significantly diverges from the values predicted by the iso-stress model for $t_m > 1$ h: Equation 6.1 (red curve in Figure 6.12(a)) progressively underestimates the experimental values of yield strength with increasing milling time. Similarly, the lower bound of the Hashin and Shtrikman (H-S) model:

$$\sigma_c = \left(\frac{\sigma_r [\sigma_r V_r + \sigma_m (1 + V_m)]}{\sigma_m V_r + \sigma_r (1 + V_m)} \right)^{-1} \qquad (Equation\ 6.2)$$

where the soft continuous matrix encapsulates the hard reinforcement [Hua15], does not properly describe the present results (green curve in Figure 6.12(a)). This indicates that calculations solely based on the volume fraction of reinforcement are not capable to predict the strengthening effect in the present materials.

This behavior can be ascribed to the bimodal composite microstructure, which is harmonic-like and consists of a continuous matrix made of composite areas with refined

reinforcement (zone 1 in Figure 6.11(b)) that encloses macro-regions with coarser and rather homogeneously distributed reinforcing particles (zone 2 in Figure 6.11(b)). Zone 1 is most likely stronger than zone 2 because of the high hardness of the Al_5Fe_2 phase [Eck11] and of the refined microstructure. The extent of zone 1 increases with increasing the milling time (Figure 6.12(b)), which would explain the higher strength than predicted by Equations 6.1 and 6.2. The strengthening contribution of the areas comprising the refined reinforcement (zone 1) can be taken into account by modifying Equation 6.1 as:

$$\sigma_c = \left(1 + V_{z1}^{1/3}\right)\left(\frac{V_r}{\sigma_r} + \frac{V_m}{\sigma_m}\right)^{-1} \qquad (Equation\ 6.3)$$

with V_{z1} being the volume fraction of zone 1 and where the choice of the cube root is in accordance with the model proposed by Gurland [Gur63] for describing the strength of WC-Co alloys.

The values of yield strength calculated using Equation 6.3 are in good agreement with the experimental data except for the material milled for 50 h (blue curve in Figure 6.12(a)), where the residual porosity and crack formation decrease the strength of the material. For small values of V_{z1} ($t_m \leq 1$ h), the strength follows the iso-stress model, as observed for Al-Fe₃Al composites with $V_{z1} = 0$ [Sha17]; the strength of the composites then raises with increasing V_{z1} for $t_m > 1$ h. Equation 6.3 of course cannot be employed to describe the strength of composites with V_{z1} approaching unity; in this case, the strengthening contribution of zone 1 will be overestimated by a factor of 2.

In order to accurately describe the strength of the present composites, therefore, both the volume fraction of reinforcement and the characteristic microstructural features describing the harmonic structure (here the extent of zone 1) have to be taken into account. Two main aspects make the choice of the amount of zone 1 the most suitable descriptive feature of the present harmonic structures. The first aspect is related to the formation of a continuous refined matrix (i.e. zone 1), which behaves like a stiff skeleton that encapsulates the softer and coarser macro-regions (zone 2) and limits their deformation in response to the applied load, increasing the overall strength. The second aspect involves the strengthening contribution resulting from the reduction of the matrix ligament size (λ), which is indirectly considered by implementing V_{z1} in Equation 6.1. The amount of fragmented Fe₃Al particles with reduced size increases with V_{z1}, which consequently reduces λ in zone 1. At the same time, the size of zone 2 progressively

decreases, giving rise to an overall reduction of λ in the entire specimen, as shown in Figure 6.12(b).
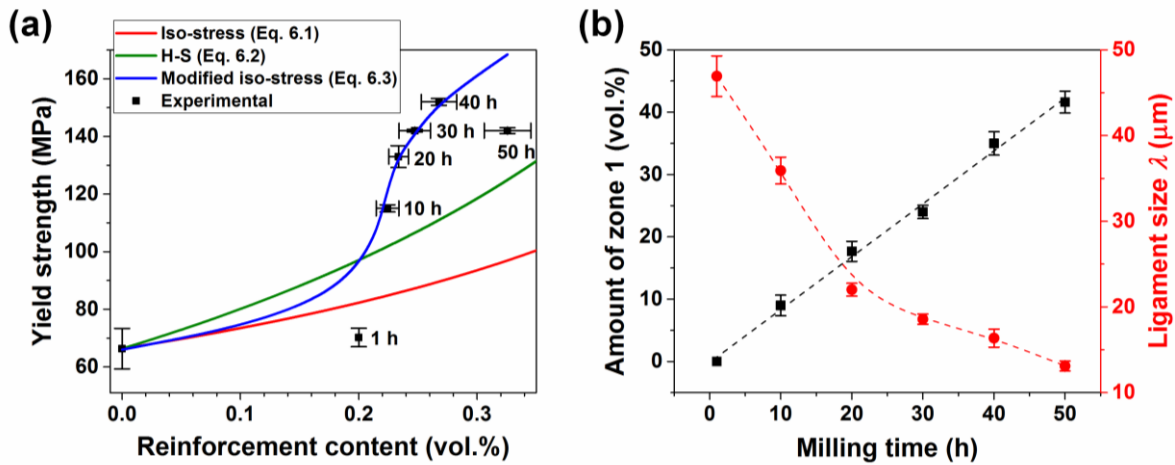

Figure 6.12 *Modeling of the strength of the composites. (a) Yield strength of the composites as a function of the volume fraction of reinforcement (cumulative amount of Fe₃Al and Al₅Fe₂): experimental data (points) and calculated values (lines) from the iso-stress model (equation 6.1), Hashin and Shtrikman (H-S) model (equation 6.2) and from the modified iso-stress model obtained by implementing the volume fraction of zone 1 (equation 6.3). (b) Amount of zone 1 and matrix ligament size of the harmonic composites as a function of the milling time.*

In this Chapter the effectiveness of the creation of harmonic structures as a method to strengthen Al-based metal matrix composites has been evaluated. To achieve this aim, Al-Fe₃Al composites with a bimodal microstructure consisting of a continuous fine-grained matrix that encloses macro-regions with coarser reinforcing particles have been synthesized by consolidation of the powder mixtures ball milled for different periods. The amount of the refined matrix, and consequently the strength of the harmonic composites, increases with increasing the milling time up to 50 h, when the higher residual porosity and the formation of cracks during mechanical loading decrease the strength of the material. For $t_m < 50$ h, the generation of the bimodal microstructure induces a significant strengthening of the harmonic composites: the strength exceeds that of the conventional material by a factor of 2, while retaining considerable plastic deformation. Modeling of the mechanical properties indicates that the strength of the present harmonic composites can be accurately described by taking into account both the volume fraction of reinforcement and the characteristic microstructural features describing the harmonic structure.

Chapter 7. Summary and outlook

Aluminum based composites are emerging as an attractive replacement for conventional materials in automotive and aerospace applications. The potential weight reduction of vehicles due to the higher values of specific strength and stiffness along with improved fatigue, wear and corrosion resistance make AMCs competitive with equivalent commercial alloys. Particulate reinforced aluminum based composites are attractive due to their iso-tropic properties, easier processing routes and lower costs compared to the fiber reinforced aluminum based composites. Recently, metallic particulate reinforcements, including metallic glasses and intermetallic phases have been successfully used to synthesize Al-based composites by powder metallurgy. The use of metallic reinforcements instead of conventional ceramics provides economical production and recyclability of AMCs. Additionally, metallic reinforcements display improved wettability and reduced difference of thermal expansion with the metallic matrix, which may thus lead to the creation of a stronger interface between matrix and reinforcement.

The strengthening of a matrix depends upon the volume fraction, particle size and distribution of the reinforcement together with the microstructural variation induced by the incorporation of the reinforcement. The reaction between matrix and reinforcement can generate new phases during processing. Such transformations may induce strengthening in MMCs, as for example reported in composites consisting of an aluminum matrix reinforced with Al-Cu-Fe quasicrystals, where the reaction generates a new phase (the ω-Al_7Cu_2Fe) and increases the strength of the material.

In this work, Al-Mg and Al-Fe_3Al composites have been successfully produced through ball milling followed by pressure assisted sintering. The effect of the volume fraction of the initial components of the composites on the creation of in-situ intermetallic phases and microstructural modifications has been evaluated. The effectiveness of the reaction between the initial components has been investigated as a strengthening method for further enhancing the mechanical properties of the composites. Finally, the effect of milling time on the microstructural refinement in Al-Fe_3Al powder mixtures and development of harmonic structures in the consolidated composites has been examined.

Reactive hot consolidation of Al-Mg powder mixtures has been used to synthesize lightweight composites reinforced with β-Al_3Mg_2 and γ-$Al_{12}Mg_{17}$ intermetallics formed in-situ during consolidation. Detailed microstructural characterization and comprehensive phase

analysis have been employed to examine the morphology of the phases in the composites and to achieve their identification and quantification. The formation of core-shell microstructures are observed in the Al-rich composites, where the Mg cores are surrounded by a double-shell of β-Al$_3$Mg$_2$ and γ-Al$_{12}$Mg$_{17}$ intermetallic phases. In the Mg-rich composites, aluminum has been fully consumed except in the composite $V = 60$. Microstructural examinations of a bilayer composites suggests that γ-Al$_{12}$Mg$_{17}$ is the first reaction product that originates at the interface between Al and Mg followed by the formation of the β-Al$_3$Mg$_2$ phase.

Microstructural and phase analysis of Al-Mg bilayer composites hot pressed at 623 K reveal the formation of a discontinuous intermetallic layer at the interface composed of β and γ phases. The higher diffusion rate of aluminum atoms in comparison to magnesium atoms suggests that intermetallic nucleation may have started with the γ phase at the Al-Mg interface followed by the formation of the β phase. Further increase of temperature to 673 K smoothens the interface and enlarges the widths of the intermetallic layers. The larger width of the β phase layer can be attributed to its higher inter-diffusion coefficient value in comparison to γ phase. The presence of oxide layer and Kirkendall's porosity at the interface between β phase and aluminum suggest that phase transformations have been occurred within the magnesium particles.

The mechanical behavior of the Al-Mg composites has been examined using room-temperature compression tests. The formation of the intermetallic phases increases the yield and compressive strengths of the composites, but decreases their plastic deformation. The strengthening effect depends on the amount of intermetallics formed during the consolidation step and, as a result, the yield strength of the composites follow iso-stress model when the data are plotted as a function of the cumulative volume percent of the intermetallic reinforcement.

In order to analyze the effectiveness of the interfacial reaction between matrix and reinforcement as a strengthening method for improving the mechanical performance of the Al-Fe$_3$Al composites, transformed and non-transformed composites have been produced by hot pressing the Al-Fe$_3$Al powder mixtures at 903 and 743 K, respectively. Detailed phase analysis and microstructural characterization of the transformed composites have been carried out to identify the phases formed during the transformation and to quantify their amount and morphology. In the Al-rich composites, a double-shell-reinforcement with Al$_5$Fe$_2$ and Al$_{13}$Fe$_4$ intermetallics surrounding the Fe$_3$Al phase is formed, while the Al matrix is progressively

consumed with increasing the reinforcement content. Conversely, in the reinforcement-rich composites only Al_5Fe_2 and residual Fe_3Al are present.

Microstructural analysis of the aluminum matrix composites containing a single mm-sized Fe_3Al particle reveals the phase sequence resulting from the Al-Fe_3Al reaction at the interface. The first phase formed is Al_5Fe_2, while $Al_{13}Fe_4$ is formed at higher temperatures between the Al matrix and Al_5Fe_2 phase. The formation of Al_5Fe_2 and $Al_{13}Fe_4$ takes place exclusively within the original Fe_3Al particles and no Fe-containing phases are observed within the Al matrix. Therefore, it can be concluded that Al diffuses into the Fe_3Al particles to form Al-rich Fe-Al phases, whereas no Fe diffusion occurs towards the Al matrix. The incomplete Al-Fe_3Al reaction and the decreased driving force for Al diffusion resulting from the reduced composition gradient in the present consolidation conditions explain the formation of the double-shell structure.

Room-temperature compression tests indicate that the phase transformation during hot pressing induces significant strengthening: yield and compressive strengths increase from 70-360 MPa and 200-500 MPa for the non-transformed ($Al + Fe_3Al$) composites to 130-1800 MPa and 550-1800 MPa for the transformed materials ($Al + Al_5Fe_2 + Al_{13}Fe_4 + Fe_3Al$). Strengthening unfortunately occurs at the expense of the plastic deformation, which is generally reduced. However, for near net shape components synthesized by powder metallurgy, where metal working and shaping is not necessary, limited plasticity would not drastically limit their application but would help to reduce the likelihood of catastrophic failure under loading. The transformed composites with 40 vol.% of initial Fe_3Al displays the maximum value of yield strength (~1820 MPa), but negligible plasticity. The transformed composite with 80 vol.% of initial Fe_3Al displays the best compromise between strength and plasticity: yield and compressive strengths exceed that of the corresponding non-transformed composite by a factor of about 2.5, while retaining appreciable plastic deformation of 7%.

Phases and microstructural modifications induced by the transformation have been correlated with the observed variations of yield strength. The iso-stress model describes well the yield strength of the non-transformed specimens. In contrast, the strength of the transformed materials does not follow the iso-stress model when considering the initial amount of Fe_3Al because of the phase and microstructure changes induced by the transformation. When the yield strength of the transformed composites are plotted as a function of the cumulative amount of

$Al_{13}Fe_4$ and Al_5Fe_2, the data can be divided into two groups according to the main soft phase (i.e. Al or Fe_3Al matrix) and the strength of the composites follows again the iso-stress model.

The effectiveness of the creation of harmonic structures as a method to strengthen Al-matrix composites has been evaluated. To achieve this aim, Al-Fe_3Al composites with a bimodal microstructure consisting of a continuous fine-grained matrix that encloses macro-regions with coarser reinforcing particles have been synthesized by consolidation of the powder mixtures ball milled for different periods.

The low energy ball milling of the initial powder mixture creates Al-Fe_3Al clusters. The average size of these clusters or macro-particles increases with increasing milling time and the size distributions of the clusters become progressively narrower. Every macro-particle (for $t_m \geq 10$ h) displays a core consisting of relatively large Fe_3Al particles homogeneously embedded in the Al matrix, which is surrounded by a shell made of Al and small, mostly sub-micron, Fe_3Al particles. This indicates that after the formation of the macro-particles at $t_m = 10$ h the microstructural refinement induced by ball milling is limited to their surface. The preferential microstructural refinement limited to the surface of the macro-particles is a necessary prerequisite for the generation of harmonic structures during subsequent powder consolidation.

The amount of the refined matrix, and consequently the strength of the harmonic composites, increases with increasing the milling time up to 50 h, when the higher residual porosity and the formation of cracks during mechanical loading decrease the strength of the material. For $t_m < 50$ h, the generation of the bimodal microstructure induces a significant strengthening of the harmonic composites: the strength exceeds that of the conventional material by a factor of 2, while retaining considerable plastic deformation. Modeling of the mechanical properties indicates that the strength of the present harmonic composites can be accurately described by taking into account both the volume fraction of reinforcement and the characteristic microstructural features describing the harmonic structure.

The results presented in this thesis indicates that powder metallurgy can be successfully used to synthesize intermetallic reinforced aluminum based composites as well as to create harmonic structures in the composites. The interfacial reaction products and generation of the harmonic structure enhance the strength of the composites. However, the mechanical behavior of these composites has to be further investigated to fully reveal their potential as structural materials. For example, the mechanical properties obtained from compression tests have to be

confirmed by conducting tensile test examinations. Furthermore, fatigue, wear and corrosion properties of the composites have to be fully evaluated.

The effectiveness of the phase transformation based strengthening can also be explored in the composites consisting of intermetallic reinforcements and heat treatable Al-based matrices. Likewise, the generation of the harmonic structures in these composites may lead to interesting results. For example, the effect of the alloying elements on the matrix-reinforcement reaction can be examined e.g., transformation temperatures, sequence of the in-situ phase transformations, together with variations in the composition, volume fraction and number of the in-situ formed phases. The compositional and microstructural changes can be linked with the altered mechanical properties of these composites. Similarly, the effect of the alloying elements on the microstructure and mechanical properties of the composites with harmonic structure can be systematically analyzed e.g., changes in the composition and width of the refined zone which encapsulates the coarse-grain cores. A systematic research can also be organized to optimize the composite processing parameters to combine the heat-treatment based strengthening with the transformation-induced strengthening.

References

[Abd14]   M. Abdellahi and M. Bahmanpour, *"A novel technology for minimizing the synthesis time of nanostructured powders in planetary mills"*, Mater. Res., 17.3. (2014) 781-791.

[Abd95]   M. Abdellaoui and E. Gaffet, *"The physics of mechanical alloying in a planetary ball mill: Mathematical treatment"*, Acta Metall. Mater., 43.3. (1995) 1087-1098.

[Afg16]   S. S. Seyyed Afghahi, M. Jafarian, M. Paidar and M. Jafarian, *"Diffusion bonding of Al 7075 and Mg AZ31 alloys: Process parameters, microstructural analysis and mechanical properties"*, Trans. Nonferrous Met. Soc. China, 26.7. (2016) 1843-1851.

[Ali14]   F. Ali, S. Scudino, M. S. Anwar, R. N. Shahid, V. C. Srivastava, V. Uhlenwinkel, M. Stoica, G. Vaughan and J. Eckert, *"Al-based metal matrix composites reinforced with Al–Cu–Fe quasicrystalline particles: Strengthening by interfacial reaction"*, J. Alloys. Compd., 607. (2014) 274-279.

[Ali12a]   F. Ali, S. Scudino, G. Liu, V. C. Srivastava, N. K. Mukhopadhyay, M. Samadi Khoshkhoo, K. G. Prashanth, V. Uhlenwinkel, M. Calin and J. Eckert, *"Modeling the strengthening effect of Al–Cu–Fe quasicrystalline particles in Al-based metal matrix composites"*, J. Alloys. Compd., 536. (2012) S130-S133.

[Ali12b]   M. Alizadeh, M. H. Paydar, D. Terada and N. Tsuji, *"Effect of SiC particles on the microstructure evolution and mechanical properties of aluminum during ARB process"*, Mater. Sci. Eng., A, 540. (2012) 13-23.

[Ali10]   M. Alizadeh and M. H. Paydar, *"Fabrication of nanostructure Al/SiCP composite by accumulative roll-bonding (ARB) process"*, J. Alloys. Compd., 492.1. (2010) 231-235.

[Alj12]   M. Aljerf, K. Georgarakis, D. Louzguine-Luzgin, A. Le Moulec, A. Inoue and A. R. Yavari, *"Strong and light metal matrix composites with metallic glass particulate reinforcement"*, Mater. Sci. Eng., A, 532. (2012) 325-330.

[All93]   J. E. Allison and G. S. Cole, *"Metal-matrix composites in the automotive industry: Opportunities and challenges"*, JOM, 45.1. (1993) 19-24.

[Ame12]   K. Ameyama and H. Fujiwara, *"Creation of harmonic structure materials with outstanding mechanical properties"*, Mater. Sci. Forum, 706. (2012) 9-16.

[And01]   I. E. Anderson and J. C. Foley, *"Determining the role of surfaces and interfaces in the powder metallurgy processing of aluminum alloy powders"*, Surf. Interface Anal., 31.7. (2001) 599-608.

[Ars91]   R. J. Arsenault, L. Wang and C. R. Feng, *"Strengthening of composites due to microstructural changes in the matrix"*, Acta Metall. Mater., 39.1. (1991) 47-57.

[Ars88]   R. J. Arsenault and S. B. Wu, *"A comparison of PM vs. melted SiC/Al composites"*, Scripta Metall., 22.6. (1988) 767-772.

[Ars86]   R. J. Arsenault and N. Shi, *"Dislocation generation due to differences between the coefficients of thermal expansion"*, Mater. Sci. Eng., 81. (1986) 175-187.

[Ars83]   R. J. Arsenault and R. M. Fisher, *"Microstructure of fiber and particulate SiC in 6061 Al composites"*, Scripta Metall., 17.1. (1983) 67-71.

[Ash87]   M. F. Ashby, *"The Modelling of Hot Isostatic Pressing.(Retroactive Coverage)"*, Hot Isostatic Pressing--Theories and Applications. (1987) 29-40.

[AST03]   ASTM E6-03, *Standard Terminology Relating to Methods of Mechanical Testing*, Annual Book of ASTM Standards, vol. 03.01, ASTM, West Conshohocken, PA, 2003.

[Azi18]   M. Azizieh, M. Mazaheri, Z. Balak, H. Kafashan and H. S. Kim, *"Fabrication of Mg/Al$_{12}$Mg$_{17}$ in-situ surface nanocomposite via friction stir processing"*, Mater. Sci. Eng., A, 712. (2018) 655-662.

[Bac03]   F.-W. Bach, Z. Babiak and T. Rothardt, *"Properties of plasma and D-gun sprayed metal-matrix-composite (MMC) coatings based on ceramic hard particle reinforced Fe-, Ni-aluminide matrix"*. International Conference Thermal Spray, 2003.

[Bai13]   Y. Bai, J. Xing, Z. Liu, S. Ma, E. Liu and Y. Gao, *"The microstructure and tribological property of in-situ Al₂O₃/Fe–25Al composites in argon atmosphere"*, Intermetallics, 38. (2013) 107-115.

[Bak95]   H. Bakker, G. F. Zhou and H. Yang, *"Mechanically driven disorder and phase transformations in alloys"*, Prog. Mater. Sci., 39.3. (1995) 159-241.

[Bak92]   H. Baker, H. Okamoto, S. Henry, G. Davidson, M. Flemming, L. Kacprzak and H. Lampman, *"Alloy phase diagrams: ASM handbook"*, Materials Park, Ohio, ASM International, Vol. 3, 1992.

[Bal15]   Ö. Balcı, K. Prashanth, S. Scudino, D. Ağaoğulları, İ. Duman, M. Öveçoğlu, V. Uhlenwinkel and J. Eckert, *"Effect of milling time and the consolidation process on the properties of al matrix composites reinforced with Fe-based glassy particles"*, Metals, 5.2. (2015) 669-685.

[Bas15]   M. R. Basariya, R. K. Roy, A. K. Pramanick, V. C. Srivastava and N. K. Mukhopadhyay, *"Structural transition and softening in Al–Fe intermetallic compounds induced by high energy ball milling"*, Mater. Sci. Eng., A, 638. (2015) 282-288.

[Ben90]   J. S. Benjamin, *"Mechanical alloying — A perspective"*, Met. Powder Rep., 45.2. (1990) 122-127.

[Ben76]   J. S. Benjamin, *"Mechanical alloying"*, Sci. Am., 234.5. (1976) 40-48.

[Ben74]   J. S. Benjamin and T. E. Volin, *"The mechanism of mechanical alloying"*, Metall. Trans., 5.8. (1974) 1929-1934.

[Bha10]   H. Bhadeshia, *"The Kirkendall Effect"*, University of Cambridge http://www.msm.cam.ac.uk/phase-trans/kirkendall.html, 4. (2010) 13.

[Boe01]   N. S.-de Boer, *"Metallische Massivglaser auf Fe-Al-PCB-(Ga-) Basis und Verbundmaterialien mit Mg-Y-Cu-Glas Matrix"*, Ph. D. Thesis, Technical University Dresden, 2001.

[Boe88]   F. R.- de Boer, R. Boom, W. Mattens, A. Miedema and A. Niessen, *"Cohesion in metals: transition metal alloys, Vol. 1"*, Amsterdam, North-Holland, 1988.

[Bre12]   S. Brennan, K. Bermudez, N. S. Kulkarni and Y. Sohn, *"Interdiffusion in the Mg-Al system and intrinsic diffusion in β-Mg₂Al₃"*, Metall. Mater. Trans. A, 43.11. (2012) 4043-4052.

[Bro76]   L. Brown and W. Stobbs, *"The work-hardening of copper-silica v. equilibrium plastic relaxation by secondary dislocations"*, Philos. Mag., 34.3. (1976) 351-372.

[Bur94]   U. Burkhardt, Y. Grin, M. Ellner and K. Peters, *"Structure refinement of the iron–aluminium phase with the approximate composition Fe₂Al₅"*, Acta Cryst. B, 50.3. (1994) 313-316.

[But06]   H.-J. Butt, K. Graf and M. Kappl, *"Physics and chemistry of interfaces"*, John Wiley & Sons, 2006.

[Cal12]   W. D. Callister Jr and D. G. Rethwisch, *"Fundamentals of materials science and engineering: an integrated approach"*, John Wiley & Sons, 2012.

[Can14]   A. Canakci, F. Erdemir, T. Varol, R. Dalmış and S. Ozkaya, *"Effects of a new pre-milling coating process on the formation and properties of an Fe–Al intermetallic coating"*, Powder Technol., 268. (2014) 110-117.

[Cha14]   A. K. Chaubey, S. Scudino, M. Samadi Khoshkhoo, K. G. Prashanth, N. K. Mukhopadhyay, B. K. Mishra and J. Eckert, *"High-strength ultrafine grain Mg–7.4%Al alloy synthesized by consolidation of mechanically alloyed powders"*, J. Alloys. Compd., 610. (2014) 456-461.

[Cha13]   S. Chatterjee, A. Sinha, D. Das, S. Ghosh and A. Basumallick, *"Microstructure and mechanical properties of Al/Fe-aluminide in-situ composite prepared by reactive stir casting route"*, Mater. Sci. Eng., A, 578. (2013) 6-13.

[Cha12]   A. K. Chaubey, S. Scudino, N. K. Mukhopadhyay, M. S. Khoshkhoo, B. K. Mishra and J. Eckert, *"Effect of particle dispersion on the mechanical behavior of Al-based metal matrix composites reinforced with nanocrystalline Al–Ca intermetallics"*, J. Alloys. Compd., 536. (2012) S134-S137.

[Cha06]   N. Chawla and K. K. Chawla, *"Metal matrix composites"*, Springer Science + Business Media, Inc., Springer, New York, 2006.

[Cha01]   N. Chawla and Y.-L. Shen, *"Mechanical behavior of particle reinforced metal matrix composites"*, Adv. Eng. Mater., 3.6. (2001) 357-370.

[Cha98a]   S. P. Chakraborty, I. G. Sharma and D. K. Bose, *"A study on the preparation of iron aluminium based intermetallic alloy by aluminothermic smelting technique"*, J. Alloys. Compd., 280.1–2. (1998) 255-261.

[Cha98b]   N. Chawla, J. W. Jones, C. Andres and J. E. Allison, *"Effect of SiC volume fraction and particle size on the fatigue resistance of a 2080 Al/SiC p composite"*, Metall. Mater. Trans. A, 29.11. (1998) 2843-2854.

[Cha96]   K. K. Chawla, *"Interfaces in metal matrix composites"*, Compos. Interface., 4.5. (1996) 287-298.

[Cha87]   K. K. Chawla, *"Composite Materials: Science and Engineering"*, in Materials Research and Engineering, Springer-Verlag, New York, 1987.

[Cha78]   K. K. Chawla and M. Metzger, *"Advances in Research on Strength and Fracture of Materials, vol. 3"*, Pergamon Press, New York, NY, USA, 1978.

[Cha72]   K. K. Chawla and M. Metzger, *"Initial dislocation distributions in tungsten fibre-copper composites"*, J. Mater. Sci., 7.1. (1972) 34-39.

[Che16]   J. Chen, C. Bao and F. Chen, *"Evolutions of microstructure and mechanical properties for Mg-Al/AlN composites under hot extrusion"*, Mater. Sci. Eng., A, 667. (2016) 426-434.

[Chu06]   B. W. Chua, L. Lu and M. O. Lai, *"Deformation behaviour of ultrafine and nanosize-grained Mg alloy synthesized via mechanical alloying"*, Philos. Mag., 86.19. (2006) 2919-2939.

[Cin13]   N. Cinca, C. R. C. Lima and J. M. Guilemany, *"An overview of intermetallics research and application: Status of thermal spray coatings"*, J. Mater. Res. Technol., 2.1. (2013) 75-86.

[Col95]   G. S. Cole and A. M. Sherman, *"Light weight materials for automotive applications"*, Mater. Charact., 35.1. (1995) 3-9.

[Cor11]   J. Corrochano, M. Lieblich and J. Ibáñez, *"The effect of ball milling on the microstructure of powder metallurgy aluminium matrix composites reinforced with MoSi_2 intermetallic particles"*, Compos. Part A Appl. Sci. Manuf., 42.9. (2011) 1093-1099.

[Cot99]   A. F. Cotton, G. Wilkinson, M. Bochmann and C. A. Murillo, *"Advanced inorganic chemistry"*, 6th edition., Wiley, New York, 1999.

[Cox52]   H. Cox, *"The elasticity and strength of paper and other fibrous materials"*, Brit. J. Appl. phys., 3.3. (1952) 72.

[Csa88]   A. Csanády, J. Günter, P. Barna and J. Mayer, *"Intermetallic phase formation in aluminium and iron thin film systems"*, Thin Solid Films, 167.1-2. (1988) 13.

[Cul78]   B. Cullity, *"Elements of X-Ray Diffraction"*, Second edition., Addision-Wesley Pub. Co. Inc., Phillippines, 1978.

[Dad12]   S. Dadbakhsh and L. Hao, *"Effect of hot isostatic pressing (HIP) on Al composite parts made from laser consolidated Al/Fe_2O_3 powder mixtures"*, J. Mater. Process. Technol., 212.11. (2012) 2474-2483.

[Das14a]   D. K. Das, P. C. Mishra, S. Singh and S. Pattanaik, *"Fabrication and heat treatment of ceramic-reinforced aluminium matrix composites - a review"*, Int. J. Mech. Mater. Eng., 9.1. (2014) 6.

[Das14b]   D. K. Das, P. C. Mishra, S. Singh and R. K. Thakur, *"Properties of ceramic-reinforced aluminium matrix composites - a review"*, Int. J. Mech. Mater. Eng., 9.1. (2014) 12.

[Dav93]   J. R. Davis, *"Aluminum and Aluminum alloys."*, ASM Specialty Handbook, ASM International, Materials Park, OH, USA, 1993.

[De11]   C. L. De Castro and B. S. Mitchell, *"The use of polymeric milling media in the reduction of contamination during mechanical attrition"*, J. Mater. Res., 17.12. (2011) 2997-2999.

[Dee96]   S. C. Deevi and V. K. Sikka, *"Nickel and iron aluminides: an overview on properties, processing, and applications"*, Intermetallics, 4.5. (1996) 357-375.

[Del87]   F. Delannay, L. Froyen and A. Deruyttere, *"The wetting of solids by molten metals and its relation to the preparation of metal-matrix composites composites"*, J. Mater. Sci., 22.1. (1987) 1-16.

[Die11]   D. Dietrich, D. Nickel, M. Krause, T. Lampke, M. P. Coleman and V. Randle, *"Formation of intermetallic phases in diffusion-welded joints of aluminium and magnesium alloys"*, J. Mater. Sci., 46.2. (2011) 357-364.

[Dir10]   G. Dirras, J. Gubicza, S. Ramtani, Q. H. Bui and T. Szilágyi, *"Microstructure and mechanical characteristics of bulk polycrystalline Ni consolidated from blends of powders with different particle size"*, Mater. Sci. Eng., A, 527.4. (2010) 1206-1214.

[Dlo93]   A. Dlouhy, N. Merk and G. Eggeler, *"A microstructural study of creep in short fibre reinforced aluminium alloys"*, Acta Metall. Mater., 41.11. (1993) 3245-3256.

[Dub11]   J. M. Dubois, E. B.-Ferré and K. Urban, *"Complex Metallic Alloys: Fundamentals and Applications"*, John Wiley & Sons, 2011.

[Eck11]   J. Eckert, J. C. Holzer, C. E. Krill and W. L. Johnson, *"Reversible grain size changes in ball-milled nanocrystalline Fe–Cu alloys"*, J. Mater. Res., 7.8. (2011) 1980-1983.

[Eck10]   J. Eckert, S. Scudino, M. Stoica, S. Kenzari and M. Sales, *"Mechanical engineering properties of CMAs"*, Complex Metallic Alloys: Fundamentals and Applications. (2010) 273-315.

[Egg00]   M. Eggersmann and H. Mehrer, *"Diffusion in intermetallic phases of the Fe-Al system"*, Philos. Mag. A, 80.5. (2000) 1219-1244.

[Eis98]   W. Eisen, B. Ferguson, R. German, R. Iacocca, P. Lee, D. Madan, K. Moyer, H. Sanderow and Y. Trudel, *"Powder metal technologies and applications"*, ASM Handbook, Vol. 7, 1998.

[El08]   T. El Kabir, A. Joulain, V. Gauthier, S. Dubois, J. Bonneville and D. Bertheau, *"Hot isostatic pressing synthesis and mechanical properties of Al/Al–Cu–Fe composite materials"*, J. Mater. Res., 23.4. (2008) 904-910.

[El01]   M. S. El-Eskandarany, *"Mechanical Alloying for Fabrication of Advanced Engineering Materials"*, Noyes Publications, Willian Andrew Publishing, New York, U.S.A, 2001.

[Esa07]   A. Esawi and K. Morsi, *"Dispersion of carbon nanotubes (CNTs) in aluminum powder"*, Compos. Part A Appl. Sci. Manuf., 38.2. (2007) 646-650.

[Est14]   I. Estrada-Guel, C. Carreño-Gallardo, C. Leyva-Porras and R. Martínez-Sánchez, *"Effect of process parameters on micro and macro-properties of an Al-based nanocomposite prepared by means of mechanical milling"*, J. Alloys. Compd., 586. (2014) S85-S89.

[Eus99]   N. Eustathopoulos, M. G. Nicholas and B. Drevet, *"Wettability at high temperatures"*, Vol. 3, Elsevier, 1999.

[Fan06]   G. J. Fan, H. Choo, P. K. Liaw and E. J. Lavernia, *"Plastic deformation and fracture of ultrafine-grained Al–Mg alloys with a bimodal grain size distribution"*, Acta Mater., 54.7. (2006) 1759-1766.

[Far15]   A. Farrokhi, A. Samadi, M. Asadi Asadabad and L. Amiri Talischi, *"Characterization of mechanically alloyed nano structured Fe₃Al intermetallic compound by X-ray diffractometry"*, Adv. Powder Technol., 26.3. (2015) 797-801.

[Fat15]   A. Fathy, O. El-Kady and M. M. M. Mohammed, *"Effect of iron addition on microstructure, mechanical and magnetic properties of Al-matrix composite produced by powder metallurgy route"*, Trans. Nonferrous Met. Soc. China, 25.1. (2015) 46-53.

[Fog03]   J. B. Fogagnolo, F. Velasco, M. H. Robert and J. M. Torralba, *"Effect of mechanical alloying on the morphology, microstructure and properties of aluminium matrix composite powders"*, Mater. Sci. Eng., A, 342.1–2. (2003) 131-143.

[För15]   W. Förster, C. Binotsch, B. Awiszus, D. Dietrich and D. Nickel, *"Interface engineering of aluminum-magnesium compounds"*, Mater. Today: Proceedings, 2. (2015) S3-S8.

[Fuj06]   H. Fujiwara, R. Akada, Y. Yoshita and K. Ameyama, *"Microstructure and mechanical property of nano-duplex materials produced by HRS process"*. Materials Science Forum, Trans Tech Publ, 503. (2006) 227-232.

[Fun72]   Y. Funamizu and K. Watanabe, *"Interdiffusion in the Al–Mg system"*, T. Jpn. I. Met., 13.4. (1972) 278-283.

[Gan08]   K. Gan and M. Gu, *"The compressibility of Cu/SiCp powder prepared by high-energy ball milling"*, J. Mater. Process. Technol., 199.1–3. (2008) 173-177.

[Gan05]   V. V. Ganesh and N. Chawla, *"Effect of particle orientation anisotropy on the tensile behavior of metal matrix composites: experiments and microstructure-based simulation"*, Mater. Sci. Eng., A, 391.1. (2005) 342-353.

[Ger05]   R. M. German, *"Powder Metallurgy and Particulate Materials Processing: The Processes, Materials, Products, Properties and Applications"*, Metal Powder Industries Federation, Princeton, New Jersey, USA, 2005.

[Gen03]   P. G. de Gennes, F. Brochard-Wyart and D. Quere, *"Capillarity and Wetting Phenomena: Drops, Bubbles, Pearls, Waves"*, Springer New York, 2003.

[Ger89]   R. M. German, *"Particle packing characteristics"*, Metal Powder Industries Federation, Princeton, New Jersey, USA, 1989.

[Ghu16]   A. Ghumatkar, S. Budhe, R. Sekhar, M. Banea and S. d. Barros, *"Influence of adherend surface roughness on the adhesive bond strength"*, Lat. Am. J. Solids Stru., 13.13. (2016) 2356-2370.

[Gia99]   E. Giacometti, N. Baluc, J. Bonneville and J. Rabier, *"Microindentation of Al-Cu-Fe icosahedral quasicrystal"*, Scripta Mater., 41.9. (1999) 989-994.

[Gie69]   B. C. Giessen, *"Developments in the structural chemistry of alloy phases"*, Springer, 1969.

[Gil83]   P. S. Gilman and J. S. Benjamin, *"Mechanical Alloying"*, Annu. Rev. Mater. Sci., 13.1. (1983) 279-300.

[Gri94]   J. Grin, U. Burkhardt, M. Ellner and K. Peters, *"Refinement of the Fe$_4$Al$_{13}$ structure and its relationship to the quasihomological homeotypical structures"*, Z. Kristallog., 209.6. (1994) 479-487.

[Gsc03]   K. Gschneidner Jr, A. Russell, A. Pecharsky, J. Morris, Z. Zhang, T. Lograsso, D. Hsu, C. H. Chester Lo, Y. Ye, A. Slager and D. Kesse, *"A family of ductile intermetallic compounds"*, Nat. Mater, 2. (2003) 587.

[Gu12]   J. Gu, S. Gu, L. Xue, S. Wu and Y. Yan, *"Microstructure and mechanical properties of in-situ Al$_{13}$Fe$_4$/Al composites prepared by mechanical alloying and spark plasma sintering"*, Mater. Sci. Eng., A, 558. (2012) 684-691.

[Gu09]   D. Gu, Z. Wang, Y. Shen, Q. Li and Y. Li, *"In-situ TiC particle reinforced Ti–Al matrix composites: Powder preparation by mechanical alloying and Selective Laser Melting behavior"*, Appl. Surf. Sci., 255.22. (2009) 9230-9240.

[Guo16]   B. Guo, J. Yi, S. Ni, R. Shen and M. Song, *"Factors affecting the microstructure and mechanical properties of Ti-Al$_3$Ti core-shell-structured particle-reinforced Al matrix composites"*, Philos. Mag., 96.12. (2016) 1197-1211.

[Gup95]   M. Gupta and M. Surappa, *"Processing-microstructure-mechanical properties of Al based metal matrix composites synthesized using casting route"*, Key Eng. Mat., 104. (1995) 259-274.

[Gur63]   J. Gurland, *"The fracture strength of sintered tungsten carbide-cobalt alloys"*, Trans. Met. Soc. AIME, 227. (1963) 1146-1150.

[Hag16]   M. Haghshenas, *"Metal–matrix composites"*, Ref. Mod. Mater. Sci. Mater. Eng., (2016) 03950-03953.

[Hal51]   E. Hall, *"The Hall-Petch Relationship"*. Proc. Phys. Soc. Ser. B, 64. (1951) 747-753.

[Han77]   N. Hansen, *"The effect of grain size and strain on the tensile flow stress of aluminium at room temperature"*, Acta Metall., 25.8. (1977) 863-869.

[Har98]   W. C. Harrigan, *"Commercial processing of metal matrix composites"*, Mater. Sci. Eng., A, 244.1. (1998) 75-79.

[Has02a]   J. Hashim, L. Looney and M. S. J. Hashmi, *"Particle distribution in cast metal matrix composites—Part I"*, J. Mater. Process. Technol., 123.2. (2002) 251-257.

[Has02b]   S. F. Hassan and M. Gupta, *"Development of a novel magnesium–copper based composite with improved mechanical properties"*, Mater. Res. Bull., 37.2. (2002) 377-389.

[Has02c]   S. F. Hassan and M. Gupta, *"Development of a novel magnesium/nickel composite with improved mechanical properties"*, J. Alloys. Compd., 335.1. (2002) L10-L15.

[Has02d]   S. F. Hassan and M. Gupta, *"Development of ductile magnesium composite materials using titanium as reinforcement"*, J. Alloys. Compd., 345.1. (2002) 246-251.

[Hel11]   E. Hellstern, H. J. Fecht, C. Garland, W. L. Johnson and W. M. Keck, *"Mechanism of Achieving Nanocrystalline AlRu By Ball Milling"*, MRS Proceedings, 132, 2011.

[Hel03]   H. Helms, U. Lambrecht and U. Höpfner, *"Energy savings by lightweighting"*, IFEU Institute for Energy-and Environmental Research. Heidelberg, 2003.

[Hen11]   D. Henkel, *"Porous iron aluminide: innovative filtration technology for refineries and clean coal applications"*, Adv. Mater. Process., 169.9. (2011) 44-46.

[Hes07]   Z. Razavi Hesabi, H. R. Hafizpour and A. Simchi, *"An investigation on the compressibility of aluminum/nano-alumina composite powder prepared by blending and mechanical milling"*, Mater. Sci. Eng., A, 454–455. (2007) 89-98.

[Hes06]   Z. R. Hesabi, A. Simchi and S. M. S. Reihani, *"Structural evolution during mechanical milling of nanometric and micrometric Al_2O_3 reinforced Al matrix composites"*, Mater. Sci. Eng., A, 428.1–2. (2006) 159-168.

[Hir96]   J. P. Hirth, *"Theory of Dislocations"*, in Physical Metallurgy, Edited by R. W. Cahn and P. Haasen, North-Holland, Amsterdam, The Netherlands, 1996.

[Hua15]   L. J. Huang, L. Geng and H. X. Peng, *"Microstructurally inhomogeneous composites: Is a homogeneous reinforcement distribution optimal?"*, Prog. Mater. Sci., 71.Supplement C. (2015) 93-168.

[Hua12]   Z. W. Huang, Y. H. Zhao, H. Hou and P. D. Han, *"Electronic structural, elastic properties and thermodynamics of $Mg_{17}Al_{12}$, Mg_2Si and Al_2Y phases from first-principles calculations"*, Physica B: Condens. Matter., 407.7. (2012) 1075-1081.

[Hua97]   B. Huang, K. N. Ishihara and P. H. Shingu, *"Metastable phases of Al–Fe system by mechanical alloying"*, Mater. Sci. Eng., A, 231.1. (1997) 72-79.

[Hum88]   F. Humphreys, *"Mechanical and physical behavior of metallic and ceramic composites"*. Proceedings of the 9th Riso International Symposium on Materials Science. S, Rockslide Denmark: Riso National Laboratory. (1988) 51-74.

[Hun93]   W. H. Hunt, T. M. Osman and J. J. Lewandowski, *"Micro-and macrostructural factors in DRA fracture resistance"*, JOM, 45.1. (1993) 30-35.

[Hut04]   E. Huttunen-Saarivirta, *"Microstructure, fabrication and properties of quasicrystalline Al–Cu–Fe alloys: a review"*, J. Alloys. Compd., 363.1-2. (2004) 154-178.

[Imm95]   J. P. Immarigeon, R. T. Holt, A. K. Koul, L. Zhao, W. Wallace and J. C. Beddoes, *"Lightweight materials for aircraft applications"*, Mater. Charact., 35.1. (1995) 41-67.

[Isr11]   J. N. Israelachvili, *"Intermolecular and surface forces"*, 3rd Edition, Academic press, USA, 2011

[Jay15]   S. Jayalakshmi and M. Gupta, *"Metallic amorphous alloy reinforcements in light metal matrices"*, Springer, 2015.

[Kai06]   K. U. Kainer, *"Metal Matrix Composites Custom-Made Materials for Automotive and Aerospace Engineering"*, Wiley-VCH, Weinheim, 2006.

[Kal02]   S. D. Kaloshkin, V. V. Tcherdyntsev, I. A. Tomilin, D. V. Gunderov, V. V. Stolyarov, Y. V. Baldokhin, I. G. Brodova and E. V. Shelekhov, *"Compsed phases and microhardness of aluminum-rich aluminum-iron alloys obtained by rapid*

quenching, mechanical alloying and high pressure torsion deformation", Mater. Trans., 43.8. (2002) 2031-2038.

[Ken14]   S. Kenzari, D. Bonina, J. M. Dubois and V. Fournée, *"Additive manufacturing of lightweight, fully Al-based components using quasicrystals"*, J. Mater. Process. Technol., 214.12. (2014) 3108-3111.

[Ken08]   S. Kenzari, P. Weisbecker, M. Curulla, G. Geandier, V. Fournee and J. M. Dubois, *"Formation and properties of Al composites reinforced by quasicrystalline AlCuFeB particles"*, Philos. Mag., 88.5. (2008) 755-766.

[Kho15a]   F. Khodabakhshi, A. Simchi, A. H. Kokabi and A. P. Gerlich, *"Friction stir processing of an aluminum-magnesium alloy with pre-placing elemental titanium powder: In-situ formation of an Al$_3$Ti-reinforced nanocomposite and materials characterization"*, Mater. Charact., 108. (2015) 102-114.

[Kho15b]   M. Sarkari Khorrami, S. Samadi, Z. Janghorban and M. Movahedi, *"In-situ aluminum matrix composite produced by friction stir processing using FE particles"*, Mater. Sci. Eng., A, 641. (2015) 380-390.

[Kim12]   J. Y. Kim, S. Scudino, U. Kühn, B. S. Kim, M. H. Lee and J. Eckert, *"Production and characterization of brass-matrix composites reinforced with Ni$_{59}$Zr$_{20}$Ti$_{16}$Si$_2$Sn$_3$ glassy particles"*, Metals, 2.4. (2012) 79-94.

[Kim01]   H. S. Kim, S. I. Hong and S. J. Kim, *"On the rule of mixtures for predicting the mechanical properties of composites with homogeneously distributed soft and hard particles"*, J. Mater. Process. Technol., 112.1. (2001) 109-113.

[Kim00]   H. S. Kim, *"On the rule of mixtures for the hardness of particle reinforced composites"*, Mater. Sci. Eng., A, 289.1–2. (2000) 30-33.

[Kim84]   Y. Kimura, Y. Mishima, S. Umekawa and T. Suzuki, *"Compatibility between carbon fibre and binary aluminium alloys"*, J. Mater. Sci., 19.9. (1984) 3107-3114.

[Kit15]   K. Kittner, A. Feuerhack, W. Förster, C. Binotsch and M. Graf, *"recent developments for the production of Al-Mg compounds"*, Mater. Today: Proceedings, 2. (2015) S225-S232.

[Koc97]   C. C. Koch, *"Synthesis of nanostructured materials by mechanical milling: problems and opportunities"*, Nanostruct. Mater., 9.1. (1997) 13-22.

[Kon15]   J. Kong, Y. Wei, J. Li, J. Huang and T. Wang, *"Microwave-assisted combustion synthesis of Fe_3Al bulk nanocrystalline intermetallic matrix composites"*, Adv. Powder Technol., 26.3. (2015) 778-782.

[Kra16]   M. Krasnowski, S. Gierlotka and T. Kulik, *"Nanocrystalline Al_5Fe_2 intermetallic and Al_5Fe_2–Al composites manufactured by high-pressure consolidation of milled powders"*, J. Alloys. Compd., 656. (2016) 82-87.

[Kra10]   M. Krasnowski and T. Kulik, *"Nanocrystalline Al–Fe intermetallics– light weight alloys with high hardness"*, Intermetallics, 18.1. (2010) 47-50.

[Kra93]   P. Krajewski, J. Allison and J. Jones, *"The influence of matrix microstructure and particle reinforcement on the creep behavior of 2219 aluminum"*, Metall. Mater. Trans. A, 24.1. (1993) 2731-2741.

[Kri81]   B. P. Krishnan, M. K. Surappa and P. K. Rohatgi, *"The UPAL process: a direct method of preparing cast aluminium alloy-graphite particle composites"*, J. Mater. Sci., 16.5. (1981) 1209-1216.

[Kwo14]   H. Kwon, M. Saarna, S. Yoon, A. Weidenkaff and M. Leparoux, *"Effect of milling time on dual-nanoparticulate-reinforced aluminum alloy matrix composite materials"*, Mater. Sci. Eng., A, 590. (2014) 338-345.

[Lag16]   M. A. Laguna-Marco, J. Sánchez-Marcos, N. Menéndez, J. Chaboy, E. Salas-Colera and C. Prieto, *"Microstructural, electronic and magnetic characterization of Fe-based nanoparticles embedded in Al matrix"*, Mater. Des., 93. (2016) 388-396.

[Lai87]   K. J. Laidler, *"Chemical kinetics"*, 3rd edition., NewYark: Harper Collins, 1987.

[Lap10a]   G. Laplanche, A. Joulain, J. Bonneville, V. Gauthier-Brunet, S. Dubois and T. El Kabir, *"Microstructural and mechanical study of an Al matrix composite reinforced by Al-Cu-Fe icosahedral particles"*, J. Mater. Res., 25.5. (2010a) 957-965.

[Lap10b]   G. Laplanche, A. Joulain, J. Bonneville, R. Schaller and T. El Kabir, *"Microstructures and mechanical properties of Al-base composite materials reinforced by Al–Cu–Fe particles"*, J. Alloys. Compd., 493.1-2. (2010b) 453-460.

[Lee13]   K. S. Lee, J. S. Kim, Y. M. Jo, S. E. Lee, J. Heo, Y. W. Chang and Y. S. Lee, *"Interface-correlated deformation behavior of a stainless steel-Al–Mg 3-ply composite"*, Mater. Charact., 75. (2013) 138-149.

[Lee08]   I. S. Lee, P. W. Kao and N. J. Ho, *"Microstructure and mechanical properties of Al–Fe in situ nanocomposite produced by friction stir processing"*, Intermetallics, 16.9. (2008) 1104-1108.

[Lee04]   M. H. Lee, J. H. Kim, J. S. Park, J. C. Kim, W. T. Kim and D. H. Kim, *"Fabrication of Ni–Nb–Ta metallic glass reinforced Al-based alloy matrix composites by infiltration casting process"*, Scripta Mater., 50.11. (2004) 1367-1371.

[Lee03a]   J.-M. Lee, S.-B. Kang, T. Sato, H. Tezuka and A. Kamio, *"Evolution of iron aluminide in Al/Fe in situ composites fabricated by plasma synthesis method"*, Mater. Sci. Eng., A, 362.1-2. (2003) 257-263.

[Lee03b]   J.-M. Lee, S.-B. Kang, T. Sato, H. Tezuka and A. Kamio, *"Fabrication of Al/Al$_3$Fe composites by plasma synthesis method"*, Mater. Sci. Eng., A343. (2003) 199-209.

[Lee02]   J.-M. Lee, S.-B. Kang, T. Sato, H. Tezuka and A. Kamio, *"microstructures and mechanical properties of Al$_3$Fe reinforced aluminum matrix composites fabricated ba a plasma synthesis method"*, Mater. Trans., 43.10. (2002) 2487-2493.

[Len66]   F. V. Lenel and G. S. Ansell, *"Creep Mechanisms and Their Role in the Sintering of Metal Powders"*, in Modern Developments in Powder Metallurgy: Volume 1

Fundamentals and Methods, Edited by H. H. Hausner, Springer US, Boston, MA (1966) 281-296.

[Li15]   C. Li, C. Chi, P. Lin, H. Zhang and W. Liang, *"Deformation behavior and interface microstructure evolution of Al/Mg/Al multilayer composite sheets during deep drawing"*, Mater. Des., 77. (2015) 15-24.

[Li99]   Z. Li, S. Schmauder and M. Dong, *"A simple mechanical model to predict fracture and yield strengths of particulate two-phase materials"*, Comp. Mater. Sci., 15.1. (1999) 11-21.

[Lie97]   M. Lieblich, J. González-Carrasco and G. Caruana, *"Thermal stability of an $AlNi_3Al$ composite processed by powder metallurgy"*, Intermetallics, 5.7. (1997) 515-524.

[Lid66]   W. G. Lidman and K. H. Moyer, *"Hot Pressing of Electrolytic Grade CR Beryllium, Modern Developments in Powder Metallurgy"*, Plenum Press, New York, 1966.

[Liu17]   Z. Y. Liu, B. L. Xiao, W. G. Wang and Z. Y. Ma, *"Modelling of carbon nanotube dispersion and strengthening mechanisms in Al matrix composites prepared by high energy ball milling-powder metallurgy method"*, Compos. Part A Appl. Sci. Manuf., 94. (2017) 189-198.

[Liu15]   W. Liu, L. Long, Y. Ma and L. Wu, *"Microstructure evolution and mechanical properties of Mg/Al diffusion bonded joints"*, J. Alloys. Compd., 643. (2015) 34-39.

[Liu12]   Z. Y. Liu, S. J. Xu, B. L. Xiao, P. Xue, W. G. Wang and Z. Y. Ma, *"Effect of ball-milling time on mechanical properties of carbon nanotubes reinforced aluminum matrix composites"*, Compos. Part A Appl. Sci. Manuf., 43.12. (2012) 2161-2168.

[Liu98]   C. T. Liu, E. P. George, P. J. Maziasz and J. H. Schneibel, *"Recent advances in B2 iron aluminide alloys: deformation, fracture and alloy design"*, Mater. Sci. Eng., A, 258.1–2. (1998) 84-98.

[Liu97]   C. T. Liu, J. Stringer, J. N. Mundy, L. L. Horton and P. Angelini, *"Ordered intermetallic alloys: an assessment"*, Intermetallics, 5.8. (1997) 579-596.

[Liu93]   C. T. Liu and K. S. Kumar, *"Ordered intermetallic alloys, part I: Nickel and iron aluminides"*, JOM, 45.5. (1993) 38-44.

[Liu90]   C. T. Liu, J. Stiegler and F. Froes, *"Ordered intermetallics"*, ASM International, Metals Handbook, Tenth Edition., 2. (1990) 913-942.

[Llo94]   D. J. Lloyd, *"Particle reinforced aluminium and magnesium matrix composites"*, Int. Mater. Rev., 39.1. (1994) 1-23.

[Loh92]   N. Loh and K. Sia, *"An overview of hot isostatic pressing"*, J. Mater. Process. Technol., 30.1. (1992) 45-65.

[Lu97]   L. Lu, M. O. Lai and S. Zhang, *"Diffusion in mechanical alloying"*, J. Mater. Process. Technol., 67.1. (1997) 100-104.

[Mab96]   M. Mabuchi, K. Kubota and K. Higashi, *"Tensile strength, ductility and fracture of magnesium-silicon alloys"*, J. Mater. Sci., 31.6. (1996) 1529-1535.

[Mal16]   A. Mallick, *"Improvement of mechanical properties in light weight Mg-based materials"*, Procedia Eng., 149. (2016) 283-287.

[Mal97]   P. K. Mallick, *"Composites engineering handbook"*, CRC Press, 1997.

[Man90]   M. Manoharan, L. Ellis and J. Lewandowski, *"Laminated composites with improved toughness"*, Case Western Reserve Univ., Cleveland, OH ,USA, 1990.

[Mas16]   M. Masmoudi, M. Mhadhbi, L. Escoda, J. J. Suñol and M. Khitouni, *"Microstructural evolution and corrosion behavior of nanocrystalline FeAl synthesized by mechanical alloying"*, J. Alloys. Compd., 657. (2016) 330-335.

[McK11]   C. G. McKamey, J. H. DeVan, P. F. Tortorelli and V. K. Sikka, *"A review of recent developments in Fe$_3$Al-based alloys"*, J. Mater. Res., 6.8. (2011) 1779-1805.

[Met16]   A. G. Metcalfe, *"Interfaces in Metal Matrix Composites: Composite Materials"*, Vol. 1, Elsevier, 2016.

[Mha13]   M. Mhadhbi, J. J. Suñol and M. Khitouni, *"Influence of heat treatments on the structure of FeAl powders mixture obtained by mechanical alloying"*, Phys. Proc., 40. (2013) 38-44.

[Mha11]   M. Mhadhbi, M. Khitouni, L. Escoda, J. J. Suñol and M. Dammak, *"Microstructure evolution and mechanical properties of nanocrystalline FeAl obtained by mechanical alloying and cold consolidation"*, J. Alloys. Compd., 509.7. (2011) 3293-3298.

[Mil91]   W. S. Miller and F. J. Humphreys, *"Strengthening mechanisms in particulate metal matrix composites"*, Scripta Metall. Mater., 25.1. (1991) 33-38.

[Mir05]   D. B. Miracle, *"Metal matrix composites – From science to technological significance"*, Comp. Sci. Tech., 65.15-16. (2005) 2526-2540.

[Mir01]   D. B. Miracle, S. L. Donaldson, S. D. Henry, C. Moosbrugger, G. J. Anton, B. R. Sanders, N. Hrivnak, C. Terman, J. Kinson and K. Muldoon, *"Composites"*, ASM handbook, Vol. 21, 10th edition., ASM international, Materials Park, Ohio, USA, 2001.

[Mis03]   R. S. Mishra, Z. Y. Ma and I. Charit, *"Friction stir processing: a novel technique for fabrication of surface composite"*, Mater. Sci. Eng., A, 341.1. (2003) 307-310.

[Mor04]   D. G. Morris, M. A. Munoz-Morris and J. Chao, *"Development of high strength, high ductility and high creep resistant iron aluminide"*, Intermetallics, 12.7-9. (2004) 821-826.

[Mor01]   B. L. Mordike and T. Ebert, *"Magnesium: Properties—applications — potential"*, Mater. Sci. Eng., A, 302.1. (2001) 37-45.

[Mor88]   A. Mortensen, J. A. Cornie and M. C. Flemings, *"Solidification processing of metal-matrix composites"*, JOM, 40.2. (1988) 12-19.

[Mos12]   E. Mostaed, H. Saghafian, A. Mostaed, A. Shokuhfar and H. R. Rezaie, *"Investigation on preparation of Al–4.5%Cu/SiCp nanocomposite powder via mechanical milling"*, Powder Technol., 221. (2012) 278-283.

[Moy07]   J. S. Moya, S. Lopez-Esteban and C. Pecharromán, *"The challenge of ceramic/metal microcomposites and nanocomposites"*, Prog. Mater. Sci., 52.7. (2007) 1017-1090.

[Mur93]   S. Murarka, *"Metallization: Theory and practice for VLSI application"*, Butterworth-Heinemann: Oxford, UK, 1993.

[Nar87]   V. C. Nardone, *"Assessment of models used to predict the strength of discontinous silicon carbide reinforced aluminum alloys"*, Scripta Metall., 21.10. (1987) 1313-1318.

[Nar86]   V. C. Nardone and K. M. Prewo, *"On the strength of discontinuous silicon carbide reinforced aluminum composites"*, Scripta Metall., 20.1. (1986) 43-48.

[Neg12]   M. Negendank, S. Mueller and W. Reimers, *"Coextrusion of Mg–Al macro composites"*, J. Mater. Process. Technol., 212.9. (2012) 1954-1962.

[Nem16a]   N. Nemati and M. Emamy, *"Evaluating Microstructure and High-Temperature Shear Behavior of Hot Extruded Al-Al$_{13}$Fe$_4$ Nanocomposite"*, Mater. Trans., 57.8. (2016) 1236-1245.

[Nem16b]   N. Nemati, M. Emamy, O. V. Penkov, J. Kim and D.-E. Kim, *"Mechanical and high temperature wear properties of extruded Al composite reinforced with Al$_{13}$Fe$_4$ CMA nanoparticles"*, Mater. Des., 90. (2016) 532-544.

[Nji01]   T. Njiokep, M. Eugene, M. Salamon and H. Mehrer, *"Growth of intermetallic phases in the Al-Mg system"*. Defect and diffusion forum, Trans Tech Publ, 194. (2001) 1581-1586.

[Ohr02]   M. Ohring, *"Mechanical Properties of Thin Films"*, in Materials Science of Thin Films (Second Edition), Edited by M. Ohring, Academic Press, San Diego (2002) 711-781

[Ozk16]   S. Ozkaya and A. Canakci, *"Effect of the B$_4$C content and the milling time on the synthesis, consolidation and mechanical properties of AlCuMg-B$_4$C nanocomposites synthesized by mechanical milling"*, Powder Technol., 297. (2016) 8-16.

[Pal12] J. C. González Palencia, T. Furubayashi and T. Nakata, *"Energy use and CO$_2$ emissions reduction potential in passenger car fleet using zero emission vehicles and lightweight materials"*, Energy, 48.1. (2012) 548-565.

[Pan15] D. Panda, L. Kumar and S. N. Alam, *"Development of Al-Fe$_3$Al nanocomposite by powder metallurgy route"*, Mater. Today: Proceedings, 2.4-5. (2015) 3565-3574.

[Pan12] A. Panteli, J. D. Robson, I. Brough and P. B. Prangnell, *"The effect of high strain rate deformation on intermetallic reaction during ultrasonic welding aluminium to magnesium"*, Mater. Sci. Eng., A, 556. (2012) 31-42.

[Par18] K. Park, J. Park and H. Kwon, *"Effect of intermetallic compound on the Al-Mg composite materials fabricated by mechanical ball milling and spark plasma sintering"*, J. Alloys. Compd., 739. (2018) 311-318.

[Pit11] S. Pitakrattanayothin, S. Naknana, P. Sumol, M. Morakotjinda, T. Yodkaew, B. Vetayanugul, R. Krataitong, N. Torsangthum and R. Tongsri, *"Preparation of PM Fe-FeAl and Fe-Fe$_2$Al$_5$ composites"*. The 25th Conference of the Mechanical Engineering Network of Thailand. (2011) 5.

[Qi13] N. Qi, M. Hu, Z. Wang, Z. Lu and C. Xie, *"Synthesis of Al/Fe$_3$Al core–shell intermetallic nanoparticles by chemical liquid deposition method"*, Adv. Powder Technol., 24.6. (2013) 926-931.

[Rag11] J. Ragani, P. Donnadieu, C. Tassin and J. J. Blandin, *"High-temperature deformation of the γ-Mg$_{17}$Al$_{12}$ complex metallic alloy"*, Scripta Mater., 65.3. (2011) 253-256.

[Ral97] B. Ralph, H. Yuen and W. Lee, *"The processing of metal matrix composites—an overview"*, J. Mater. Process. Technol., 63.1-3. (1997) 339-353.

[Ram96] N. Ramakrishnan, *"An analytical study on strengthening of particulate reinforced metal matrix composites"*, Acta Mater., 44.1. (1996) 69-77.

[Reu29] A. Reuss, *"Calculation of the flow limits of mixed crystals on the basis of the plasticity of monocrystals"*, Z. Angew. Math. Mech, 9. (1929) 49-58.

[Roh86]   P. K. Rohatgi, R. Asthana and S. Das, *"Solidification, structures, and properties of cast metal-ceramic particle composites"*, Int. Met. Rev., 31.1. (1986) 115-139.

[Roy06]   D. Roy, B. Basu, A. Basu Mallick, B. V. Manoj Kumar and S. Ghosh, *"Understanding the unlubricated friction and wear behavior of Fe-aluminide reinforced Al-based in-situ metal–matrix composite"*, Compos. Part A Appl. Sci. Manuf., 37.9. (2006) 1464-1472.

[Sah91]   P. Sahoo and M. J. Koczak, *"Analysis of in situ formation of titanium carbide in aluminum alloys"*, Mater. Sci. Eng., A, 144.1-2. (1991) 37-44.

[Sal18]   O. O. Salman, A. Funk, A. Waske, J. Eckert and S. Scudino, *"Additive manufacturing of a 316L steel matrix composite reinforced with CeO_2 particles: process optimization by adjusting the laser scanning speed"*, Technologies, 6.1. (2018) 25.

[Sal13]   M. D. A. Saldaña and S. I. Martínez-Monteagudo, *"Oxidative Stability of Fats and Oils Measured by Differential Scanning Calorimetry for Food and Industrial Applications"*, in Applications of Calorimetry in a Wide Context - Differential Scanning Calorimetry, Isothermal Titration Calorimetry and Microcalorimetry, Edited by A. A. Elkordy, InTech, Rijeka (2013) Ch. 19.

[Sam65]   S. Samson, *"The crsytal structure of the phase β Mg_2Al_3"*, Acta Cryst., 19.3. (1965) 401-413.

[Sar17]   S. Sardar, S. K. Karmakar and D. Das, *"Ultrasonic assisted fabrication of magnesium matrix composites: a review"*, Mater. Today: Proceedings, 4.2, Part A. (2017) 3280-3289.

[Saw14]   C. Sawangrat, O. Yamaguchi, S. K. Vajpai and K. Ameyama, *"Application of harmonic structure design to biomedical Co-Cr-Mo alloy for improved mechanical properties"*, Mater. Trans., 55.1. (2014) 99-105.

[Sch90]   G. B. Schaffer and P. G. McCormick, *"Displacement reactions during mechanical alloying"*, Metall. Trans. A, 21.10. (1990) 2789-2794.

[Sch89]   G. B. Schaffer and P. G. McCormick, *"Reduction of metal oxides by mechanical alloying"*, Appl. Phys. Lett., 55.1. (1989) 45-46.

[Scu09a]   S. Scudino, G. Liu, K. G. Prashanth, B. Bartusch, K. B. Surreddi, B. S. Murty and J. Eckert, *"Mechanical properties of Al-based metal matrix composites reinforced with Zr-based glassy particles produced by powder metallurgy"*, Acta Mater., 57.6. (2009) 2029-2039.

[Scu09b]   S. Scudino, G. Liu, M. Sakaliyska, K. B. Surreddi and J. Eckert, *"Powder metallurgy of Al-based metal matrix composites reinforced with β-Al₃Mg₂ intermetallic particles: Analysis and modeling of mechanical properties"*, Acta Mater., 57.15. (2009) 4529-4538.

[Scu08]   S. Scudino, K. B. Surreddi, S. Sager, M. Sakaliyska, J. S. Kim, W. Löser and J. Eckert, *"Production and mechanical properties of metallic glass-reinforced Al-based metal matrix composites"*, J. Mater. Sci., 43.13. (2008) 4518-4526.

[Sen16]   L. Senčekova, M. Palm, J. Pešička and J. Veselý, *"Microstructures, mechanical properties and oxidation behaviour of single-phase Fe₃Al (D0₃) and two-phase α-Fe,Al (A2)+Fe₃Al (D03) FeAlV alloys"*, Intermetallics, 73. (2016) 58-66.

[Sha18]   R. N. Shahid and S. Scudino, *"Strengthening of Al-Fe₃Al composites by the generation of harmonic structures"*, Sci. Rep., 8.1. (2018) 64841-64812.

[Sha17]   R. N. Shahid and S. Scudino, *"Microstructural strengthening by phase transformation in Al-Fe₃Al composites"*, J. Alloys. Compd., 705. (2017) 590-597.

[Shi92]   N. Shi, B. Wilner and R. Arsenault, *"An FEM study of the plastic deformation process of whisker reinforced SiC/Al composites"*, Acta Metall. Mater., 40.11. (1992) 2841-2854.

[Sik96]   V. K. Sikka, *"Processing of Aluminides"*, in Physical Metallurgy and processing of Intermetallic Compounds, Edited by N. S. Stoloff and V. K. Sikka, Springer US, Boston, MA (1996) 561-604.

[Sin16]   A. Singh, K. Solanki, M. Manuel and N. Neelameggham, *"Magnesium Technology 2016"*, Springer International Publishing, 2016.

[Sin15]   H. Sina, J. Corneliusson, K. Turba and S. Iyengar, *"A study on the formation of iron aluminide (FeAl) from elemental powders"*, J. Alloys. Compd., 636. (2015) 261-269.

[Sko14]   K. G. Skorpen, E. Mauland, O. Reiso and H. J. Roven, *"Novel method of screw extrusion for fabricating Al/Mg (macro-)composites from aluminum alloy 6063 and magnesium granules"*, Trans. Nonferrous Met. Soc. China, 24.12. (2014) 3886-3893.

[Son10]   M. Song, Y. He and S. Fang, *"Yield stress of SiC reinforced aluminum alloy composites"*, J. Mater. Sci., 45.15. (2010) 4097-4110.

[Ste07]   W. Steurer, *"The Samson phase, β-Mg$_2$Al$_3$, revisited"*, Z. Kristallog., 222.6. (2007) 259-288.

[Sto03]   V. V. Stolyarov, R. Lapovok, I. G. Brodova and P. F. Thomson, *"Ultrafine-grained Al–5 wt.% Fe alloy processed by ECAP with backpressure"*, Mater. Sci. Eng., A, 357.1-2. (2003) 159-167.

[Sto00]   N. S. Stoloff, C. T. Liu and S. C. Deevi, *"Emerging applications of intermetallics"*, Intermetallics, 8.9–11. (2000) 1313-1320.

[Sto98]   N. S. Stoloff, *"Iron aluminides: present status and future prospects"*, Mater. Sci. Eng., A, 258.1–2. (1998) 1-14.

[Sto66]   N. S. Stoloff and R. G. Davies, *"The mechanical properties of ordered alloys"*, Prog Mater Sci, 13.1. (1966) 84.

[Su97]   H. L. Su, M. Harmelin, P. Donnadieu, C. Baetzner, H. J. Seifert, H. L. Lukas, G. Effenberg and F. Aldinger, *"Experimental investigation of the Mg-Al phase diagram from 47 to 63 at.% Al"*, J. Alloys. Compd., 247.1. (1997) 57-65.

[Sur13a]   S. Suresh, *"Fundamentals of metal-matrix composites"*, Elsevier, 2013.

[Sur13b]   C. Suryanarayana and N. Al-Aqeeli, *"Mechanically alloyed nanocomposites"*, Prog. Mater. Sci., 58.4. (2013) 383-502.

[Sur03]   M. K. Surappa, *"Aluminium matrix composites: Challenges and opportunities"*, Sadhana, 28.1. (2003) 319-334.

[Sur01a]   C. Suryanarayana, *"Mechanical alloying and milling"*, Prog. Mater. Sci., 46.1–2. (2001) 1-184.

[Sur01b]   C. Suryanarayana, E. Ivanov and V. V. Boldyrev, *"The science and technology of mechanical alloying"*, Mater. Sci. Eng., A, 304. (2001) 151-158.

[Svo17]   J. Svoboda and F. D. Fischer, *"Incorporation of vacancy generation/annihilation into reactive diffusion concept – Prediction of possible Kirkendall porosity"*, Comp. Mater. Sci., 127. (2017) 136-140.

[Tan05]   F. Tang, M. Hagiwara and J. M. Schoenung, *"Formation of coarse-grained inter-particle regions during hot isostatic pressing of nanocrystalline powder"*, Scripta Mater., 53.6. (2005) 619-624.

[Tan04]   F. Tang, I. E. Anderson, T. Gnaupel-Herold and H. Prask, *"Pure Al matrix composites produced by vacuum hot pressing: tensile properties and strengthening mechanisms"*, Mater. Sci. Eng., A, 383.2. (2004) 362-373.

[Tan03]   F. Tang, I. E. Anderson and S. B. Biner, *"Microstructures and mechanical properties of pure Al matrix composites reinforced by Al-Cu-Fe alloy particles"*, Mater. Sci. Eng., A, 363.1. (2003) 20-29.

[Tay91]   M. Taya, *"Strengthening mechanisms of metal matrix composites"*, Mater. Trans., JIM., 32.1. (1991) 1-19.

[Thü93]   F. Thümmler and R. Oberacker, *"An In troduction to Powder Metallurgy"*, The Institute of Materials Series on Powder Metallurgy, The Institute of Materials, London, UK, 1993.

[Tjo04]   S. C. Tjong and H. Chen, *"Nanocrystalline materials and coatings"*, Mater. Sci. Eng., R, 45. (2004) 88.

[Tjo00]   S. C. Tjong and Z. Y. Ma, *"Microstructural and mechanical characteristics of in situ metal matrix composites"*, Mater. Sci. Eng., R, 29.3–4. (2000) 49-113.

[Tor03]   J. M. Torralba, C. E. da Costa and F. Velasco, *"P/M aluminum matrix composites: an overview"*, J. Mater. Process. Technol., 133.1–2. (2003) 203-206.

[Tre74]   R. E. Tressler, *"Interfaces in oxide reinforced metals"*, in Interfaces in Metallic Matrix Composites: Composite Materials, Edited by, Academic Press New York, vol. 1. (1974) 286-301.

[Tsa16]   A. P. Tsai, K. Aoki, A. Inoue and T. Masumoto, *"Synthesis of stable quasicrystalline particle-dispersed Al base composite alloys"*, J. Mater. Res., 8.1. (2016) 5-7.

[Und85]   E. E. Underwood, *"Metals Handbook"*, 9th edition., ASM International, Metal Park, OH, USA, 1985.

[Upa97]   G. S. Upadhyaya, *"Powder metallurgy technology"*, Cambridge Int. Science Publishing, 1997.

[Urb04]   K. Urban and M. Feuerbacher, *"Structurally complex alloy phases"*, J. Non-Cryst. Solids, 334-335. (2004) 143-150.

[Urb97]   K. Urban, M. Feuerbacher and M. Wollgarten, *"Mechanical behavior of quasicrystals"*, MRS Bulletin, 22.11. (1997) 65-68.

[Vaj16a] S. K. Vajpai, M. Ota, Z. Zhang and K. Ameyama, *"Three-dimensionally gradient harmonic structure design: an integrated approach for high performance structural materials"*, Mater. Res. Lett., 4.4. (2016) 191-197.

[Val00]   R. Z. Valiev, R. K. Islamgaliev and I. V. Alexandrov, *"Bulk nanostructured materials from severe plastic deformation"*, Prog. Mater. Sci., 45.2. (2000) 103-189.

[Var02]   R. A. Varin, *"Intermetallic-reinforced light-metal matrix in-situ composites"*, Metall. Mater. Trans. A, 33.1. (2002) 193-201.

[Var01]   R. A. Varin, *"Intermetallics: crystal structures"*, in Encyclopedia of materials: Science and technology, Edited by K. Buschow, Elsevier, Oxford (2001) 9913.

[Vog86] M. Vogelsang, R. J. Arsenault and R. M. Fisher, *"An in situ HVEM study of dislocation generation at Al/SiC interfaces in metal matrix composites"*, Metall. Trans. A, 17.3. (1986) 379-389.

[Voi89] W. Voigt, *"Ueber die Beziehung zwischen den beiden Elasticitätsconstanten isotroper Körper"*, Ann. Phys., 274.12. (1889) 573-587.

[Wan15a] Z. Wang, K. G. Prashanth, A. K. Chaubey, L. Löber, F. P. Schimansky, F. Pyczak, W. W. Zhang, S. Scudino and J. Eckert, *"Tensile properties of Al–12Si matrix composites reinforced with Ti–Al-based particles"*, J. Alloys. Compd., 630. (2015) 256-259.

[Wan15b] Z. Wang, S. Scudino, M. Stoica, W. Zhang and J. Eckert, *"Al-based matrix composites reinforced with short Fe-based metallic glassy fiber"*, J. Alloys. Compd., 651. (2015) 170-175.

[Wan14] Y. Wang, M. Song, S. Ni and Y. Xue, *"In situ formed core–shell structured particle reinforced aluminum matrix composites"*, Mater. Des., 56. (2014) 405-408.

[Wan08] J. Wang, Y. Li and W. Huang, *"Interface microstructure and diffusion kinetics in diffusion bonded Mg/Al joint"*, React. Kinet. Catal. L., 95.1. (2008) 71-79.

[Wan06] S. J. Wang, G. Q. Wu, R. H. Li, G. X. Luo and Z. Huang, *"Microstructures and mechanical properties of 5 wt.% Al_2Y_p/Mg–Li composite"*, Mater. Lett., 60.15. (2006) 1863-1865.

[Wan02] Y. Wang, M. Chen, F. Zhou and E. Ma, *"High tensile ductility in a nanostructured metal"*, Nature, 419. (2002) 912.

[Wei15] Q. Wei, S. Li, C. Han, W. Li, L. Cheng, L. Hao and Y. Shi, *"Selective laser melting of stainless-steel/nano-hydroxyapatite composites for medical applications: Microstructure, element distribution, crack and mechanical properties"*, J. Mater. Process. Technol., 222. (2015) 444-453.

[Wu12] Y. Wu, G.-Y. Kim and A. M. Russell, *"Effects of mechanical alloying on an Al6061–CNT composite fabricated by semi-solid powder processing"*, Mater. Sci. Eng., A, 538. (2012) 164-172.

References

[Xue15]   Y. Xue, R. Shen, S. Ni, D. Xiao and M. Song, *"Effects of sintering atmosphere on the mechanical properties of Al-Fe particle-reinforced Al-based composites"*, J. Mater. Eng. Perform., 24.5. (2015) 1890-1896.

[Yam02]   A. Yamazaki, *"Mechanical alloying of magnesium and Mg-Al alloys with MnO_2 and Fe_2O_3"*, J. Jpn. Inst. Light Metals, 52. (2002) 421-425.

[Yas17]   Yashpal, Sumankant, C. S. Jawalkar, A. S. Verma and N. M. Suri, *"Fabrication of aluminium metal matrix composites with particulate reinforcement: a review"*, Mater. Today: Proceedings, 4.2. (2017) 2927-2936.

[Ye04]   H. Z. Ye and X. Y. Liu, *"Review of recent studies in magnesium matrix composites"*, J. Mater. Sci., 39.20. (2004) 6153-6171.

[You15]   K. J. Young, *"Synthesis and characterization of bulk metallic glasses, composites and hybrid porous structures by powder metallurgy of metallic glassy powders"*, Ph.D. Thesis, Technical University Dresden, 2015.

[Yu06]   P. Yu, K. B. Kim, J. Das, F. Baier, W. Xu and J. Eckert, *"Fabrication and mechanical properties of Ni–Nb metallic glass particle-reinforced Al-based metal matrix composite"*, Scripta Mater., 54.8. (2006) 1445-1450.

[Zam13]   M. Zamanzade, H. Vehoff and A. Barnoush, *"Effect of chromium on elastic and plastic deformation of Fe_3Al intermetallics"*, Intermetallics, 41. (2013) 28-34.

[Zha17a]   H. Zhang, Y. Zhao, Y. Yan, J. Fan, L. Wang, H. Dong and B. Xu, *"Microstructure evolution and mechanical properties of Mg matrix composites reinforced with Al and nano SiC particles using spark plasma sintering followed by hot extrusion"*, J. Alloys. Compd., 725. (2017) 652-664.

[Zha17b]   Y. S. Zhang, Y. H. Zhao, W. Zhang, J. W. Lu, J. J. Hu, W. T. Huo and P. X. Zhang, *"Core-shell structured titanium-nitrogen alloys with high strength, high thermal stability and good plasticity"*, Sci. Rep., 7. (2017) 40031-40038.

[Zha15]   M. Zhao, Z. Zhou, J. Tan, Q. Ding and M. Zhong, *"Effects of ball milling parameters on microstructural evolution and mechanical properties of W-3% Y composites"*, J. Nucl. Mater., 465. (2015) 6-12.

[Zha08]   Z. Zhang and D. L. Chen, *"Contribution of Orowan strengthening effect in particulate-reinforced metal matrix nanocomposites"*, Mater. Sci. Eng., A, 483-484. (2008) 148-152.

[Zha06]   Z. Zhan, Y. He, D. Wang and W. Gao, *"Low-temperature processing of Fe–Al intermetallic coatings assisted by ball milling"*, Intermetallics, 14.1. (2006) 75-81.

[Zha05]   D. L. Zhang, S. Raynova, C. C. Koch, R. O. Scattergood and K. M. Youssef, *"Consolidation of a Cu–2.5vol.% Al$_2$O$_3$ powder using high energy mechanical milling"*, Mater. Sci. Eng., A, 410. (2005) 375-380.

[Zha04]   D. L. Zhang, *"Processing of advanced materials using high-energy mechanical milling"*, Prog. Mater. Sci., 49.3. (2004) 537-560.

[Zol13]   A. Zolriasatein, R. A. Khosroshahi, M. Emamy and N. Nemati, *"Mechanical and wear properties of Al-Al$_3$Mg$_2$ nanocomposites prepared by mechanical milling and hot pressing"*, International Journal of Minerals, Metallurgy, and Materials, 20.3. (2013) 290-297.

[Zol15]   A. Zolriasatein and A. Shokuhfar, *"Homogenizing annealing heat treatment effects on the microstructure, hardness and thermal behavior of Al$_{12}$Mg$_{17}$ complex metallic alloy"*, Mater. Des., 75. (2015) 17-23.

Acknowledgement

I would like to convey my special thanks to Mrs. Brit Präßler-Wüstling and Mrs. Janett Schuster for their kind assistance in administrative matters with patience and smile on the faces. The help of Mrs. Mann with humble, cooperative and polite attitude at Ausländerbehörde (Welcome Center) of Dresden is highly admirable and I am extremely thankful to her.

I am extremely thankful to Prof. Dr. Hasan Bin Awais, Assoc. Prof. Dr. Fahad Ali and Asst. Prof. Mr. Naeel-ul-Haq Tariq for motivation and help which they have provided me for the pursuance of my higher studies and taking care of all official and non-officials matters in Pakistan to make my life tension free in Germany.

I owe special gratitude to Deutscher Akademischer Austauschdienst (DAAD) also known as The German Academic Exchange Service for providing financial support under the Program of Research Grants for Doctoral Candidates and Young Academics and Scientists in Germany (57048249). I would like to express my sincere thanks to the German Nation because this funding was paid from their tax money. It was not possible for me to do my PhD without this financial support. I am highly obliged to Mrs. Dagmar Beerwerth and Mrs. Dagmar Hosseini-Razi for their impassioned role in the smooth and uninterrupted execution of DAAD Scholarship, along with the moral support and taking care of official and social matters. In addition to that, I am thankful to Dr. Thomas Gemming the acting director of Institute for Complex Materials (IKM) in IFW for the financial support to present my research work at several forums, and finally to wrap up and write up my research work.

I would like to thank all friends in Dresden for organizing refreshing pleasure sessions which were highly effective to release the stress. By the way, many thanks to them as well who always tried to pile-up the stress but stayed futile.

I extend my heartfelt thanks from the core of my heart to my family for their everlasting love, continuous encouragement and consistent motivation throughout this venture. I express my earnest thanks to Ch. Ahmed Ali, Ch. Muhammad Nawaz and Ch. Ahmed Nawaz for standing beside my family in Pakistan to interact with local administration. I am extremely grateful and indebted to Mr. Raees Khan and his grandfather for their unforgettable and unpayable support. I would like to thank all family members who suffered due to my absence and all relatives, friends and colleagues, especially Mr. Muhammad Siddique who supported my family by proving himself an elder brother and never let us feel that I am not in Pakistan.

(Hafiz Rub Nawaz Shahid)

List of publications

(2018-2014)

1. <u>R. N. Shahid</u>, S. Scudino, "*Strengthening of Al-Fe$_3$Al composites by the generation of harmonic structures*" Sci. Rep, vol.8, p. 6484, 2018, DOI:10.1038/s41598-018-24824-y

2. P. Ramasamy, <u>R. N. Shahid</u>, S. Scudino, J. Eckert and M. Stoica, *''Influencing the crystallization of Fe$_{80}$Nb$_{10}$B$_{10}$ metallic glass by ball milling''* J. Alloy Comp, vol. 725, p. 227, 2017

3. <u>R. N. Shahid</u>, S. Scudino, "*Microstructural strengthening by phase transformation in Al-Fe$_3$Al composites*" J. Alloy Comp, vol. 705, p. 590, 2017

4. S. Scudino, <u>R. N. Shahid</u>, B. Escher, M. Stoica, B. S. Li, and J. J. Kruzic, *"Mapping the cyclic plastic zone to elucidate the mechanisms of crack tip deformation in bulk metallic glasses"* Appl. Phys. Lett, p. 110, 081903 (2017); DOI: 10.1063/1.4977001

Erklärung

Hiermit versichere ich, dass ich die vorliegende Arbeit ohne unzulässige Hilfe Dritter und ohne Benutzung anderer als der angegebenen Hilfsmittel angefertigt habe; die aus fremden Quellen direkt oder indirekt übernommenen Gedanken sind als solche kenntlich gemacht. Bei der Auswahl und Auswertung des Materials sowie bei der Herstellung des Manuskripts habe ich Unterstützungsleistungen von folgenden Personen erhalten: Prof. Dr. Jürgen. Eckert und Dr. Sergio. Scudino. Weitere Personen waren an der geistigen Herstellung der vorliegenden Arbeit nicht beteiligt. Insbesondere habe ich nicht die Hilfe eines kommerziellen Promotionsberaters in Anspruch genommen. Dritte haben von mir keine geldwerten Leistungen für Arbeiten erhalten, die in Zusammenhang mit dem Inhalt der vorgelegten Dissertation stehen. Die Arbeit wurde bisher weder im Inland noch im Ausland in gleicher oder ähnlicher Form einer anderen Prüfungsbehörde vorgelegt und ist auch noch nicht veröffentlicht worden. Dissertation wurde an der TU Dresden am Institut für Werkstoffwissenschaft der Fakultät Maschinenwesen unter der wissenschaftlichen Betreuung durch Prof. Dr.-Ing. habil. Dr. h.c. Jürgen Eckert angefertigt. Die Promotionsordnung der Fakultät Maschinenwesen der TU Dresden aus dem Jahre 2001 erkenne ich an.

Hafiz Rub Nawaz Shahid
Dresden, 12.09.2018